Characterization of heat transfer rates in an air to phase change material thermal storage unit for integration in air handling units

by

Sarah Suzanne Wert

A thesis submitted to the Faculty of Graduate and Postdoctoral Affairs in partial fulfillment of the requirements for the degree of

Master of Applied Science

in

Mechanical Engineering

Carleton University
Ottawa, Ontario

Abstract

Space heating accounts for 55% of the total energy demand in the commercial sector in Canada. Improvement in energy efficiency and energy storage in this area can have a significant impact on total energy demand. Phase change materials (PCM) have been shown to be a viable medium for thermal energy storage having larger storage capacity per mass than conventional sensible heat storage materials.

For this thesis, an air-loop was designed, constructed and instrumented to characterize the heat transfer rates and energy storage potential of a small scale PCM thermal energy storage (TES) unit. The air-loop was designed to provide the necessary inlet conditions to the PCM TES unit. The storage unit was custom made and housed multiple aluminum flat plates (450 mm x 300 mm x 10 mm) filled with PCM (RT44HC). The plates were aligned in two rows of 29. A gap of 11 mm existed between each plate to allow air (the heat transfer fluid (HTF)) to pass. Overall, three variables were studied for the characterization: the HTF flow rates, the initial temperature of the PCM and the HTF inlet temperature.

An empirical model was created in TRNSYS with the values determined from the characterization of the PCM TES. This model with data from a real commercial building AHU was used to simulate a PCM TES integrated into an AHU using the integration method of strategic heating with the goal of reducing peak power during start-up. This was but one of multiple methods of PCM TES integration into an AHU. The simulation results were compared to the AHU without PCM TES to determine whether any energy improvements were achieved. It was determined that by adding the PCM TES the start-up peak power could be reduced by 35 kW.

Acknowledgements

I would like to thank my supervisors Dr. Cynthia A. Cruickshank and Dr. Dominic Groulx for their guidance, support and patience over the course of the project.

I would like to thank my colleagues from the Solar Energy Systems Laboratory at Carleton University for their support and friendship. I would like to acknowledge the additional guidance of PhD candidate Chris Baldwin particularly with the experimental instrumentation and equipment.

I would like to express my appreciation to Public Services and Procurement Canada for funding this project and providing data from the air handling units of one of the federal buildings.

I would also like to thank my parents, my sister and my fiancé for their overwhelming support and encouragement.

Table of Contents

List of Tables

List of Figures

Nomenclature

$c_{\mathrm{p,a}}$ Specific Heat of Air (kJ/kg·K)

$c_{\mathrm{p,l}}$ Specific Heat of PCM Liquid Phase (kJ/kg·K)

$c_{\mathrm{p,s}}$ Specific Heat of PCM Solid Phase (kJ/kg·K)

E_{st} Cumulative Energy Storage (kJ)

m Total Mass of PCM (kg)

T_{f} Final Temperature (°C)

T_{i} Initial Temperature (°C)

T_{m} Melting Temperature (°C)

q_{i} Instantaneous Heat Transfer (kW)

$\dot{V}$ Volumetric Flow Rate (m^3/s)

Δh_{m} Heat of Fusion of PCM (kJ/kg)

Δt Time interval (s)

ΔT Temperature Difference (°C)

ρ Density of Air (kg/m^3)

Abbreviations

AHU Air Handling Unit

GHG Green House Gases

HTF Heat Transfer Fluid

HVAC Heating, Ventilation and Air Conditioning

PCM Phase Change Material

TES Thermal Energy Storage

1 Chapter: Introduction

1.1 Background

According to the International Energy Outlook 2016 report, the world's energy consumption will increase by 48% by 2040 [1]. Energy consumption is correlated with emission of greenhouse gases (GHG) as most of the global energy is still produced with fossil fuels [1, 2]. Thus, this increase will result in an elevation of GHG emissions which has harmful effects on the environment and contributes to climate change [3]. Also, since the American energy crises that occurred in the 1970s, it has been emphasized that fossil fuels are a limited resource in which the world is heavily dependent that must be preserved through reduction of use and increased efficiency [4]. As a result, the cost of energy has increased causing concerns for its future affordability [1]. It is for these reasons that advancements in technologies which will result in reduction of GHG emissions, in either reduction of energy consumed or increased efficiency, and in improved affordability of energy, are necessary.

One area where there is potential for improvement is space heating in the commercial building sector. According to Natural Resources Canada, space heating accounted for 55% of the total energy consumption in the commercial building sector in Canada in 2013 [5]. One strategy to reduce energy consumption for space heating in the commercial building sector involves the use of thermal energy storage (TES) incorporated into air handling units (AHUs), a commonly used space heating device. Although there are many types of TES systems, an air to phase change material (PCM) TES system was chosen as a good candidate for the desired application. When selected properly, the PCM would go through its phase change transition during the storing-discharging cycle of the TES, and contribute its latent heat of fusion to the overall energy storage density of the system. Thus, for the same amount of energy storage, PCM will require less space

than a sensible TES such as a concrete slab or water [6]. Another reason an air-PCM TES would be appropriate for this application is because the air in the AHU can be used as the heat transfer fluid (HTF). This makes incorporating the air-PCM TES to the ventilation ducting or to the AHU structure itself a logical approach.

Due to the general low conductivity of PCM resulting in low heat transfer rates, any PCM TES must be properly designed for the desired application [7]. The PCM TES will have different heat transfer rates for each application which presently cannot be determined numerically. For this reason, heat transfer rates of the various PCM TES systems designed are characterized experimentally. At the time of this thesis, PCM heat transfer rates have not yet been characterized for the application of integration into an AHU for space heating. Thus, the heat transfer rates of the PCM TES design for implementation into an AHU was characterized by experiment and then the information gathered was used to simulate how the AHU would react to the integration of the air-PCM TES before a full scale model is pursued.

1.2 Air Handling Unit (AHU)

Air handling units are commonly used as the main piece of equipment in the heating, ventilation and air conditioning (HVAC) system of commercial and office buildings. Its two primary functions are to achieve the necessary air changes per hour required for the building and to condition the air within the building to a desired temperature. The AHU is normally connected to an air distribution system using duct work to distribute the conditioned fresh air throughout the building. The air distribution system can vary in design, however, this study will focus only on heat transfer rates within the AHU [8].

AHUs can vary in their components. For instance, some are used for heating only and others only for cooling [8]. For this study, there was the opportunity to obtain data from the AHUs

of a federal government office building in Ottawa. A basic schematic of the AHUs is shown in Figure 1.1 depicting the main components of the AHU for this specific building. The main components are the fan, the dampers, the filter, the heating heat exchanger and the cooling heat exchanger. The fan pulls in the return air (the stale air from within the building denoted by T_inside in Figure 1.1) and circulates it through the AHU. The dampers are used to control and separate the air. The dampers are controlled so that most of the air will be recirculated and continue through the AHU but a smaller percentage is exhausted to the outdoors while the same percentage of fresh outdoor air (denoted by T_outside in Figure 1.1) enters the AHU. The return air and the fresh outdoor air are combined to form what is known as the mixed air. The mixed air passes through the filter which will remove large particulates. The heating and cooling heat exchangers are used to condition the mixed air to the desired temperature.

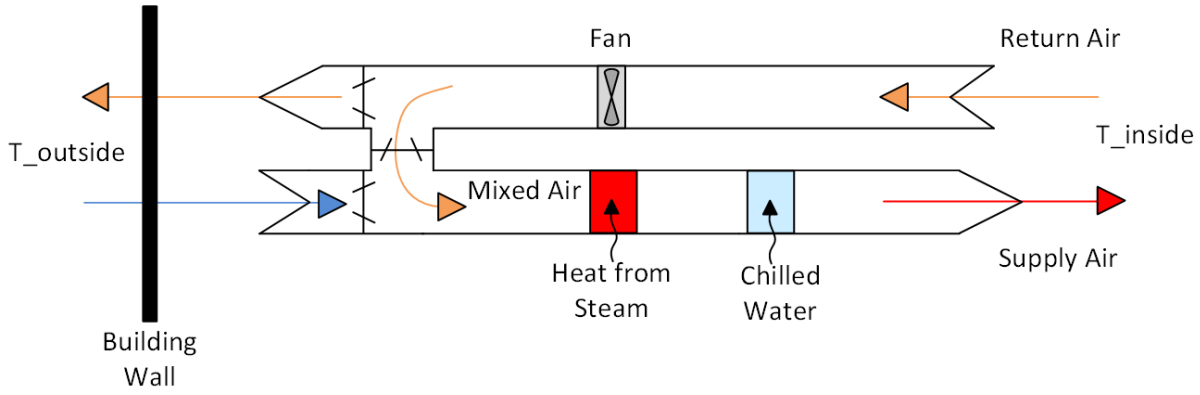

Figure 1.1 Schematic of AHU Base Model

The control of the AHU from the government building dictates that the heating is only operational in the winter and the cooling is only operational in the summer. The HTF used for the heating heat exchanger is steam and chilled water for the cooling heat exchanger. As this study will only look at storage during winter, the cooling heat exchanger shall not be considered. However, the incorporation of PCM storage for both heating and cooling would be recommended as a continuation of this work.

1.3 Phase Change Materials

Phase change materials (PCMs) are materials that have the ability to store energy through latent heat released during a phase transition at the materials designated transition temperature or temperature range [7]. Figure 1.2 demonstrates how a material can store energy gradually through sensible heat over a temperature difference and how the same material can also store a large amount of energy isothermally through latent heat at its melting point. Most PCMs used for thermal storage store latent heat during the solid to liquid transition, mainly because transition from liquid to gas would result in large volume and pressure changes; whereas liquids and solids have more similar volumes so they can more easily be stored in the same smaller container economizing on space [7]. This study will focus on solid to liquid PCMs.

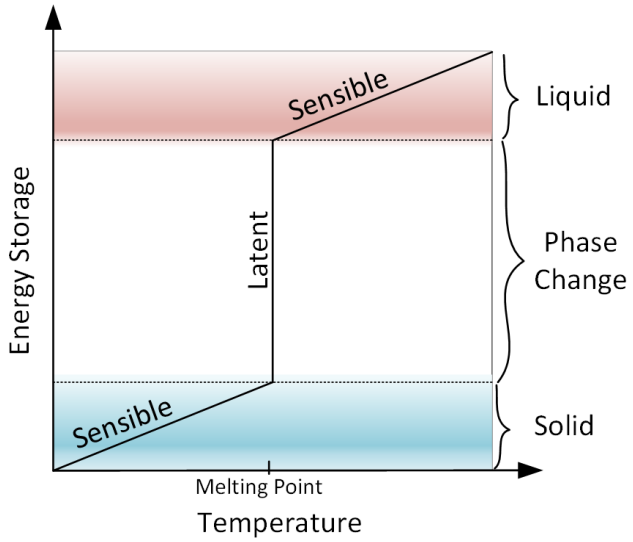

Figure 1.2 Example of how Latent and Sensible Heat is Stored with Respect to Temperature [7]

The biggest drawback to using PCMs in TES is known as 'the rate problem', see Subsection 2.2.3 [7]. This refers to the problems encountered with regards to the heat transfer rates that occur within the system. Due to 'the rate problem', it is important to experimentally characterize the heat transfer rates that occur in a PCM TES before implementation of the application.

1.4 Methods of Incorporating PCM into AHUs

There are three different methods presented below that could be used to incorporate a PCM TES into an AHU. This study will only explore the first method of incorporation through TRNSYS AHU simulations with an empirical model created from the experimental heat transfer characterization results. Note that even though the heating source of the building data used in the study is steam, the results of this study could be applied to any thermal energy heating source for instance; natural gas, electricity, geothermal, etc. This will allow the findings to be applicable to multiple buildings and not be limited to buildings using a specific heating source.

1.4.1 Incorporation Method 1: Strategic Heating

The first incorporation method is for thermal storage strategic heating based on outdoor temperatures, see Figure 1.3 for the PCM TES placement in the AHU and air flow circulation for both charging and discharging cycles. With this method, the PCM is charged during the daytime when the outside temperatures are higher thus requiring less energy from the heater in the AHU to condition the air and discharge either during the night or early morning where temperatures are lower and additional energy is required.

During charging, a fraction of the supply air which is at room temperature, is sent to the PCM where it is afterwards recirculated and added to the mixed air. During discharging, all the fresh air required is taken directly from outside to the PCM storage, where it is preheated then moved back to the AHU as part of the mixed air. The temperature difference across the heater should be reduced which will thus reduce the energy required from the heater. The building data obtained showed a large peak in needed power during the morning startup of the AHU. This method would reduce this peak helping the system operate more efficiently with a more consistent rate throughout the day. This application would be most beneficial in areas were commercial

buildings are charged electricity prices based on the peak power used. Thus, if this method is successful in reducing the peak load, the cost of electricity will be reduced for all hours of the day.

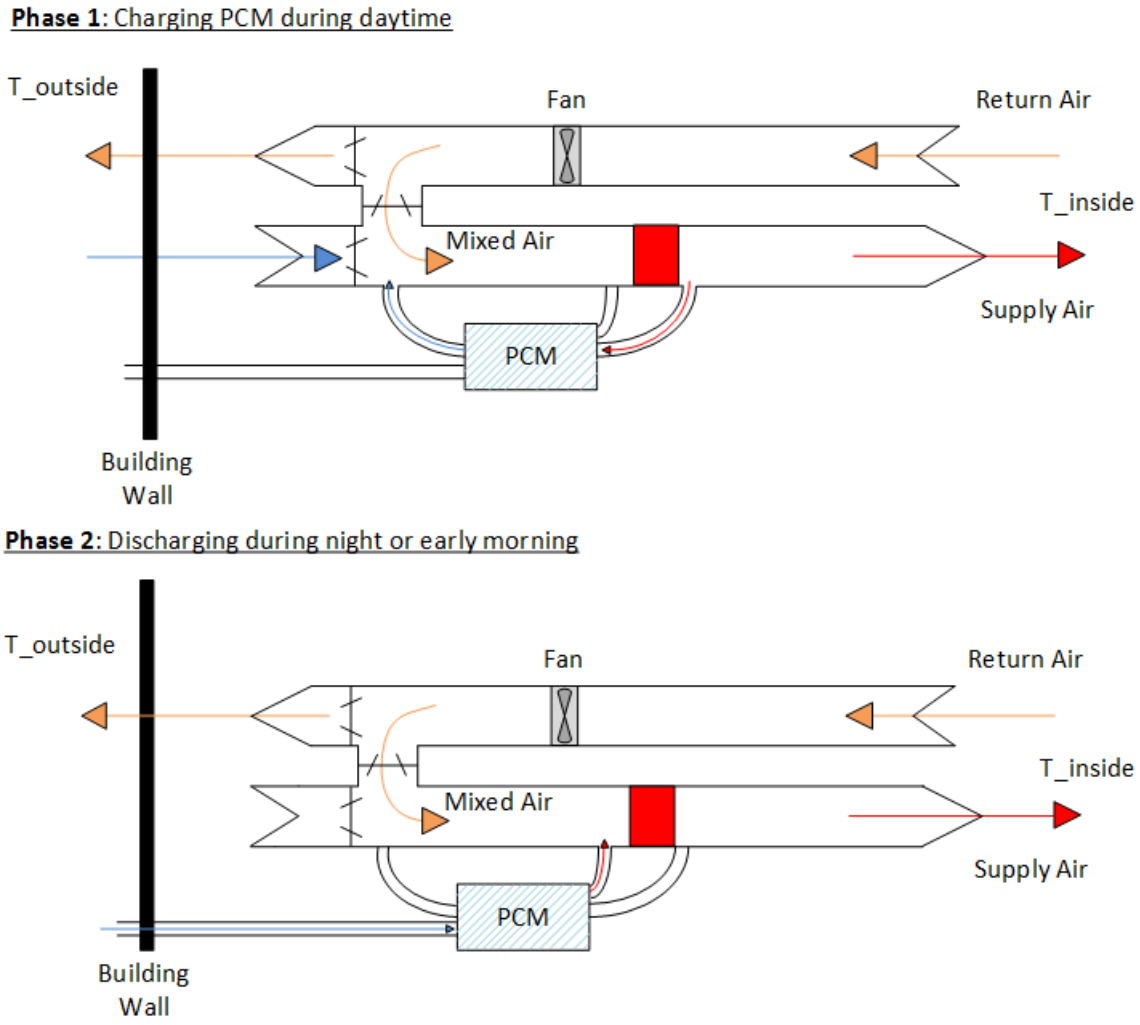

Figure 1.3 PCM Incorporation Method 1, Strategic Heating, with Air Flow Shown for Charging and Discharging Cycles

1.4.2 Incorporation Method 2: Peak Shaving

The second method is for peak shaving, see Figure 1.4 for the PCM TES placement in the AHU and air flow circulation for both charging and discharging cycles. With this method, the PCM is charged during off-peak hours by a secondary heater circulating air through a closed loop.

This method could have also worked by charging the PCM with the AHU heater but the secondary heater allows for more freedom to choose the inlet charging temperature. Generally, a higher charging temperature is desired to be able to use a PCM with a higher melting temperature creating a larger temperature difference between charging and discharging temperatures which will increase the sensible heat storage available in the material and increase the overall heat transfer rates. The PCM is discharged to the cold outdoor intake air during on-peak hours decreasing the amount of heat transfer required from the AHU heater when energy is more expensive.

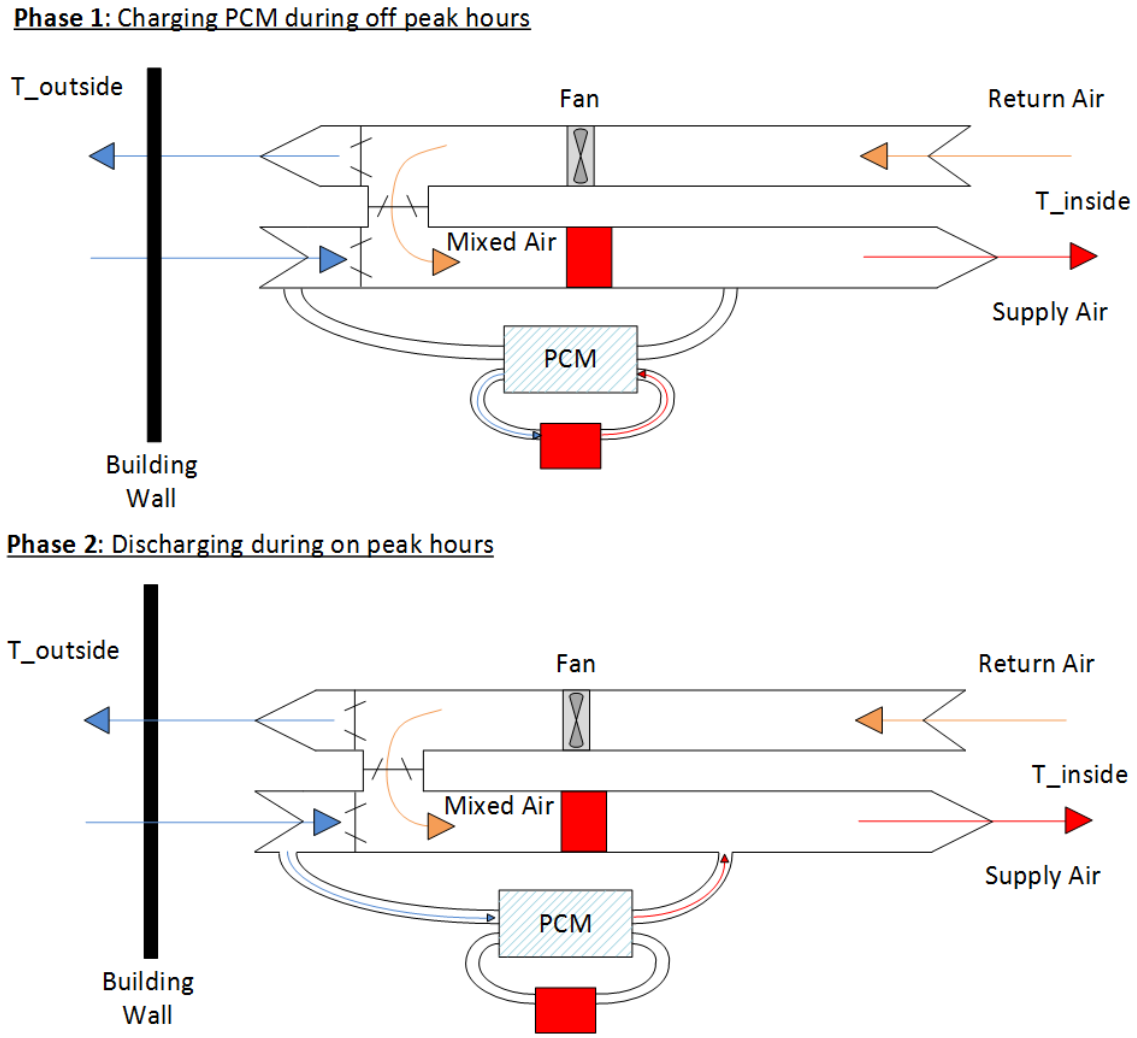

Figure 1.4 PCM Incorporation Method 2, Time-of-Use Peak Shaving, with Air Flow Shown for Charging and Discharging Cycles

This application will only work for areas with time-of-use pricing such as the province of Ontario and only if electric heaters are used. The application focusses on financial savings by redistributing the load when its prices are lower. There is also an environmental benefit to this method. The electricity consumed during peak loads is generally produced with fossil fuels such as coal and oil. By shaving the peak, the need to burn these environmentally harmful fuels is reduced.

1.4.3 Incorporation Method 3: Heat Recovery

The third method is for heat recovery, see Figure 1.5 for the PCM TES placement in the AHU and air flow circulation for both charging and discharging of each unit. This method consists of two PCM storage units separated by a layer of insulation or located in separate areas. The concept of recovering heat from the exhaust to be directly transferred to the intake has been explored in the past and is currently commercially available [9, 10].

The heat recovery system proposed here is a newer concept with only one previous study [11]. Instead of transferring the heat directly, the energy is stored to be used later. The PCM thermal storage units are in constant operation both charging from the exhaust room temperature air and discharging to the cool outdoor air at the same time. Once the charging unit has reached the total energy storage capacity, the airflows in both units switch and charging and discharging is reversed. A series of dampers would be one possible strategy for switching the airflow of the units. The PCM heat recovery method would need to be compared to conventional heat recovery units to determine whether there were any improvements. This method, if proven to be functional in future studies, could be useful in arctic climates where conventional heat exchangers do not function due to freezing problems, although the current study will not focus on this particular topic.

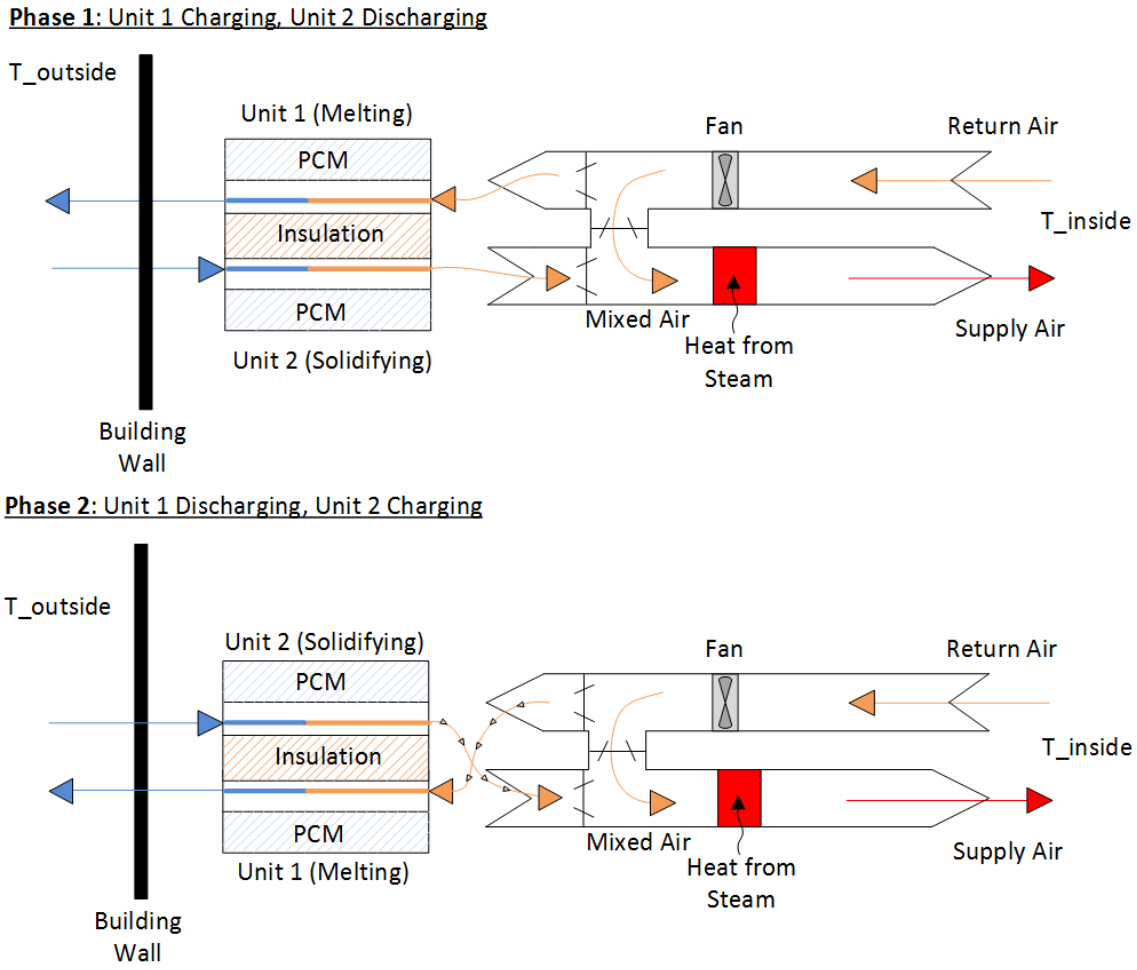

Figure 1.5 PCM Incorporation Method 3, Heat Recovery, with Air Flow Shown for Charging and Discharging of Each Unit

1.5 Objectives

The main objectives of this study is to determine the thermal and energy behavior of an integrated PCM TES system into an AHU using a laboratory scale experimental device and use the knowledge gained to create an empirical model in TRNSYS for full scale simulations of the AHU. All the sub-objectives of this study are listed as follows:

1. Analyze temperatures and flows present in a commercial building's AHU, completed previously and presented in final report to Public Services and Procurement Canada [12];

2. Design, construct and characterize an air-loop and containment area for experimental testing;
3. Design a configuration for the selected PCM including encapsulation type;
4. Analyze heat transfer rates and total energy storage in the PCM configuration;
5. Create a new TRNSYS type of the PCM configuration using a performance map of the experimental data;
6. Create TRNSYS simulations of the first method for incorporating the TES PCM into the AHU that utilizes the data from the existing commercial building and analyze the results with comparisons to simulations of the AHU without the PCM.

1.6 Contributions

The following are the contributions of this research:

1. The construction, instrumentation and programming of an air-loop to be used for the experimentation of PCM and future project;
2. Characterization of air flow and temperature through the PCM box of the air-loop
3. Characterization of PCM TES unit described using a range of values for temperature and flow rate that would be seen in an AHU;
4. The creation of an empirical model in TRNSYS which could be used to predict how various integration methods would affect the performance of the AHU in a TRNSYS simulation
5. Presented simulation results predicting how the Integration Method 1: Strategic Heating would affect the performance of the AHU

1.7 Organization of Research

The information presented in this thesis is the results of research conducted over the span of two years in the Carleton Solar Energy Systems Laboratory. This study consisted of the first

phase of a multi part research project. The overall goals of the thesis is to build an experimental heated and cooled air-loop, to experimentally characterize a PCM TES design and run preliminary simulations of a PCM TES system integrated into an AHU for a typical commercial building.

The study is presented and arranged into the following chapters:

Chapter 1 Introduction: presents a background on the subject matter of the study and outlines the research objectives;

Chapter 2 Literature Review: provides an overview of more detailed information and relevant studies that have been done in the past on this subject;

Chapter 3 Experimental Set-up and Procedure: provides a detail explanation of the experimental set-up including instrumentation positioning, design selection explanations, test procedures and control sequence programming;

Chapter 4 Experimental Set-up Characterization: presents characterization of the velocities and temperatures observed within the experimental set-up;

Chapter 5 Experimental Results: presents the experimental results and discussion of the heat transfer rates and energy study performed on the PCM TES systems;

Chapter 6 Modelling Approach: provides a description of how the PCM TES empirical model was created with the model's associated limitations and the layout of the TRNSYS simulation with and without the PCM;

Chapter 7 TRNSYS Simulation Results: presents the results of the simulations of the first PCM TES incorporation method with comparison to a base AHU;

Chapter 8 Conclusions and Future Work: summarizes the key results, presents the conclusions of the study and provides recommendations for future work.

2 Chapter: Literature Review

2.1 Introduction

Incorporating PCM for HVAC applications have been studied since Turnpenny *et al.* came up with the novel idea for space cooling with PCM in 2000 [13]. Since then, multiple studies have been performed on the subject, each with slight variations in design and application such as space cooling, space heating, ventilation or a combination. In 2013, the International Energy Agency included a chapter pertaining to the integration of PCM into central HVAC systems in their Annex 23: Energy storage in buildings of the future. The chapter focused on discussing various studies on the specified subject [14]. It was made clear from the differences between the studies that there was no single design that would function ideally for all applications pertaining to HVAC systems. Although, incorporating PCM could be successful if the design and PCM selection was customized for a desired application. For this reason studies pertaining to incorporating PCM for HVAC applications are application specific.

The following section will provide further details on PCMs and the general characterizations of PCM TES systems, a discussion of previous studies focused on incorporating PCM for HVAC applications, on PCM TES modelling, and provide some concluding remarks.

2.2 Phase Change Material in Further Details

Phase change materials were briefly discussed in Subsection 1.3 describing how PCM have the ability to store both sensible and latent heat. Sensible heat is the energy required to cause a change in temperature of a material whereas latent heat is the energy required to change the phase of a material, for instance ice into liquid water [15]. Phase change materials have a higher energy density then sensible storage materials, meaning they have the capacity to store more energy for the same quantity of material. This principle was demonstrated by Turnpenny [16] in which he

compared the energy from his PCM TES device weighing 200 kg to the energy of a passive concrete slab which would require 5 tons (4536 kg) of concrete for the same energy storage capacity [16].

This section is included to provide additional details regarding PCMs. The information should provide for a better understanding of the properties that result in the usefulness to TES systems, how PCMs are classified, and of the rate problem which strongly influences PCM TES design.

2.2.1 PCM Properties

There are several properties that are taken into consideration when choosing a PCM for a TES application. The most relevant are melting point, latent heat, thermal conductivity, stability of the material, supercooling, and safety [7].

The most important property is the melting point of the PCM. It is vital that the melting point be within the temperature range used during storage, otherwise phase change will not occur. Latent heat from the phase change is used to determine the amount of energy that can be stored for a given mass of PCM during the phase transition [7]. Energy density could also be considered an important property if space for the TES unit is a concern. Thermal conductivity gives an indication of the rate of which energy can be transferred [17]. Phase change materials are considered to have low thermal conductivity values in general which in turn suppress the heat transfer rates encountered in PCM TES devices [18]. Stability of the material is required as it would be uneconomical to replace the PCM in the storage unit regularly once installed for operation. In this context stability would mean a material that would not rust its container, would not degrade over time and would be able to endure the many thermal cycles performed over the lifetime of the unit without significant changes in its properties [7]. Supercooling is related to a delay in the release of

latent heat during solidification which occurs when a PCM must be cooled to temperatures well past the solidification point to start crystalizing [19]. This is undesirable as this lower temperature may be out of the application's operating temperature range in which case only the sensible heat would be recovered. Supercooling is more prevalent in some PCM than in others which will be further discussed in the next section. It is thus important to choose a PCM with little to no supercooling present. Safety of the PCM is a major concern if it is to be put into commercial circulation. It is crucial that the PCM be of low toxicity, low flammability risk and not react violently [7].

2.2.2 Types of PCM

There are many different materials that can be used for PCM applications. These materials are typically divided into three main categories; organic, inorganic and eutectic mixtures, which can be further divided into subcategories, see Figure 2.1 [4, 20, 21, 22]. There are several advantages and disadvantages associated with the different PCM main categories.

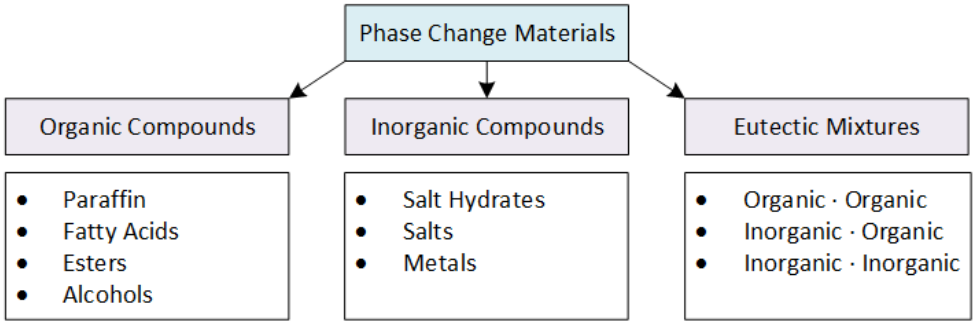

Figure 2.1 Classification of PCMs [20] [21]

Organic compounds are generally abundantly available, inexpensive and easy to work with [23]. Paraffin wax are often used as PCM for electronic thermal management due to having a melting range that varies between 35°C and 70°C depending on the hydrocarbon structures [23, 24]. Fatty acids have lower melting points than paraffin waxes making them good to use for human comfort applications [23, 25]. Both fatty acids and esters are advantageous to building material

application such as being integrated into gypsum and concrete because they are from renewable sources, are nontoxic, are biodegradable and easily recyclable [7, 25]. Some key advantages to organic compounds are that they are chemically and physically stable, they have high repeatability of performance meaning they will not break down or experience separation and they have decent latent heat values around 200-300 kJ/kg for paraffin waxes and 100-200 kJ/kg for fatty acids [23]. Organic compounds are flammable from their hydrocarbon nature however they generally have flash points around 200°C which is normally higher than the operating temperature range of the application [23]. Some container materials such as stainless steel function well with organic compounds but many materials such as aluminum, copper and brass are susceptible to corrosion from fatty acids [27]. The major disadvantage to organic compounds is low thermal conductivity ranging around 0.2 W/mK for many paraffin waxes [7, 23].

Inorganic compounds have a wide range of melting points from 40°C to just above 100°C for salt hydrates [7]. They are widely used for applications with higher melting points that are outside the organic compound range such as for solar energy applications [7, 23]. In comparison to organic materials; inorganic materials have similar latent heat values; higher thermal conductivity improving heat transfer rates; smaller density changes from liquid to solid making them easy to contain and; have generally higher overall density [4, 21, 22, 23]. Inorganic compounds can be divided into three major categories; salt hydrates, salts and metals. Salt hydrates with latent heat values around 100 to 300 kJ/kg are more commonly used but have a few key disadvantages [7]. First, they exhibit significant instabilities due to the hydrates potentially dehydrating during the heating cycle leading to breakdown of the material [23]. Second, some salts, such as calcium chloride hexahydrate-based, exhibit a high potential of sub-cooling critically affecting the heat transfer rate during cooling and making control strategies for application

challenging [28]. Finally, they are aqueous salt solutions in their molten states which makes them extremely corrosive the certain types of metal containers [7]. Metals are mainly used for high temperature applications [7, 29] however there are some metals such as Cesium and Gallium that have the potential to be used in low temperature applications [23]. Metals have some of the highest thermal conductivity, for instance Gallium having a melting temperature of 29.8°C has a thermal conductivity of 29.4 W/mK. The main disadvantages to metals is their high densities and low latent heat values [23]. There is also unfortunately still a lack in research of several key properties before these metal PCMs should be used for commercial applications [29].

Eutectic mixtures are a combination of organic and inorganic alloys. They are created to achieve improved PCM properties. As many eutectic mixtures are fabricated by corporations, there can be limited data available regarding their thermophysical properties. Some key improvements that were achieved through eutectic mixtures are a sharp melting temperature with no segregation and congruent phase-change. This allows for better control during PCM TES strategies [4, 20, 21, 22, 30].

2.2.3 The Rate Problem

The largest problem when it comes to energy storage in a PCM TES system, as previously mentioned in Subsection 1.3, is 'the rate problem' [7]. 'The rate problem' refers to challenges with heat transfer rates to and from the PCM in TES systems, and results in part from the normally low values of thermal conductivity of the PCM [7, 16, 30, 31]. This makes it challenging to obtain the energy storage required in the desired amount of time for a given application; and even more challenging to design the TES system for a specific heat transfer rates.

The theoretical amount of total energy of which a specified mass of PCM can store has been established and commonly used in previous studies [4, 7, 32, 33, 34]; it will be presented in

Chapter 3. The rate at which this energy is stored is not as simple to determine. The heat transfer rate is dependent on multiple factors such as thermal conductivity of the PCM, geometry of the encapsulation, the temperature of the HTF, the flow rate of the HTF and the initial temperature of the PCM, as well as the nature and strength of the various heat transfer processes in the PCM (conduction, natural convection), etc. [7, 14, 16, 31, 33, 34, 35]. Thus, various PCM TES applications will charge and discharge at different rates necessitating the need for characterizing the heat transfer rates of each system individually since no simple heat exchanger design rule currently exist for PCM heat exchanger. Fortunately, having so many factors influencing heat transfer provides multiple opportunities to manipulate the heat transfer rate in order to overcome 'the rate problem'. Many solutions focus on the geometry of the encapsulations such as adding fins [16, 33] and having thinner encapsulation decreasing thermal resistance of the wall [31, 36, 37] for heat transfer. Another popular solution is to vary the inlet temperature and flow rate of the HTF until desired charging times are achieved [31, 33, 37, 38].

2.3 PCM TES General Characterization

A TES system consists of a device that stores energy into a medium generally through heat transfer from a HTF. A PCM TES utilizes PCM as the energy storage medium. The design of TES systems can vary greatly through different encapsulation methods and strategies for interaction of the HTF with the storage medium. The device generally operates with a charging phase storing energy and a discharging phase dissipating the stored energy from the medium. However, there are some devices in existence that charge and discharge simultaneously [39]. This section will discuss how heat transfer occurs in PCM TES and the different PCM TES designs from previous studies.

2.3.1 Heat Transfer Modes

It is important to know how heat is transferred from the HTF to the PCM in the storage unit. Murray et al. [34] preformed a study on a cylindrical PCM storage tank demonstrating the heat transfer mechanisms during melting and solidification through observations of temperature nodes at various elevations within the tank [34]. It was found that conduction was the dominating mode of heat transfer at the start of the melting process as the nodes at different elevations read the same temperature. After a certain time, faster melting was observed at the top of the tank. This occurred because energy was displaced upward by natural convection once the PCM became liquid. It was concluded that conduction dominates the heat transfer process at the beginning of melting but changes to convection dominant after a sufficient amount of PCM becomes liquid. During solidification, the temperature remained independent from tank height until completion. This demonstrated that conduction dominates throughout the entire solidification process [34]. Multiple other studies have come to the same conclusions [31, 33, 38, 40]. Liu et al. [38] offered the explanation for conduction domination during solidification was due to solid PCM forming on the heat transfer surfaces creating an ever-increasing thermal resistance limiting the impact of natural convection in the remaining liquid PCM [38].

2.3.1 Types of PCM Encapsulation

The size, shape and wall thickness of the encapsulation in which the PCM is contained will have an effect on the overall heat transfer rate of the storage unit as discussed previously. The following are types of PCM encapsulation that have been used in previous studies specifically for applications where air was used as the HTF.

Although cylindrical encapsulation is popular with liquid HTF such as water heaters and solar collectors [33, 34, 38, 41], it is less common to see a cylindrical geometry for air-PCM

applications such as ventilation systems. Turnpenny et al. [16] used a cylindrical geometry, see Section 2.4.1 for further experimental details, however his set up was space consuming requiring the area of an entire small room [16]. Since then, air-PCM studies have focused on either geometries that are more easily integrated into ductwork such as flat plates and shell and tube; or capitalized on the low density property of air compared to liquids by filling the cylinder as a pack bed with microencapsulation or spherical encapsulation.

Arkar *et al.* [37] and Nagano *et al.* [42] are two examples of pack bed cylinders used for air-PCM applications. Arkar *et al.* [37] created an air-PCM TES by filling a cylinder (diameter = 0.34 m) with PCM encapsulated spheres (diameter 50 mm and wall thickness of 1 mm) to be placed in the ventilation system of low-energy houses. The cylinder contained 35 rows of spheres, creating a packed bed with a porosity of 0.388. The flow rate used was 50 to 200 m^3/h. The experiment was successful, changing the storage unit temperature by 0.1 K/min during charging [37, 43]. Nagano et al. [42] used microencapsulated granules which consisted of paraffin wax absorbed into granulated porous ceramics measuring between 1 to 3 mm. A TES was created by filling a cylinder (50 mm diameter) with the PCM granules and flowing air (the HTF) through the cylinder. The PCM granules TES was successful in storing energy requiring about 7 to 8 hours for complete charging or discharging of the PCM. It was observed that this method eliminated supercooling [43]. Cylindrical pack beds have been proven to work well due to the increased PCM area in contact with the HTF, however filling the spherical encapsulation or microencapsulation can be labor intensive and expensive.

Multiple studies for air-PCM shell-and-tube have been done in the past [11, 44, 45, 46, 47]. These studies focused on two main configurations. The first consists of tubes coiled inside a PCM filled cylinder with air as the HTF passing through the tubes also referred to as tube-in-tank. Tay

et al. [44] used a tube-in-tank method in a study that investigated the usefulness of this configuration storage in a cooling tower application for night time building cooling. The study demonstrated that the tube-in-tank configuration was able to store the same amount of energy as a sensible heat storage unit in a smaller volume of about 18 times [44]. The second configuration consists of multiple PCM filled tubes in a confinement in which the HTF passes through. Promoppatum et al. [11] used a crossflow shell-and tube configuration with staggered tubes in a heat recovery application in an HVAC system, see Section 2.4.3 for further experimental details. The configuration consisted of 360 PCM filled tubes places in an air duct with storage dimensions of 30 cm by 30 cm by 85 cm long. The key benefit of this configuration is that the total amount of PCM can be easily adjusted by removing or adding tubes [11].

The majority of air-PCM studies however, are performed with flat plate encapsulation due to their simplicity to work with, symmetry and ease of fabrication [14, 31, 32, 36, 48, 49, 50, 51, 52, 53]. Zelba *et al.* [36] compared the use of a shell and tubes encapsulation vs flat plate encapsulation for HVAC applications and found that the flat plate method had some key advantages. Heat transfer can be controlled with a flat plate encapsulation by varying the encapsulation thickness. The flat plate has a high area to volume ratio and there is a decrease of pressure drop in the air compared to with shell and tube [36].

2.4 Previous Studies of Air-PCM TES Incorporated into HVAC Systems

The use of air-PCM TES for incorporation into HVAC applications has been studied over the past two decades. There have been many advances over that time. A large focus of the research has gone into the design and improvement of ‘free cooling’ or the application of air-PCM TES for air conditioning. This technology has had many studies and is now well developed. The other focus is on space heating applications. There are fewer studies that have been made in this area, of which

the majority focus on strategies for time-of-use energy rates which reduce the on-peak loads by storing heat during off-peak hours. Other space heating TES PCM studies utilize solar energy to charge the PCM [50]. There has also been some new developments for PCM TES used for heat recovery applications in the ventilation system [11].

2.4.1 Free Cooling

Free cooling refers to the storage of latent heat taken from air either entering or circulating through a building during the day when the temperature is warm and then released into the cool night air. The result will provide a certain amount of cooling for the building during the day. Free cooling provides an economical solution to keep temperatures at a livable level throughout the summer months. There have been multiple studies performed for free cooling in the past [13, 16, 31, 36, 37, 48, 51, 54, 55, 56] [57, 58]. The following are three examples of free cooling studies.

Turnpenny *et al.* [16] is the first to experiment with the free cooling concept while using PCMs as the storage medium. Previously, free cooling had only existed in application by storing sensible heat exclusively in high density materials such as concrete [16]. Turnpenny *et al.* [16] had a set-up that consisted of ten heat pipes embedded part way into ten cylinders filled with PCM, positioned in a circular configuration with the exposed heat pipe ends in the center of a room within close proximity to a ceiling fan with a span of 1200 mm. The PCM used was salt hydrate $Na_2SO_4 10H_2O$ with 1.5% added borax nucleating agent [13]. In addition, there were three vents leading outside. One vent was positioned near the ceiling fan and the other two were positioned near the floor. At night, all vents would be open and the cool night air would be directed by the fan to pass over the heat pipes which released the stored energy from the PCM extracted from the air during the day, and exit from the floor vents [16]. Turnpenny *et al.* [16] successfully

demonstrated the use of PCM with free cooling methods to prevent a room from overheating during average UK summer conditions [16].

Weinläder *et al.* [55] implemented free cooling into a ventilated cooling ceiling application [55]. This application was tested for average size rooms such as a conference room in an office building. The configuration consists of placing one layer of plate encapsulated PCM for 56% of the ceiling area leaving a gap for air to pass between the PCM layer and the ceiling. The PCM used was DELTA-COOL 24 with a total mass of 180 kg. There was a supply and an exhaust vent at either side of the room within the gap. These vents move outdoor air within the gap to charge the PCM at night and are closed during the day as the room air circulates through the gap. The system was monitored over a long-term program resulting in significant cooling potential over the course of the summer [55].

Monodraught has made PCM free cooling commercially available with their low energy cooling and ventilation system known as Cool-Phase [54]. This device is composed of a flat plate encapsulation design. The system is designed for installation for large room applications. The configuration consists of a duct leading to the outside providing fresh air into the Cool-Phase device with a fan. The air can then be cooled by what is referred to as “thermal batteries” which refers to the PCM. The system is fully automated, monitoring the CO_2 levels within the room for adequate ventilation as well as the outdoor and room temperatures for efficient operation. There are four modes of operation. At nighttime, the PCM will release its stored heat to the incoming fresh air. During the day, the fresh air will either be vented directly into the room if the temperature outside is lower than the indoor temperature, be passed over the PCM before entering the room if the temperature outside is lower but cannot meet cooling load, or the indoor air will be recirculated

over the PCM with the minimal fresh air required for ventilation if the outdoor temperature is warmer than the indoor temperature [54].

PCM free cooling has been proven to be viable for cooling, however, when compared to other cooling devices such as air conditioners they are not as reliable as there can be instability in the system. Free cooling is greatly dependent on the outdoor air temperature. If the temperature is not within a certain range, the PCM will not completely solidify which will shorten the melting period as discovered by Arkar *et al.* [37]. If the melting period is shortened, cooling will not last the desired time-period and the indoor temperature has the opportunity to rise above comfort levels.

2.4.2 Time-of-Use Heating

The application used for latent heat thermal energy storage (LHTES) for heating has been limited to experiments demonstrating phase change materials storage potential for the reduction of peak power consumption. Time-of-use pricing was implemented in several countries in an attempt to reduce peak power demands. It does so by increasing the price of electricity during the hours of highest demand and provides a discounted price during hours of low demand. PCM storage can be used to shift the cost of electrical heating by storing energy during off-peak hours to be used for heating during on-peak hours.

Stathopoulos et al. [59] experimented with placing PCM storage with a flat plate design directly into a section of the ventilation system. The design consisted of seventeen 18 mm thick aluminum plates positioned vertically with fins between the gaps. The entire heat exchanger including insulation had dimensions of 1.05 by 0.8 by 0.25 m. The PCM used was Microtek 37 paraffin with a melting temperature of 37°C and latent heat of 227 kJ/kg. Two fans forced air to flow through two electrical resistances producing heat after which the air would flow through the

section of ducting containing the PCM storage before entering the room [14, 59]. During the off-peak hours the electrical heaters would provide enough heat to both charge the PCM TES and to heat the space to a comfortable level. During on-peak hours, the electric heater would turn off and the stored heat in the PCM will be used to heat the space. The experiment was successful in sustaining comfort levels during on-peak hours [14, 59].

Lin et al. [38] experimented with placing the PCM in a floor based heating system. The PCM used was paraffin with a melting temperature of 52°C and a latent heat of 200 kJ/kg. The floor layering consisted of insulation, an electric heater, PCM, an air gap with supports and a floor covering. Imbedded within the floor coverings were an inlet and outlet fan used to circulate air under the floor for heating. The electric heaters would be turned on between the hours of 23:00 to 7:00 to heat the PCM and the floor. At 9:00 until 16:00 the fans would circulate the indoor air through the PCM which would release its stored energy warming the air to heat the space [60]. The experiment was successful in shifting electrical usage to the off-peak hours while maintaining comfort levels [60].

2.4.3 Heat Recovery

Heat recovery by definition is the transfer of energy between an outgoing airstream to an incoming airstream [61]. There are two main mechanisms used to achieve heat recovery; the heat recovery wheel also known as the desiccant wheel and the heat exchanger also known as the heat recovery ventilator. Both devices are currently being implemented into AHUs for energy efficiency improvement [62, 63].

The heat recovery wheel is a device used for heat recovery which may utilize both sensible and latent energy. Physically it consists of a wheel that is separated into sections to divide the incoming and outgoing air. Sensible heat is transferred through the separation walls that divide the

two airstreams as well as from a small amount of air that remains from the other airstream due to the motion of the wheel [61]. Heat recovery wheels transfer latent heat by use of a desiccant. In this instance, the moisture in the air is considered the PCM, however, there is no actual PCM stored within this device. The desiccant simply absorbs water vapour from one airstream and releases it into another [61].

The heat exchangers commercially available that are used for heat recovery utilize sensible heat. The airstreams from both the exhaust and intake pass through a core where heat is exchanged generally through a thin wall [64, 65]. This design exchanges heat from one stream to the other directly and does not need to be stored. There is the possibility that storing the heat in PCM before transferring it could be more effective. There is a cross-section shell-and-tube PCM heat exchanger newly developed by Promoppatum *et al*. [11] that applies this new method [11]. This design is similar to the one proposed in Chapter 1 in that it is composed of two heat exchangers that alternate between charging and discharging based on a control strategy. This paper focused heavily on numerical modelling of the system and optimization of design. It lacked the presentation of heat transfer rates and a demonstration of the successful implementation of the design for the application [11].

2.5 Modelling of PCM

Testing a LHTES system in full can become quite large and expensive. For this reason many LHTES application designs have been proven with a combination of both experimental testing and computerized modelling. Usually, the experimental tests are performed on the specific PCM storage system to determine its properties during the phase change process and the results are imported into the model of the application to determine successfulness of the proposed design. Arkar *et al.* [37] utilized this method to investigate free cooling in heavy and light weight low

energy buildings. The design consisted of two spherical encapsulated PCM storage units strategically placed within a mechanical ventilation system [37]. Arkar *et al.* [37] created a numerical model of a function in the form of a Fourier series based off experimental data obtained that was used to predict the temperature outlet of the PCM storage. The temperatures obtained were inputted into a TRNSYS model simulating various scenarios for the building ventilation design [37]. Lin *et al.* [60] also created a model based on his experimental results and succeeded in optimizing the design for different environmental conditions [60]. Dolado *et al.* [49] developed an empirical model from experimental results of a real-scale air PCM TES with a flat plate design for free cooling application to be able to successfully characterize melting and solidification of the PCM [49].

2.6 Conclusions

The literature review reveals that the understanding of PCM is well developed. There is a good classification system of the different types of materials and their properties are defined. The 'rate problem' has been identified as an obstacle to overcome when dealing with PCM for TES applications. PCM TES has been extensively studied. There is a good grasp for which modes of heat transfer are present during the melting and solidification cycles. Many strategies and encapsulation designs have been studied. These studies have demonstrated that multiple designs can be successful at storing energy. The most researched air PCM TES incorporation into the HVAC system was 'free cooling' for air conditioning applications and peak shaving/saving for space heating applications. The literature is lacking in HVAC applications on the commercial scale with studies either focused on houses or on one large room within a building. As large AHUs are primarily used for commercial buildings, there were no studies that were found which integrated the PCM TES for AHU applications.

3 Chapter: Experimental Set-up and Procedure

An experimental set-up was constructed, instrumented and commissioned in order to evaluate the behavior of a scaled air-PCM storage unit under controlled laboratory conditions with the desire to implement the design in a full-scale prototype TRNSYS simulation. The experimental set-up is composed of two components, the air-loop and the PCM box. A schematic outlining the placement of the equipment and instrumentation can be seen in Figure 3.1. A labeled image of the experimental set-up can be seen in Figure 3.2. Note that the air-loop was suspended by cables anchored to the ceiling of the laboratory whereas the PCM box rested on the laboratory floor.

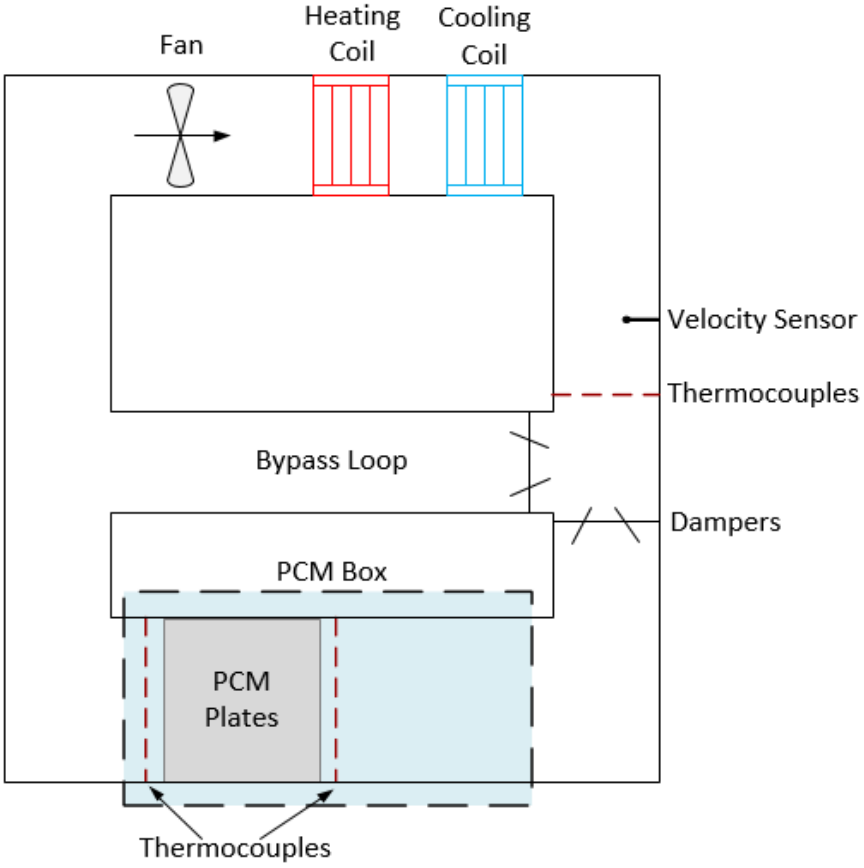

Figure 3.1 Schematic of Experimental Set-Up

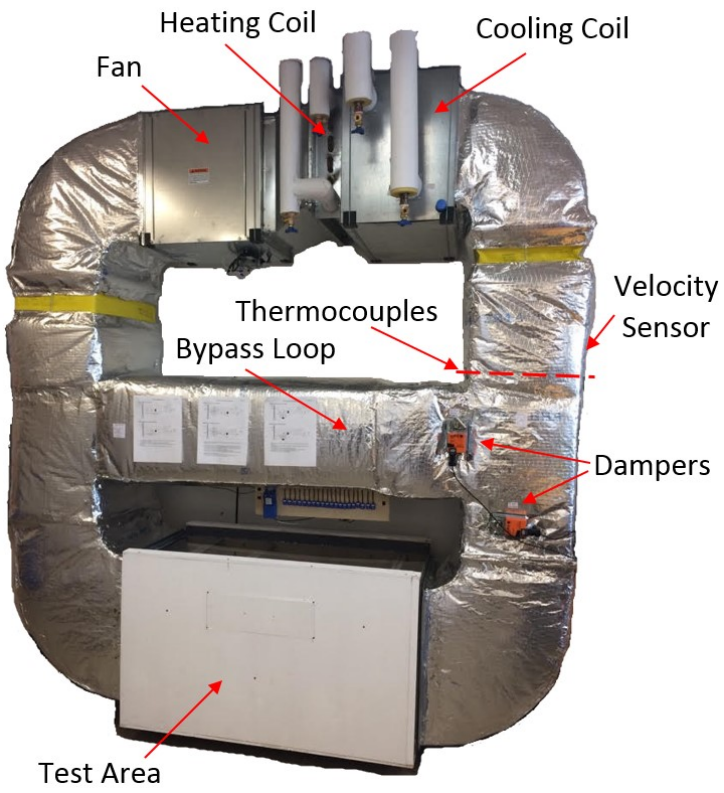

Figure 3.2 Labeled Image of Experimental Equipment

3.1 Air-loop Design

The air-loop was designed and built to condition air to temperatures and flow rates that would be encountered should a storage unit be integrated into a commercial building's AHU. The air is conditioned using three pieces of equipment; a centrifugal inline fan, a heating coil and a cooling coil placed in that order. The air flow through the loop is generated by a GREENHECK SQ-130HP-VG direct drive centrifugal inline fan as shown in Figure 3.3 a). The air flow generated by the fan is unidirectional moving the air in the direction of the heating and cooling coils. The fan was rated at 890 CFM (1512 m^3/h) for a static pressure of 1.2 in. water. A GREENHECK HW58S01A09-15x28-RH hot water coil with a capacity of 9.4 kW was used to heat the incoming air, see Figure 3.3 b). A GREENHECK CW58S06S12-15x24-RH chilled water thermacoil with a capacity of 10.7 kW was used to cool the incoming air, see Figure 3.3 c). The coils used water as

their HTF drawn from the water mains of the building where the experimental set-up was located on the Carleton University Campus. The air temperature range achievable in the air-loop was directly dependent on the temperature of the water resulting in a maximum and minimum air temperature of 85˚C and 18˚C respectively. The water flow to the cooling coil was controlled by a BELIMO LF24-SR actuator and the water flow to the heating coil was controlled by a BELIMO TFB24-SR actuator. Both actuators and the fan were controlled by PID controllers requiring feedback for the temperature sensors within the duct, see Table 3-1 for PID values.

Table 3-1 Proportional (P), Integral (I), Derivative (D) Values for Control of the Fan and Both Actuators for the Conditioning Coils

Equipment	Proportional (P)	Integral (I)	Derivative (D)
Fan	0.004	0.001	0.000
Cooling Actuator	0.010	1.000	0.000
Heating Actuator	1.000	0.040	9.000

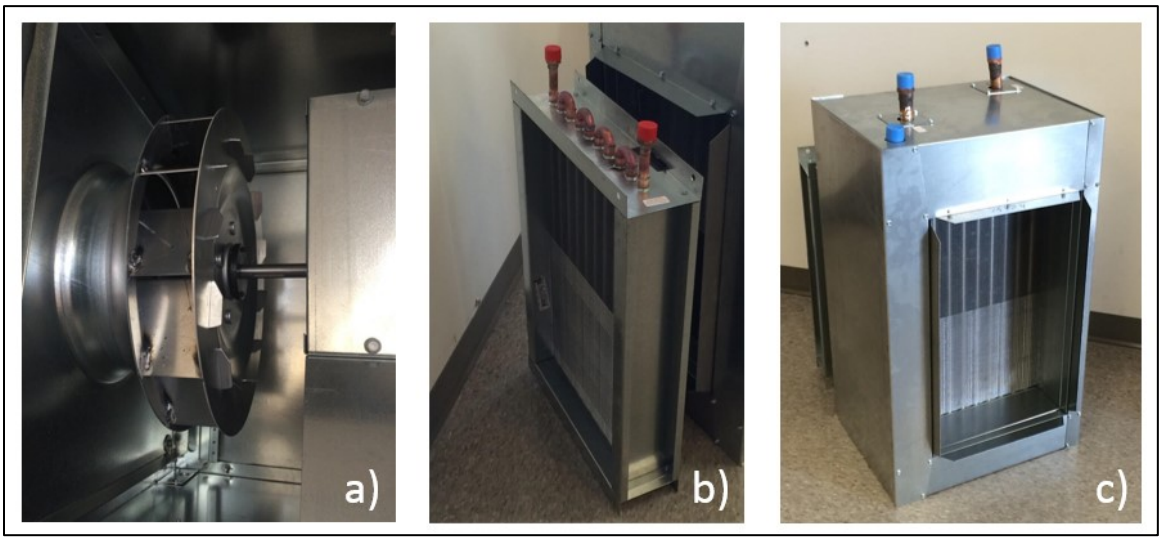

Figure 3.3 a) GREENHECK SQ-130HP-VG Direct Drive Centrifugal Inline Fan, b) GREENHECK HW58S01A09-15x28-RH Hot Water Coil, c) GREENHECK CW58S06S12-15x24-RH Chilled Water Thermicoil

Two dampers controlled by BELIMO LMB24-3 actuators were used in the air-loop to control the path of the flow. One damper was positioned at the entrance to the bypass loop and the

other in the path of the PCM box. The actuators were programmed to have one damper completely open while the other was completely closed. This ensured that all the air flow would either enter the bypass loop or the PCM box. The bypass loop had the purpose of circulating the air until a desired air temperature was obtained. Once achieved, the dampers would activate, allowing the air to enter the PCM box. The bypass loop was important to obtain desired inlet temperatures when switching from charging to discharging and vice-versa.

The duct work has dimensions of 0.381 m (15 in.) by 0.6096 m (24 in.) throughout the majority of the air-loop and varying dimensions in the elbows to the fan and the PCM box. The size of the air-loop was chosen to accommodate the desired flow rate and to integrate properly with the required dimensions of the PCM box. Turning vanes were also added to the elbows duct before and after the PCM box in an attempt to improve flow development through the box.

3.2 PCM BOX DESIGN

The PCM box was designed and built to contain the PCM during testing. The following section will provide details of the PCM box's design.

3.2.1 PCM Encapsulation

Several encapsulation methods were considered for this study. The first consideration was whether to use macroencapsulation or microencapsulation. Macroencapsulation was chosen as it was considered sufficient for the needs of the study and microencapsulation has increased complexity that would consume both time and money. A flat plate encapsulation method was chosen for this experiment. There are a couple reasons for which this encapsulation method was selected. First, flat plates are commonly used in previous PCM applications [14, 31, 32, 36, 48, 49, 50, 51]. These past experiments have been successful in demonstrating PCMs storage ability to improve systems indicating the flat plate is a successful encapsulation method. Second, the flat

plates are easy and cost effective to implement. The focus of this thesis is to demonstrate how PCM could improve AHUs and not to optimize the storage capacity. That would be recommended for future work.

The PCM was encapsulated using the Rubitherm flat plate aluminum cases, see Figure 3.4. The aluminum case has dimensions of 450 mm x 300 mm x 10 mm.

Figure 3.4 Rubitherm PCM Encapsulated Aluminum Case

The Rubitherm PCM encapsulation aluminum case was selected for several reasons. First, the plates are prefabricated and filled with the selected PCM by Rubitherm. The PCM was immediately ready for testing as soon as it arrived in the laboratory. Second, using prefabricated plates took advantage of Rubitherm's expertise. Rubitherm has already experimented and determined the optimal amount with which to fill the plates: filling it with too little PCM and storage capacity would be lost, with possibly lower energy transfer rates but too much and the plates could break and leak during the expansion that accompanies phase change. This exact problem happened to Lazaro *et al.* [31] before changing to the Rubitherm plates concluding that a better designed plate was better to have than a PCM with improved specifications [31]. Third, multiple successful experiments have been completed in the past that have used these plates in their studies [31, 55]. This demonstrates that the plates are a successful design for PCM energy

storage. Finally, using a commercially available plate would make any future prototypes more easily transferable to an economical scale.

3.2.2 Box Configuration

Figure 3.5 shows various views of the PCM box with PCM configuration. This 3D model was created by using Google Sketch up during the design phase. The model's main purpose was to ensure that the dimensions of each component would fit properly during the construction phase.

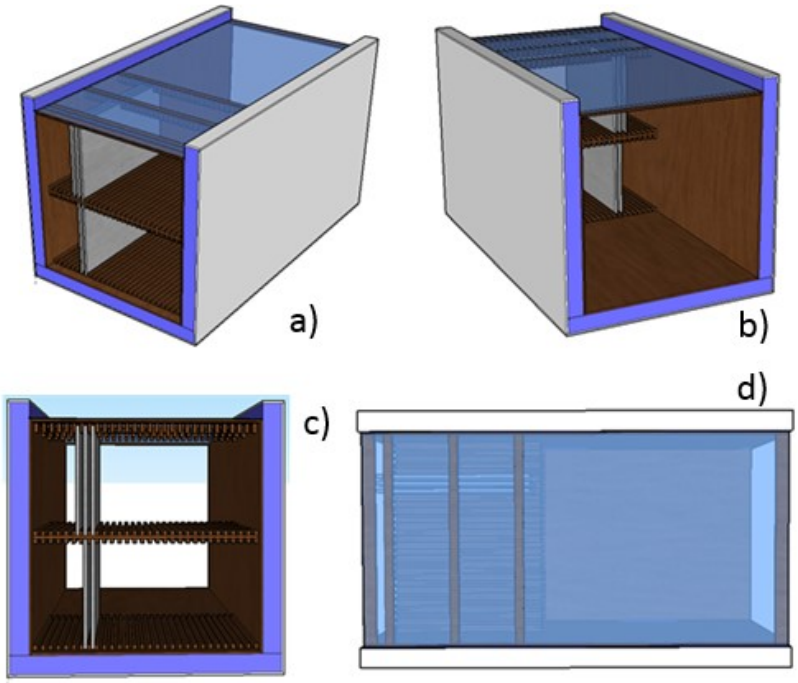

Figure 3.5 Images of PCM Box done in Google Sketch up before Construction. a) and b) Images Showing Opposite Sides, c) End View d) Top View

An end view of the PCM box with material labels can be seen in Figure 3.6. The PCM box outer surfaces were insulated using a 2 in. thick layer of insulation (RSI 1.4) to minimize heat loss from the box. An inner and outer layer of ½ in. plywood was used to encase the insulation on three sides. A sheet of Plexiglass, located at the top of the PCM box was inserted to allow for visual observation of the box interior during testing. When not under observation, the Plexiglass was covered by a layer of insulation.

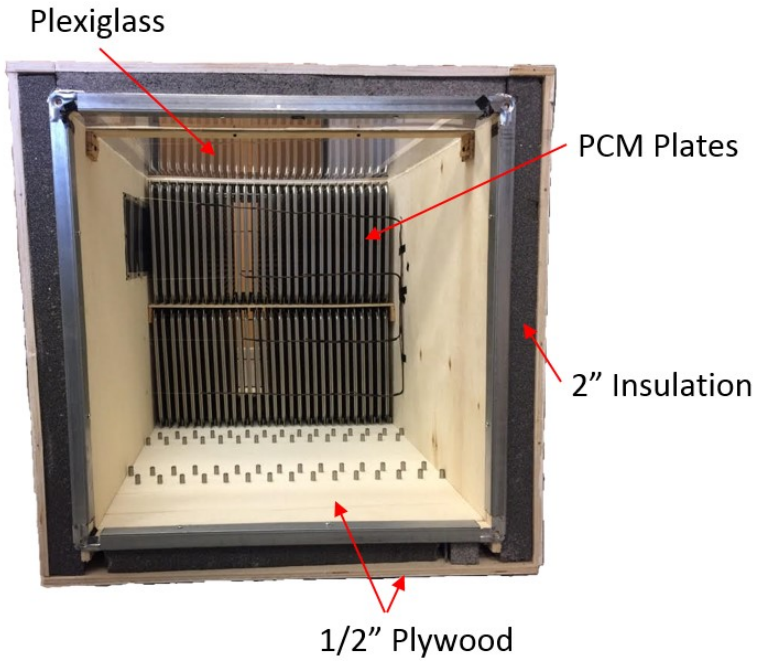

Figure 3.6 Picture of the Interior Cross Sectional View of the PCM Box with Construction Materials Outlined

The plates are stacked in two rows at the end of the PCM box furthest from the air flow entrance. This was done in an attempt to give the incoming air space for the flow to become fully developed after the elbow. Each row contains 29 PCM filled plates with a 0.011 m air channel between each plate, for a total of 58 plates.

There were several iterations of how the plates would be held in place. The requirements were as follows:

- The plates need to be able to slide into position for easy removal and insertion.
- The holder needed to be strong enough to hold the plates both vertically and horizontally. In order to test various orientations, the box would be flipped on its side, however this would only be done in future studies.
- The holder needed to let the air flow pass over the plates unimpeded
- Would like to be able to see the plates were the Plexiglas was located

These requirements were implemented so that the box configuration could be versatile and various configurations could be achieved in future studies. The plates sit in between the base plate at the bottom of the box, the middle plate in between the two rows of PCM and the top bars in between the PCM plates and the Plexiglas. The first iteration consisted of nailing 1 in. height 10 mm wide pieces of wood to the base plate, on both sides of the middle plate and to the top bars. This iteration can be seen in the 3D model in Figure 3.5. However, after some consideration it was realized that the wood was too thin and would split. The next iteration was to have the base plate, middle plate and top bars be made of thicker wood in which grooves could be cut using CNC machining and an AutoCAD model. Unfortunately, the price for the thicker wood pieces was outside the available budget. The final iteration was to use ¾ in. metal dowels. The dowels were positioned two in between each PCM plate on the base plate, middle plate and top bars. The dowels in the middle plate were centered through the plate in order to hold both rows of PCM plates. It can be noted from Figure 3.6 that the dowels on the base plate extend to the first half of the box. This was done so that another column of PCM plates could be added if desired. The PCM box fully constructed can be seen in Figure 3.7. Additional details regarding the construction of the PCM box were included in Appendix A.

Figure 3.7 Fully Constructed PCM Box

3.3 PCM Selection

The PCM was selected based on its properties, specifically trying to obtain the highest heat storage capacity as possible, and on the melting temperature that would meet the requirements for integration into an AHU. For this application, the return temperature and the supply temperature could be used as the charging temperature. However, in some strategies, such as time-of-use shaving, an auxiliary heater could be used to elevate the charging temperature. The temperature used during discharging would be provided by the outdoor winter air being taken in by the intake of the AHU. This temperature would thus be dependent on the weather.

The main purpose of integrating a PCM TES into the AHU is to preheat this frigid outdoor air during the discharge cycles. These temperatures would be considered below zero. As previously indicated, the air-loop equipment had a minimum temperature of 18°C. Fortunately, heat transfer within the system is not dependent on the inlet and outlet temperatures specifically but rather on the temperature difference between the air stream and the PCM, with the PCM melting temperature playing a major role in this temperature difference. Thus, to simulate the desired negative temperatures, the experiments focused on obtaining the temperature differences by using higher temperatures within the range of the equipment.

This decision also allows for multiple strategies with various melting temperatures to be analyzed with one PCM selection. This concept is demonstrated in Figure 3.8 for an experimental PCM with a melting temperature of 44 ˚C and an application PCM with a melting temperature of 18°C. The return temperature of 19°C would correlate to 45°C and the minimum application temperature possible would be -8°C corresponding to the experimental minimum temperature of 18˚C. A PCM melting temperature of 44°C was chosen as it was demonstrated to achieve the desired corresponding maximum and minimum application temperatures.

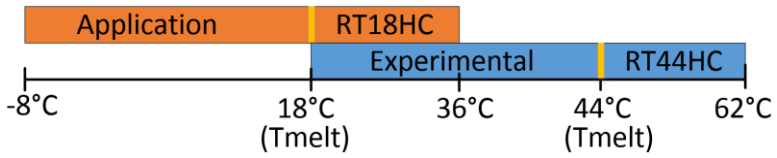

Figure 3.8 Temperature Conversion from Experimental to Application, where the Yellow Line Represents the Melting Temperature of the PCMs.

In order for the test strategy to succeed, the properties of the PCM chosen for testing must be similar to the properties of other PCMs that have melting temperatures that would function in real world implementation. For these reasons, RT44HC was selected. RT44HC is an organic material (paraffin wax) with similar heat storage capacity, specific heat capacity, density, and volume expansion and heat conductivity as RT18HC, RT11HC and RT5HC, see Appendix B for properties. This PCM also has a considerably high heat storage capacity. The properties of RT44HC are listed in Table 3-2 [66].

Table 3-2 Properties of RT44HC [66]

Property	Value
Melting area	41-44°C
Solidification area	44-40°C
Heat storage capacity with temperature range of 35°C to 50°C	250 kJ/kg
Latent heat of fusion*	220 kJ/kg
Specific heat capacity	2 kJ/kg K
Density solid	0.8 kg/l
Density liquid	0.7 kg/l
Heat conductivity	0.2 W/m-K
Volume expansion	12.5 %

*Latent heat of fusion was calculated in Section 4.2.1, see Eq. (4.5).

3.4 Instrumentation

In the experimental set-up, four parameters could be measured and recorded through various sensors. Those parameters are; temperature, velocity, pressure and relative humidity. All the instruments and the equipment were controlled with LabVIEW through the data acquisition

device (DAQ) model number NI cDAQ-9188. The DAQ with the signal cards inserted can be seen in Figure 3.9. The wiring diagram of the set-up can be seen in Appendix C.

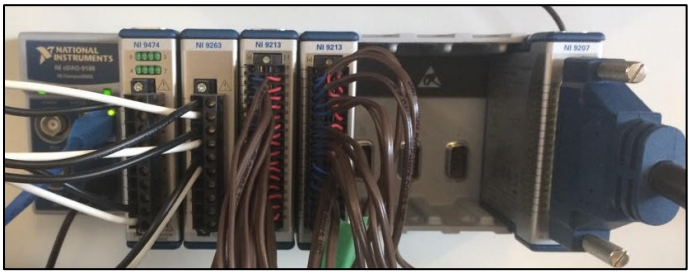

Figure 3.9 Data Acquisition with Signal Cards

3.4.1 Temperature

The temperature was measured with Type T calibrated thermocouples with an uncertainty of ±0.88˚C. Further details are available in Appendix D for thermocouple calibration, Appendix E for temperature measurement error and Appendix F for dynamic response time. Temperature measurements were taken in the air-loop and the PCM box.

The location of thermocouples within the air-loop is shown in the experimental set-up schematic seen in Figure 3.1 to be just above the bypass loop. There were five thermocouples positioned to form an X pattern as seen in Figure 3.10 across the area of the duct. The measurements from these thermocouples were averaged to determine a single temperature for the conditioned air. The location was chosen as it was at the end of a straight section of duct to allow for flow development but before the flow was directed by the dampers.

The conditioned air temperature measurement was used by the LabVIEW program to control the air temperature within the loop. The heating and cooling coils have an automated actuator which regulate the water flow rate to the coils as previously discussed. The signal to the valves is provided by PID controllers within LabVIEW which compares the temperature setpoint to the average temperature measurement.

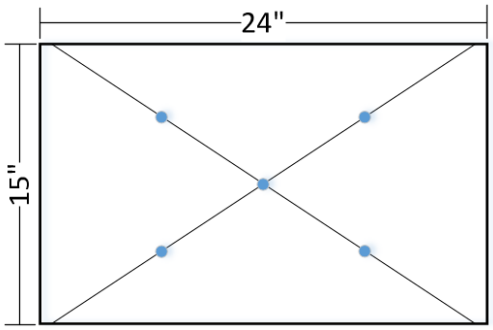

Figure 3.10 Thermocouple Position within Duct. Location shown in Figure 3.1

The thermocouples within the PCM box were located in two 2D planes at the inlet and outlet of the PCM plates. Each location had eight thermocouples for a total of sixteen thermocouples in the PCM box. Both inlet and outlet thermocouples had the same configuration as seen in Figure 3.10 andFigure **3.11**. This particular configuration was chosen to obtain an even distribution of temperature measurements so that both the perimeter and the interior values were taken into consideration. Note that the thermocouples were held in place by electrical tape to fishing lines that were tied to screws on both side of the box. These temperature measurements were recorded during testing and used to determine heat transfer across the PCM plates.

Figure 3.11 Temperature Measurement Positions at oth the Inlet and Outlet of the PCM Storage Area

3.4.2 Velocity

A Cambridge Accusense F900 series air velocity sensor as seen in Figure 3.12 was used to measure velocity. The velocity sensor had a range of 0.15 m/s to 5 m/s. The velocity measurement had an uncertainty of ±6.5% of the readings for values above 1 m/s. Further details regarding the velocity measurement error are in Appendix G. The velocity sensor was positioned just above the thermocouples in the air-loop seen in Figure 3.1 as that location offered the greatest potential for flow development before entering the PCM box. The LabVIEW program used the velocity measurement to send feedback to a PID controller used to control the output signal of the fan to maintain the velocity setpoint. The velocity sensor was additionally used to determine the velocity profile within the PCM box, see section 4.1.

Figure 3.12 Cambridge Accusense F900 Series Air Velocity Sensor

3.4.3 Other Measurements

The pressure difference across the PCM plates and the relative humidity within the air-loop were measured for monitoring purposes. An Ashcroft model number CXLdp, seen in Figure 3.13 a), with a range of 1 inH_2O was installed placing the tubing along the back side of the PCM box wall on either side of the PCM plates. The relative humidity transmitter was an OMEGA model number HX92BV2 with a range of 0 to 100% relative humidity, seen in Figure 3.13 b). The sensor was placed in the duct across from the bypass loop just below the thermocouples in X formation.

a) 

b) 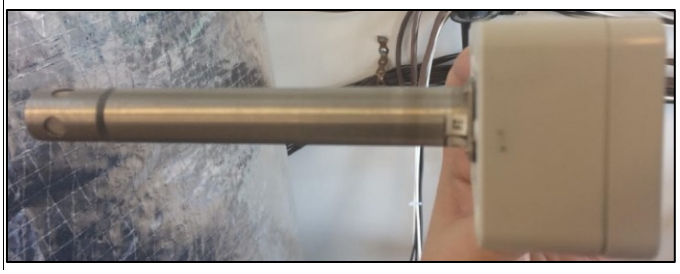

Figure 3.13 a) Ashcroft CXLdp Differential Pressure Sensor, b) OMEGA HX92BV2 Relative Humidity Transmitter

3.5 Full Cycle Test Procedure

The experimental procedure used for characterizing the PCM-TES system was referred to as the full cycle test procedure. A flow chart of the control sequence used by the LabVIEW program of the full cycle test procedure can be seen in Figure 3.14. This test was composed of three phases. The first phase known as the initializing temperature phase, shown in yellow, would heat or cool the PCM plates to the desired initial temperature. The initial temperature of the PCM would have an effect on the sensible heat component of the total storage capacity thus, it was important to set the initial temperature of the PCM plates at the start of the test. The second phase was the charging cycle. This phase would ensure a constant heating setpoint until the inlet and outlet temperatures reached the same value indicating that the PCM was fully charged.

The final phase was the discharging cycle. Similar to the charging cycle, this phase would ensure a constant cooling setpoint until the inlet and outlet temperatures reached the same value indicating that the PCM was completely discharged. The data from the full cycle test was recorded every minute which was exported to an excel file at the end of the test.

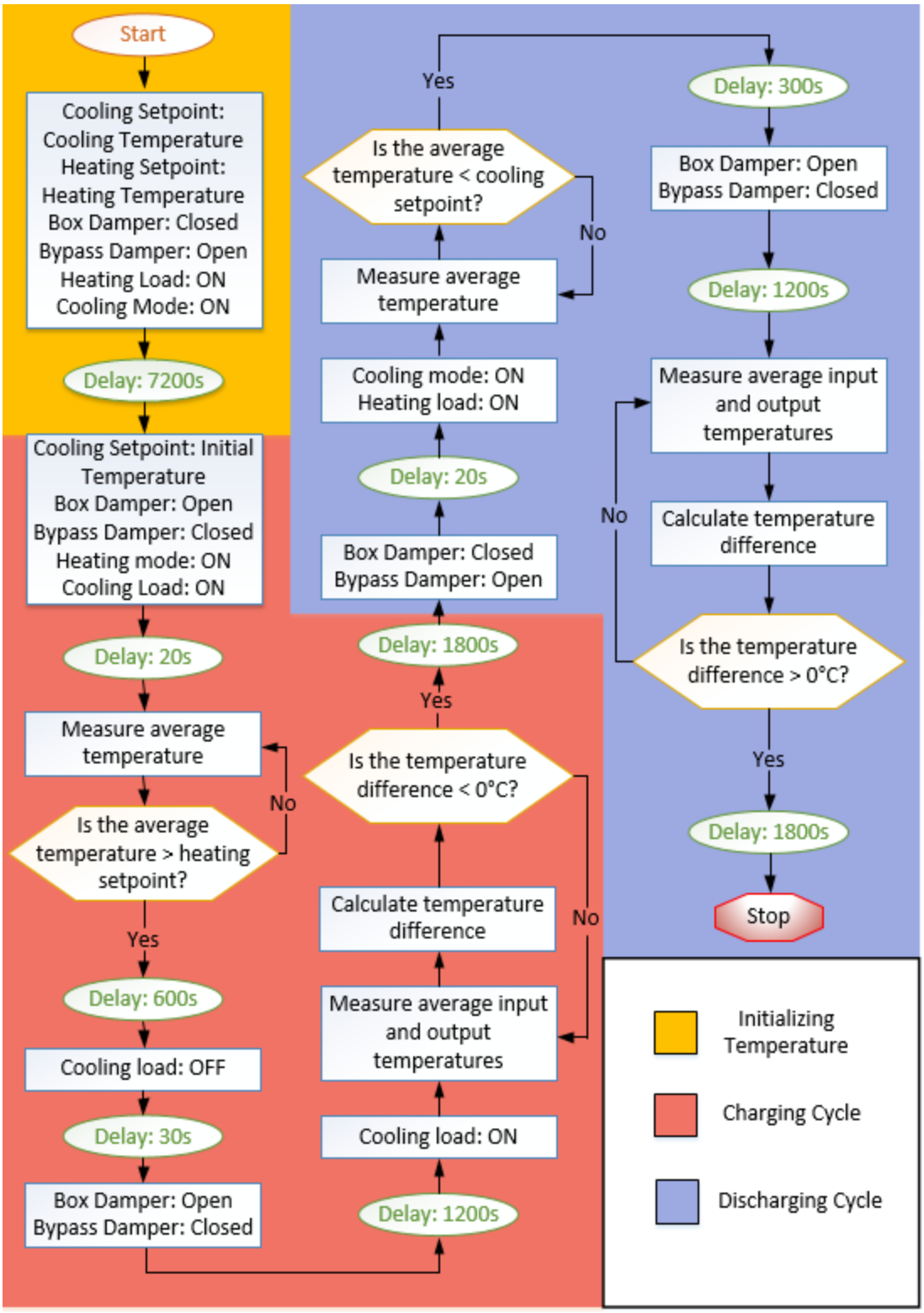

Figure 3.14 Flow Chart of Full Cycle Test LabVIEW Control Procedure

3.6 LabVIEW Control Panel

As previously discussed, a control program was written in LabVIEW for the full cycle test procedure. Figure 3.15 and Figure 3.16 show the front panel designed for the operation and monitoring of the test. The front panel was divided into four sections; controls, inlet temperature sensors, outlet temperature sensors and analysis.

The controls panel was used to set the desired parameters of the test (Figure 3.15). This included initial temperature, cooling temperature, heating temperature and flow rate. This section monitored the damper positions, heating or cooling mode, velocity in the duct and in the PCM box, the five in duct thermocouple temperatures with their mean, the pressure difference across the plates, the relative humidity, the heat load, the cool load and the flow rate. The graph was used to monitor changes in temperature over time.

The inlet and outlet temperature sensors sections were used to monitor the temperature from the 16 thermocouples in the PCM box (Figure 3.16). The blue boxes show the sensors configuration matching Figure 3.11. These boxes are also programmed to change colour to red at temperature above the melting temperature of 44˚C. The image shows the orientation of the sensors in the PCM box. The graphs at the bottom of the panel section once again allow for the monitoring of changes in temperature over time.

The analysis section was included to provide a preview of the results as the experiment progressed, Figure 3.16. The top graph in the section allows for comparing the average inlet and outlet temperature and temperature difference over time. The bottom graph shows changes in instantaneous heat transfer over time. Monitoring the results during the experiment provided feedback as to whether problems were occurring during operation and aided greatly with troubleshooting solutions or improvements.

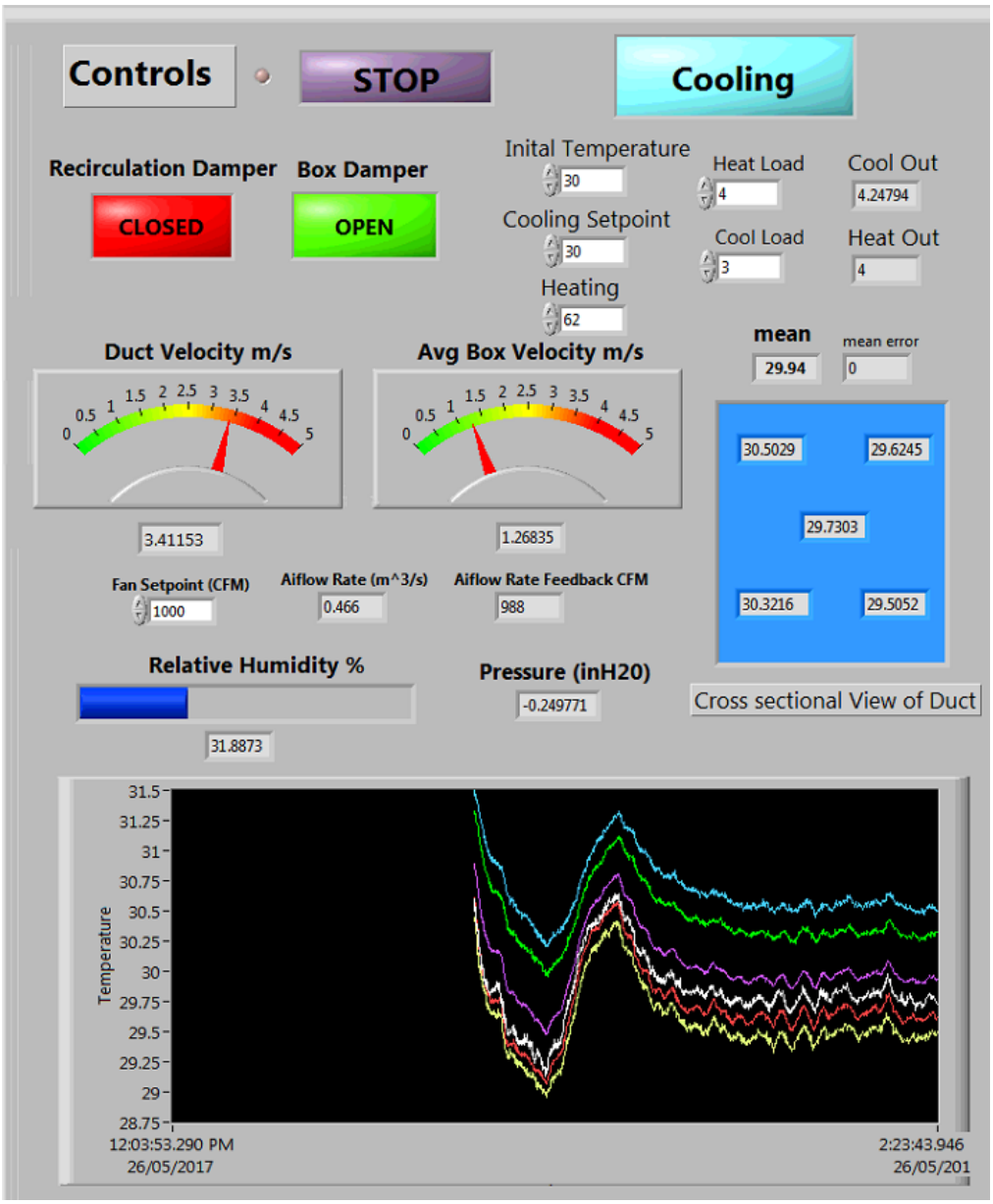

Figure 3.15 LabVIEW Front Panel Controls Section

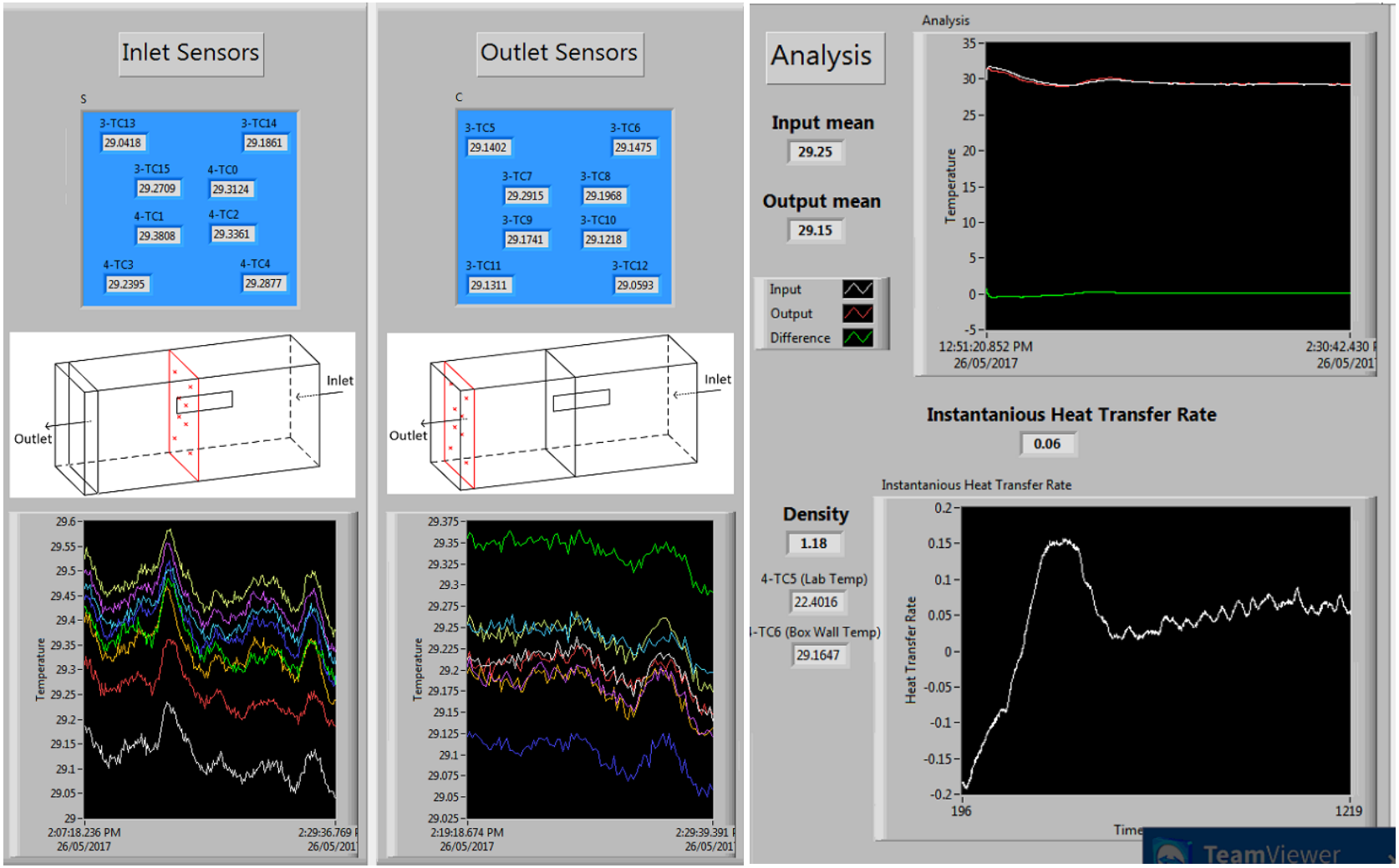

Figure 3.16 LabVIEW Front Panel Inlet Sensors, Outlet Sensors and Analysis Section

This chapter provided an overview of the experimental setup. This included the equipment and sensor placement within the air-loop, the TES geometry, the chosen PCM for experimentation, the PCM characterization procedure and the LabVIEW control program. The following chapter will describe the characterization of experimental tests performed in the air-loop.

4 Chapter: Experimental Set-up Characterization

This section will present and discuss the characterization of the experimental set-up. The characterization focused primarily on the velocity and temperature profiles occurring within the PCM box at the inlet of the PCM plates.

4.1 Velocity Profile

The velocity profile was determined at the inlet of the PCM plates in order to obtain a better understanding of how the air was entering the PCM storage area and interacting with the PCM plates. Any discrepancy in flow could result in faster or slower heat transfer rates in certain areas of the storage unit. The results from the velocity profile were also used in the LabVIEW programming.

4.1.1 Velocity Profile Test Procedure

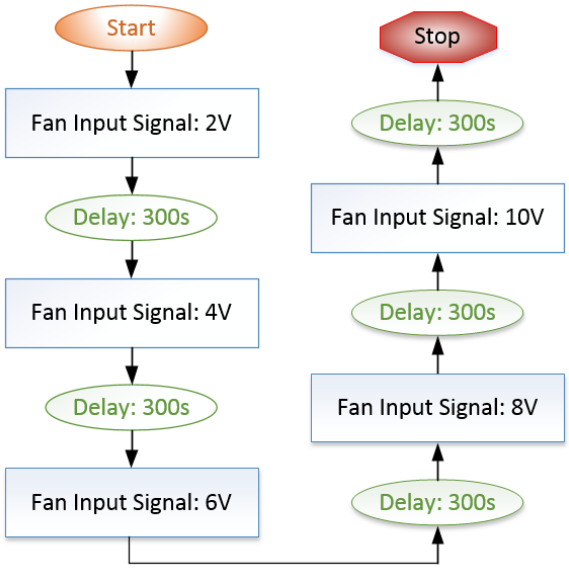

Figure 4.1 Flow Chart of Velocity Profile Test Procedure

The velocity profile test procedure was used during all testing of the velocity profile. A flow chart for this test procedure is shown in Figure 4.1. The procedure consisted of sending an initial 2 V signal to the fan's input for 300 s and then increasing the signal by 2 V increments each

subsequent 300 s until the maximum signal input of the fan, 10 V, was attained. The velocity would be recorded every 3 s for 100 readings per interval.

4.1.2 First Configuration

In order to determine the velocity profile within the PCM box, the Cambridge Accusense F900 series air velocity sensor was positioned in 8 different locations in a 2D plane 5 in. away from the inlet of the PCM plates. Due to the wall-mounting constraint of the velocity sensor, the velocity could only be measured along the perimeter. The measurement positions are shown in Figure 4.2.

Figure 4.2 Velocity Sensor Locations of First Velocity Profile Configuration

Only one velocity sensor was available for this study. Thus at each location, a separate test was performed before moving the velocity sensor to a new location. Each test followed the velocity profile test procedure, enabling the results to be treated as if they had come from one test with multiple sensors. The velocity profile test was also performed with the velocity sensor in its duct location, see Figure 3.1. The correlation between the monitored velocities inside the duct to the velocity within the box is important since it allows for the determination of the velocity within

the box during a full cycle test based on the only measured velocity during those tests; the velocity measured in the duct.

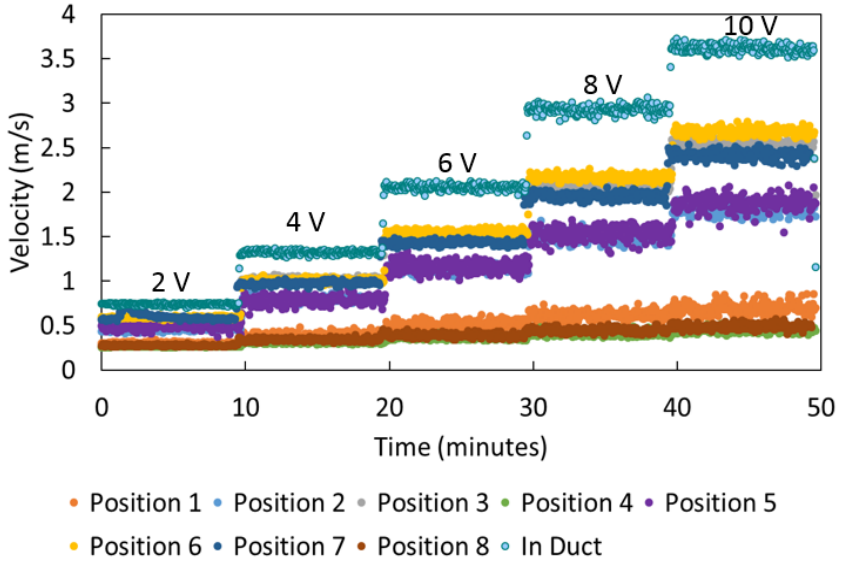

Figure 4.3 Velocity Measurements over Time for 8 Sensor Locations of First Configuration and in Duct Location

It is observed from Figure 4.3 that the velocity is symmetrical in the box from side to side. However, the velocity at the top of the box is drastically lower than the velocity close to the bottom of the box. It was noted that the velocity does not decrease linearly from the top to the bottom of the box. The velocity measured at the middle positions (2 and 5) is significantly closer to the velocity observed at the bottom of the box. This unevenly distributed velocity is mainly due to the 90° elbow in the duct before the PCM box in which the momentum of the flow causes fluid separation from the top of the box and forces most of the air flow to the bottom of the box. Clearly, positioning the PCM as far from the inlet of the PCM box is not enough to render the flow fully developed. The velocity measurements within the duct have a significantly higher velocity than the highest measured velocity within the box. This is due to two causes. First, the area of the duct is smaller than the area of the box, which leads to higher measured velocities for equal flow rates.

Second, the sensor was positioned near the outside radius of an elbow, where it can be assumed it measured the maximum velocity in that cross-section of the duct.

4.1.3 Second Configuration

Since it had been determined that the velocity is approximately symmetrical from side to side, it was possible to obtain a more detailed velocity profile by measuring the velocity linearly from top to bottom. The second sensor configuration can be seen in Figure 4.4. It is composed of 11 velocity sensor linear positions with 2in distance between each sensor. The sensor was once again mounted to the wall. In Figure 4.4 the velocity sensor can be seen installed in Position 6.

Figure 4.4 Velocity Sensor Locations of Second Velocity Profile Configuration

The graph, shown in Figure 4.5, represents the velocity from the top of the box (0 m) to the bottom of the box (0.606 m) for the five different fan signal settings which cover the range of the fan. The general trend observed was that the velocity is relatively low at the top of the box significantly increasing after 0.1 m which corresponds roughly to Position 2. The velocity then increases almost gradually until the bottom. It was noted that the velocity relative to box height follows the same trend as the fan signal increases.

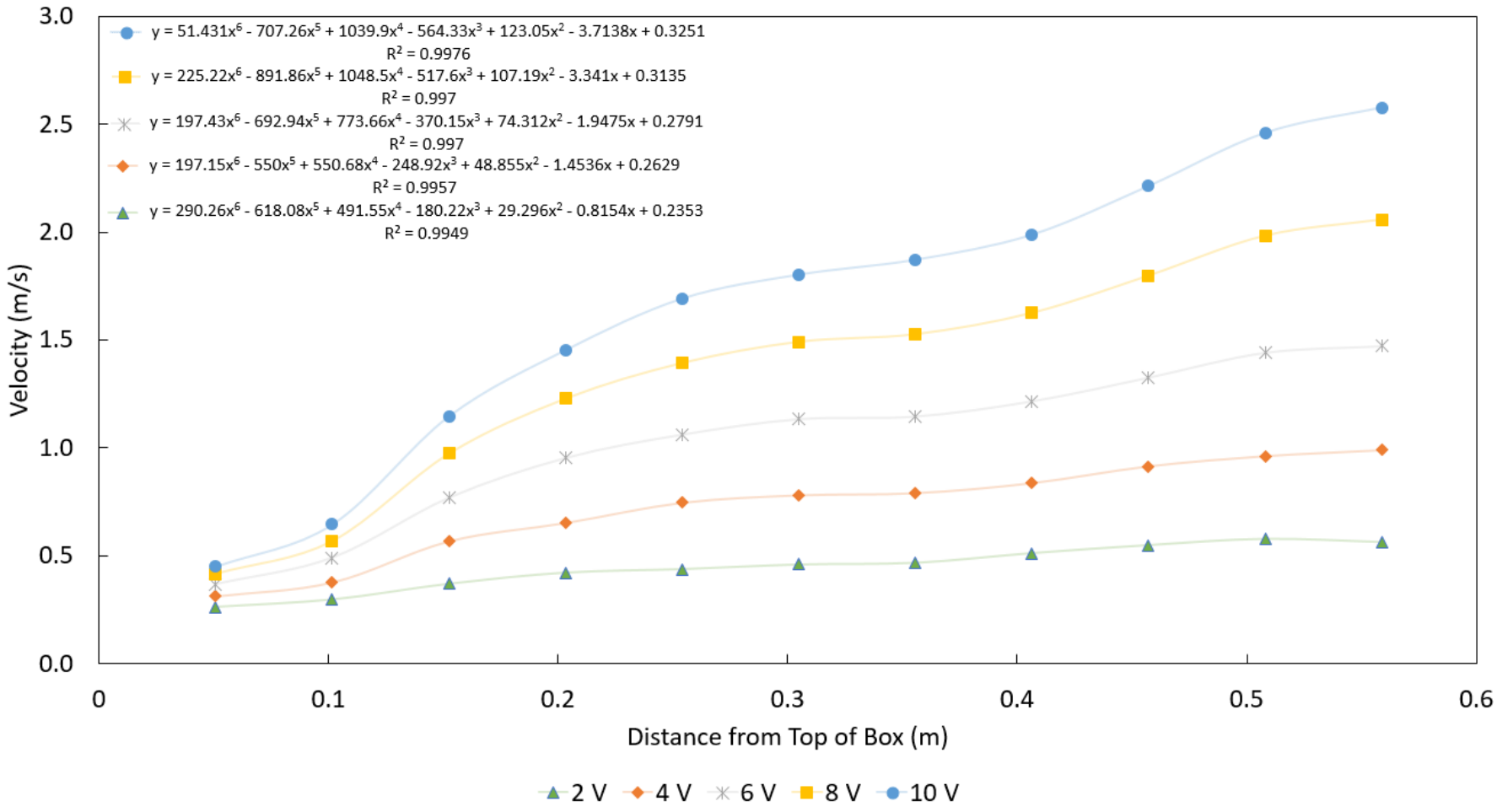

Figure 4.5 Velocity Profile at Inlet of PCM Plates from Top (0 m) to Bottom (0.606 m) for Five Fan Input Signals Covering Range of Fan

It was important to be able to relate the velocity measured by the sensor in the duct to the velocity profile in the PCM box as the sensor would only be placed in the duct location during testing of the PCM. Equations were determined for each of the five fan signal curves in Figure 4.5. The integral of the equations was taken to find the area under the curve which was then divided by the box height (0.606 m) to give an average velocity for the five fan signals.

The velocity inside the PCM box was correlated to the in-duct velocity by matching the average PCM velocity to its corresponding in-duct velocity measurement for each of the five fan signals, see Figure 4.6. Thus, the LabVIEW program will receive the velocity measurement at the duct location, determine the corresponding velocity with the PCM box using the correlating equation in Figure 4.6 and then multiply by the box area to determine the flow rate within the PCM box. The flow rate measurement was compared to a setpoint value through a PID controller which controlled the input signal to the fan, see Appendix H for comparison of flow rate values to the manufacture specified flow rate curve of the fan. It was determined that the maximum flow rate at 10 V was 1299 CFM (2207 m^3/h).

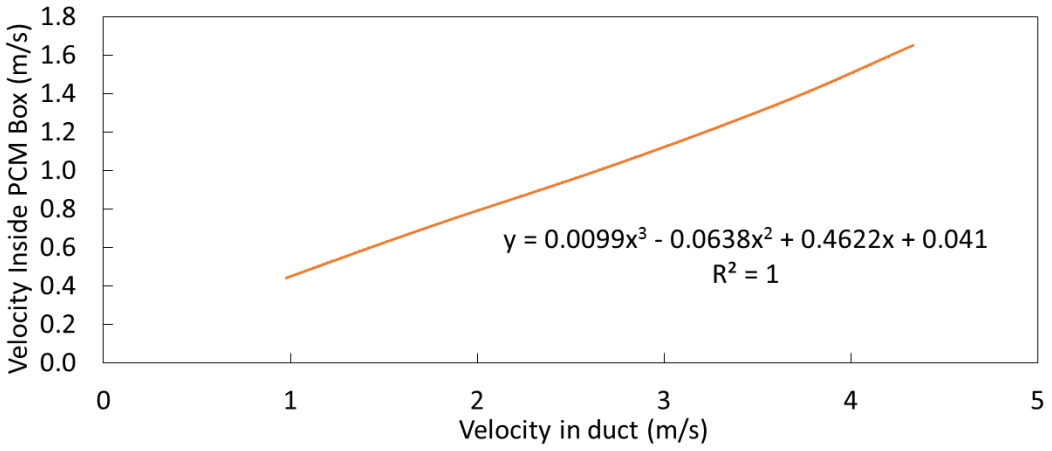

Figure 4.6 Correlating Average Velocity Profile to Velocity Measurement in Duct

4.2 Theory and Uncertainty

Characterizing the heat transfer rate or power during charging and discharging is of central importance for the design of PCM TES prototypes for integration into the AHUs of commercial buildings. This section will outline the equations used to determine heat transfer rate and energy storage of the PCM TES unit and the associated uncertainties.

4.2.1 Theory

For this study, only the total amount of heat transferred to the HTF will be measured as local heat transfer processes occurring within the PCM units are known from the literature. As the HTF does not undergo a phase change it will only transfer heat sensibly which can be experimentally calculated by:

$$q_{\mathrm{i}} = \dot{V}\rho c_{\mathrm{p}}\Delta T \tag{4.1}$$

where q_{i} is the instantaneous heat transfer rate, $\dot{V}$ is the volumetric flow rate, ρ is the density of the HTF fluid, c_{p} is the specific heat of the HTF fluid and ΔT is the temperature difference between the inlet and the outlet of the PCM TES. Many studies on PCM TES applications have used this equation to determine heat transfer of the system [7, 16, 31, 33, 34, 35, 43, 49]. Equation (4.1) is dependent on the experimental measured values of velocity and temperature. The volumetric flow rate was determined by using the box velocity, discussed in Section 4.1.3, and multiplying it by the cross-sectional area of the box. The inlet and outlet temperatures were an average of 8 thermocouple readings each, see Figure 3.11 for thermocouple positioning. The temperature difference was determined by using the average inlet and outlet temperature values. Finally, the density was varied based on the average inlet temperature. In addition, heat transfer to the surroundings would have a minimal effect on the instantaneous heat transfer rate. The theoretical

heat loss, see Appendix I for further calculations, was subtracted from the instantaneous transfer rate at every interval for more realistic results.

The cumulative energy storage also called energy capacity of the system can be determined experimentally by:

$$E_{\mathrm{st}} = \sum q_{\mathrm{i}}\, \Delta t \tag{4.2}$$

where E_{st} is the cumulative energy storage of the PCM, q_{i} is the instantaneous heat transfer rate, see Eq. (4.1), and Δt is the time interval between measurements [7, 31, 32, 33]. The cumulative energy storage will be referred to as "energy stored".

The theoretical energy capacity of the PCM TES unit can be calculated from:

$$E_{\mathrm{st}} = m\left[c_{\mathrm{p,s}}(T_{\mathrm{m}} - T_{\mathrm{i}}) + \Delta h_{\mathrm{m}} + c_{\mathrm{p,l}}(T_{\mathrm{f}} - T_{\mathrm{m}})\right] \tag{4.3}$$

where m is the total mass of the PCM, $c_{\mathrm{p,s}}$ is the specific heat of the solid state of the PCM, $c_{\mathrm{p,l}}$ is the specific heat of the liquid state of the PCM, T_{m} is the melting temperature, T_{i} is the initial temperature of the PCM, T_{f} is the final temperature of the PCM and Δh_{m} is the latent heat of fusion. Equation 4.3 demonstrates both the sensible and latent heat storage capacity within its three terms [4, 7, 33, 34, 35].

The mass of the PCM within the PCM box was determined by weighing all 58 plates in the PCM box using a kitchen scale with an error of ±0.5g. The mass was summed and the mass of the aluminum encapsulation containers taken from manufacture specifications was subtracted for the final PCM mass, see Appendix J. The total mass for the PCM was determined to be 29.6 kg. The latent heat of fusion was determined by rearranging Eq. (4.3) using the manufactured specific heat storage capacity of 250 kJ/kg ±7.5% for a temperature range of 35˚C to 50˚C:

$$\Delta h_{\mathrm{m}} = \frac{E_{\mathrm{st}}}{m} - c_{\mathrm{p,s}}(T_{\mathrm{m}} - T_{\mathrm{i}}) - c_{\mathrm{p,l}}(T_{\mathrm{f}} - T_{\mathrm{m}}) \tag{4.4}$$

$$\Delta h_{\mathrm{m}} = 250\,\frac{\mathrm{kJ}}{\mathrm{kg}} - 2\,\frac{\mathrm{kJ}}{\mathrm{kgK}}(44℃ - 35℃) - 2\,\frac{\mathrm{kJ}}{\mathrm{kgK}}(50℃ - 44℃) = 220\,\frac{\mathrm{kJ}}{\mathrm{kg}} \pm 19\,\frac{\mathrm{kJ}}{\mathrm{kg}} \quad (4.5)$$

Additional energy storage would have occurred in the form of sensible heat to the additional materials between the inlet and outlet temperature sensors. This would have included the aluminum of the encapsulation of the PCM and the ½" plywood boards surrounding three sides of the PCM. The additional energy storage, see Appendix K for calculation details, was added to the theoretical energy storage value. The additional energy storage was determined to store energy on an order of magnitude less than the PCM storage and contributed a significant yet minimal amount to the overall theoretical energy storage capacity.

4.2.2 Uncertainty

The box velocity error was a combination of two factors; the velocity error present when the velocity profile was created called the box velocity experimental error and the velocity error from the correlation equation during testing, Eq. (4.6).

$$\delta v_{\mathrm{B}} = \sqrt{\left(\delta v_{\mathrm{B(experimental)}}\right)^2 + \left(\delta v_{\mathrm{B(correlation)}}\right)^2} \quad (4.6)$$

where δv_{B} represents the box velocity error during a test following the full cycle test procedure. The velocity error from the velocity profile test would simply be the error of the sensor. The correlation equation derived from Figure 4.6 was:

$$v_{\mathrm{B}} = 0.0099 v_{\mathrm{D}}^3 - 0.0638 v_{\mathrm{D}}^2 + 0.4622 v_{\mathrm{D}} + 0.041 \quad (4.7)$$

where v_{B} represents average box velocity and v_{D} represents the velocity measurement in the duct. The derivative of the correlation equation multiplied by the error of the velocity sensor, see Eqs (4.8) and (4.9), provided the error from the correlation equation during testing.

$$\frac{\partial v_{\mathrm{B}}}{\partial v_{\mathrm{D}}} = 3(0.0099) v_{\mathrm{D}}^2 - 2(0.0638) v_{\mathrm{D}} + 0.4622 \quad (4.8)$$

$$\delta v_{\mathrm{B(correlation)}} = \frac{\partial v_{\mathrm{B}}}{\partial v_{\mathrm{D}}}(\delta v_{\mathrm{D}}) = [3(0.0099) v_{\mathrm{D}}^2 - 2(0.0638) v_{\mathrm{D}} + 0.4622][0.065 v_{\mathrm{D}}] \quad (4.9)$$

The error of velocity measurement determined during the uncertainty analysis of the sensor was 6.5% of the reading, see Appendix G. Inserting the values into Eq. (4.6) provided the final equation used to determine velocity error within the box:

$$\delta v_{\mathrm{B}} = \sqrt{(0.065 v_{\mathrm{B}})^2 + ([3(0.0099)v_{\mathrm{D}}^2 - 2(0.0638)v_{\mathrm{D}} + 0.4622][0.065 v_{\mathrm{D}}])^2} \quad (4.10)$$

The volumetric flow rate was calculated by multiplying the integrated box velocity by height and the length of the PCM box. The area of the box was 0.372 m². The PCM box was custom made and measured out with a measuring tape with an error of ±0.0005 m which is converted to ±0.0007 m² for the area. The velocity and area errors are combined using error propagation for multiplication:

$$\delta \dot{V} = \left|\dot{V}\right| \sqrt{\left(\frac{\delta v_{\mathrm{B}}}{v_{\mathrm{B}}}\right)^2 + \left(\frac{\delta A}{A}\right)^2} \quad (4.11)$$

where $\delta \dot{V}$ represents the volumetric flow rate error, $\dot{V}$ represents the volumetric flow rate value, δA represents the area error and A represents the area of the box.

The temperature uncertainty from a single thermocouple was determined to be ±0.88˚C, see Appendix E. The average inlet and outlet temperature errors were determined using propagation of error for addition:

$$\delta T_{\mathrm{in}} = \delta T_{\mathrm{out}} = \sqrt{8(\delta T)^2} = \sqrt{8(0.88)^2} = \pm 2.5℃ \quad (4.12)$$

where δT_{in} represents the error of the average inlet temperature, δT_{out} represents the error of the average outlet temperature and δT represents the error of a single thermocouple measurement.

The error of the temperature difference of the inlet and outlet, used in the instantaneous heat transfer rate equation, was determined using error propagation for addition:

$$\delta \Delta T = \sqrt{(\delta T_{\mathrm{in}})^2 + (\delta T_{\mathrm{out}})^2} = \sqrt{2(2.5)^2} = \pm 3.5℃ \quad (4.13)$$

where $\delta\Delta T$ represents the error or the temperature difference, δT_{in} represents the error of the average inlet temperature and δT_{out} represents the error of the average outlet temperature.

The instantaneous heat transfer rate error was determined using error propagation for multiplication:

$$\delta q_{\text{i}} = |q| \sqrt{\left(\frac{\delta \dot{V}}{\dot{V}}\right)^2 + \left(\frac{\delta \Delta T}{\Delta T}\right)^2 + \left(\frac{\delta c_{\text{p}}}{c_{\text{p}}}\right)^2 + \left(\frac{\delta \rho}{\rho}\right)^2} \tag{4.14}$$

where δq_{i} is the instantaneous heat transfer rate error, $\delta \dot{V}$ is the volumetric flow rate error calculated from Eq.(4.6), $\delta\rho$ is the density error of the HTF fluid which was derived from the density equation with respect to inlet temperature, δc_{p} is the error of the specific heat of the HTF fluid and $\delta\Delta$T is the temperature difference error, see Eq. (4.13). The specific heat capacity of air for the temperature range used was 1.005 kJ/ (kg K). Between 40˚C to 60˚C the specific heat capacity of air changes to 1.009 kJ/ (kg K) resulting in an error of 0.004 kJ/ (kg K).

The cumulative energy storage error was determined by adding the error propagation for multiplication of the energy storage values at every time interval:

$$Q_{\text{i}} = q_{\text{i}} * \Delta t \tag{4.15}$$

$$\delta Q_{\text{i}} = |Q_{\text{i}}| \sqrt{\left(\frac{\delta q_{\text{i}}}{q_{\text{i}}}\right)^2 + \left(\frac{\delta \Delta T}{\Delta T}\right)^2} = |Q_{\text{i}}| \left(\frac{\delta q_{\text{i}}}{q_{\text{i}}}\right) \tag{4.16}$$

$$\delta E_{\text{st}} = \sum \delta Q_{\text{i}} \tag{4.17}$$

where Q_{i} is the energy stored per time interval, δQ_{i} is the error of the energy stored per time interval and δE_{st} is the cumulative energy storage error.

4.3 Analysis of a Single Full Cycle Test

A detail analysis for a single full cycle test is presented below. The following test had an initial temperature setpoint of 18˚C, a heating setpoint of 62˚C, a cooling setpoint of 18˚C and a

flow rate setpoint of 800 CFM (1359 m³/h). The analysis focused on velocity, flow rate, temperature, instantaneous heat transfer rate and cumulative heat transfer.

The volumetric flow rate for both the charging and discharging cycles can be seen in Figure 4.7 and Figure 4.8 respectively with upper and lower error limits. It was observed that the volumetric flow rate follows the setpoint well with slight oscillations.

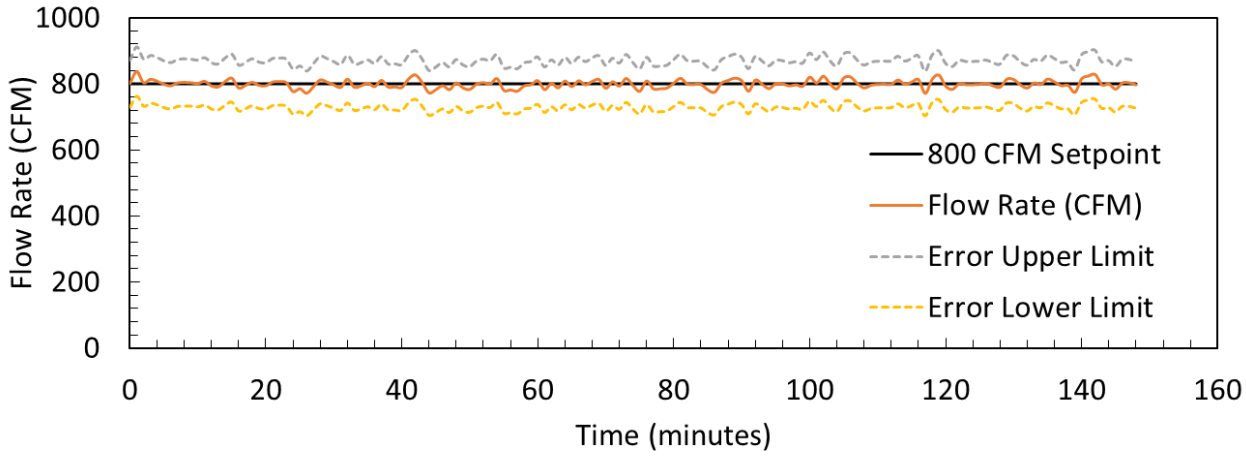

Figure 4.7 Volumetric Flow Rate during PCM Charging cycle with Upper and Lower Errors

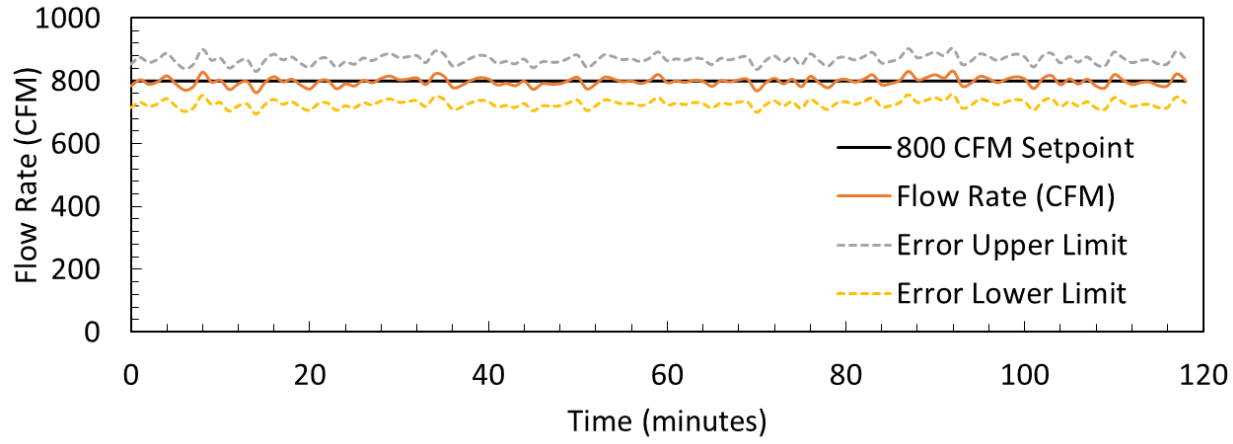

Figure 4.8 Volumetric Flow Rate during PCM Discharging cycle with Upper and Lower Errors

The temperature measurements from all 16 thermocouples in the PCM box are shown in Figure 4.9 for the charging cycle and in Figure 4.10 for the discharging cycle. It is noted that at the beginning of the cycles the inlet temperatures do not start at the setpoint temperature. The cycle

begins as soon as the box damper is opened allowing flow of the HTF in the PCM box. Thus, the air within the PCM box was still at the temperature from the previous cycle and needs a minute for the incoming air to move the stagnant air previously present.

Upon observing the inlet temperatures, it was noted that the temperature measurements at the bottom of the box are slightly higher and become gradually lower for charging in Figure 4.9 and the opposite was observed of the inlet temperature measurements during discharging in Figure 4.10. This is due to transient values. This transition is most prevalent at the start of the sequence when the temperature of the air-loop has not yet stabilized creating a larger inlet temperature difference between the top and the bottom of the box. During charging, there was oscillation present due to the PID controller. These oscillations were caused by slight transient temperatures throughout the charging sequence which was observed by the slight top to bottom inlet temperature differences over the oscillations.

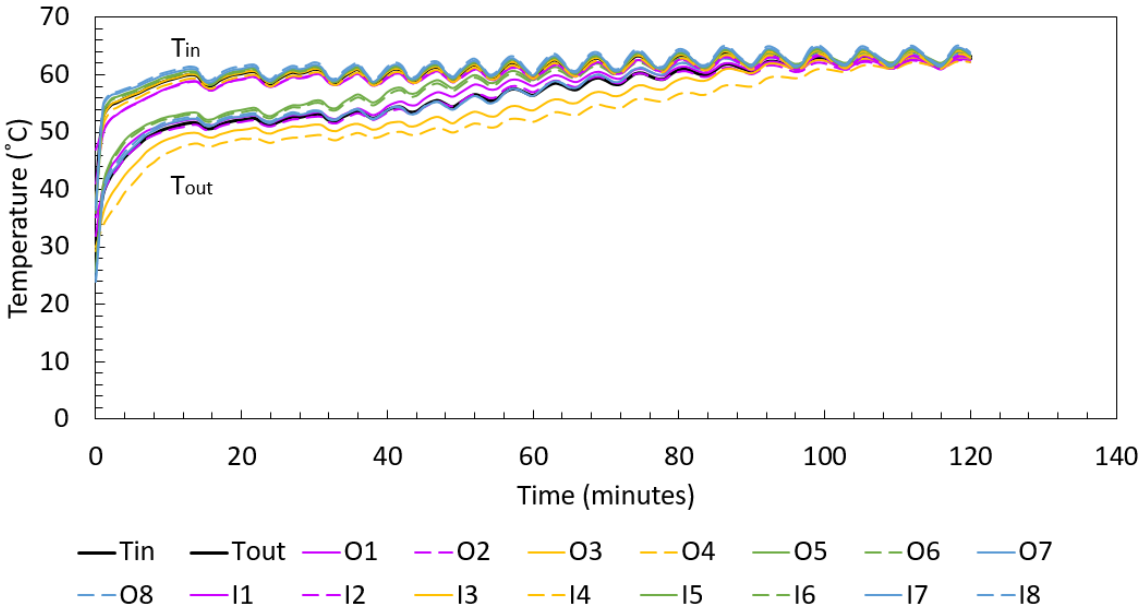

Figure 4.9 Temperature Measurements of all 16 Inlet and Outlet Thermocouples during the Charging Cycle with Averages Shown in Black

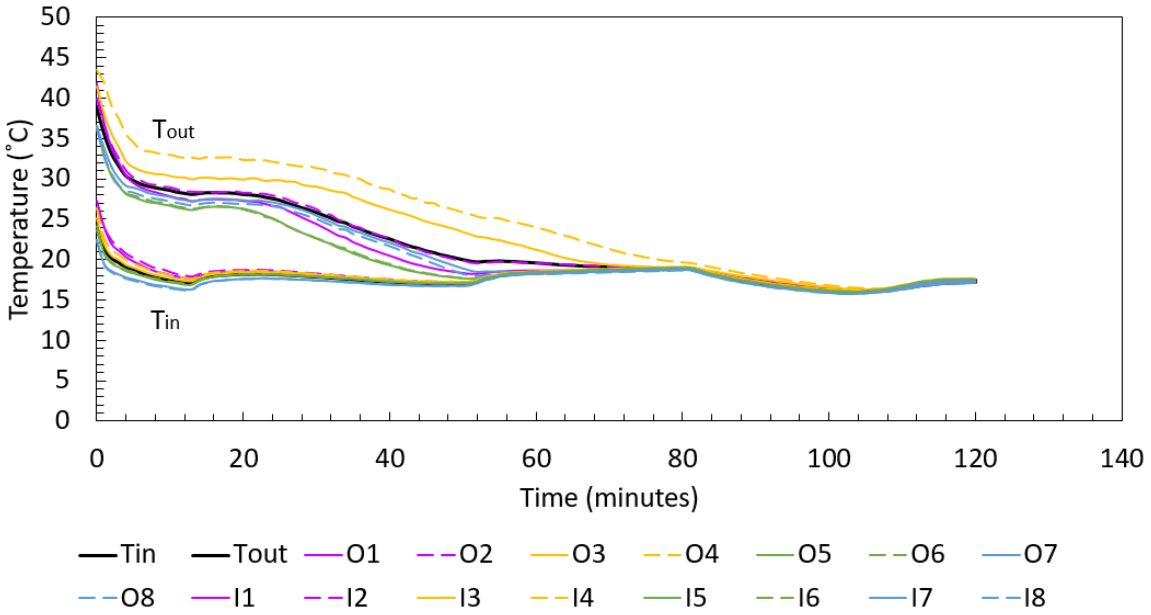

Figure 4.10 Temperature Measurements of all 16 Inlet and Outlet Thermocouples during the Discharging Cycle with Averages Shown in Black

The outlet temperatures were observed to have significant temperature differences from top to bottom. The two top and two bottom outlet temperature measurements produced similar values. The two higher middle values, demonstrated by the yellow lines in Figure 4.9 and Figure 4.10, had significantly lower temperatures during charging and significantly higher values during discharging. Finally, the two lower middle values, demonstrated by green in Figure 4.9 and Figure 4.10, had the highest temperatures during charging and the lowest temperatures during discharging. In an attempt to explain this phenomenon, the boundary layer was determined indicating an internal flow between the plates. The Reynolds number would vary vertically in the gaps of the PCM storage unit as it has been shown that the velocity varies vertically. The Reynolds number was approximated to be between 1529 using the maximum recorded velocity of 1.41 m/s and 477 using the minimum recorded velocity of 0.44 m/s. This flow is thus approximated to be laminar. According to Bergman *et al.* [67] the Nusselt number of a laminar internal flow is independent of the Reynolds number, thus independent from velocity [67]. Thus, this phenomenon

cannot be explained with simple thermal dynamic principles and would require further testing in future studies for a better understanding of internal heat transfer rates occurring within the unit.

The temperature difference between the inlet and outlet thermocouples was determined and can be seen in Figure 4.11 for the charging cycle and in Figure 4.12 for the discharging cycle. The instantaneous heat transfer rate for the charging and discharging cycles are demonstrated in Figures 4.13 and 4.14 respectively with upper and lower error limits displayed.

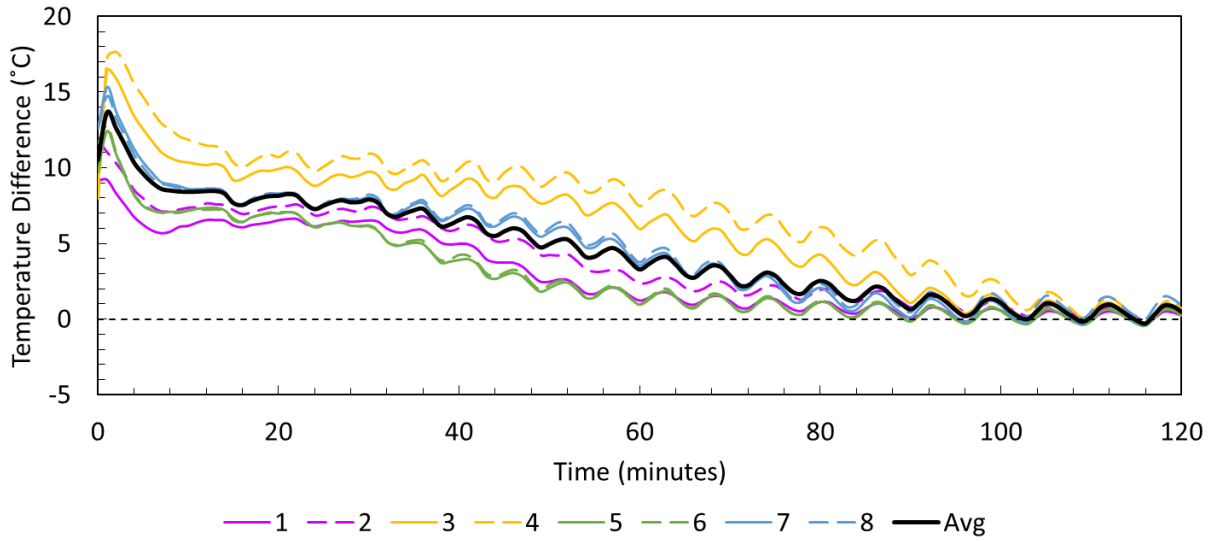

Figure 4.11 Temperature Difference of 8 Positions with Average for Charging Cycle

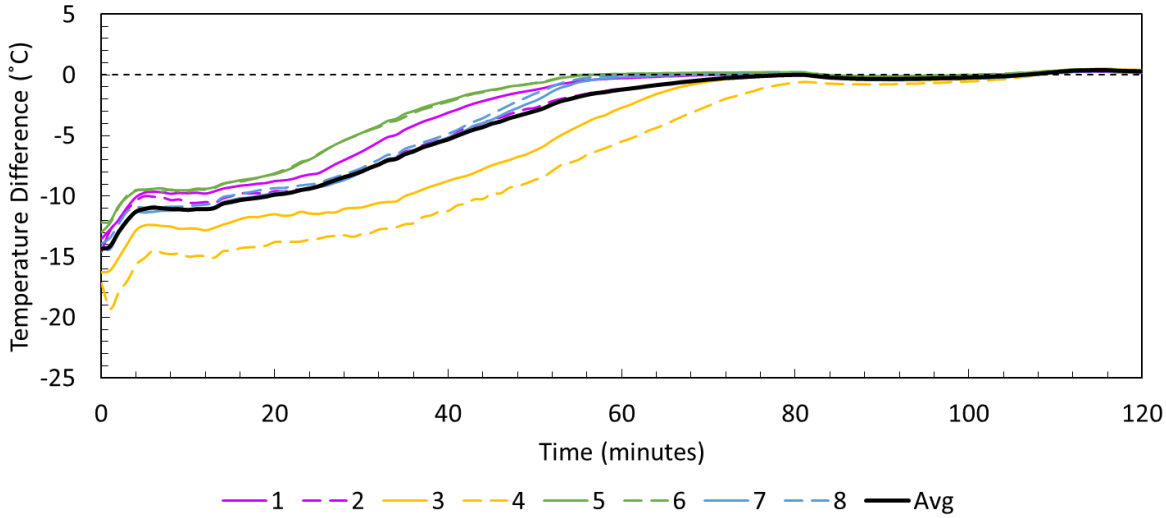

Figure 4.12 Temperature Difference of 8 Positions with Average for Discharging Cycle

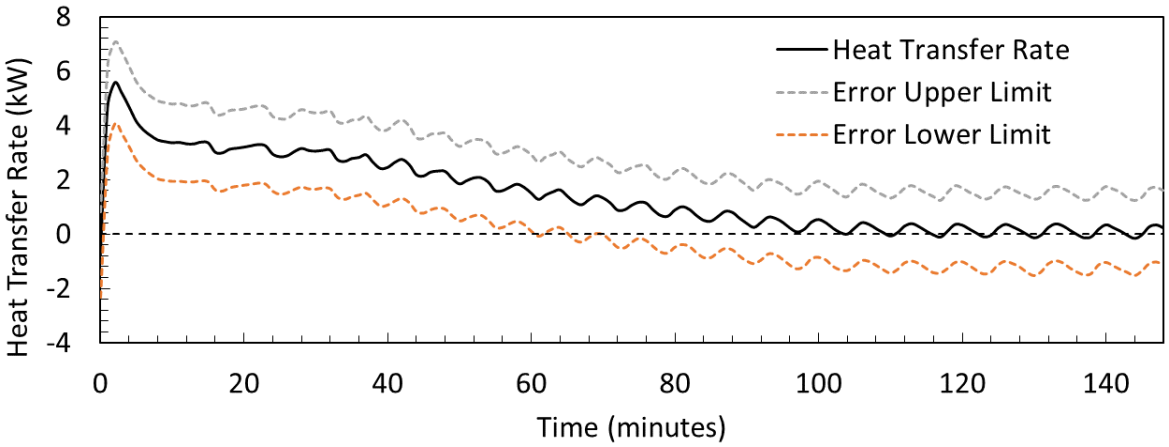

Figure 4.13 Instantaneous Heat Transfer Rate during the Charging cycle with Error Limits

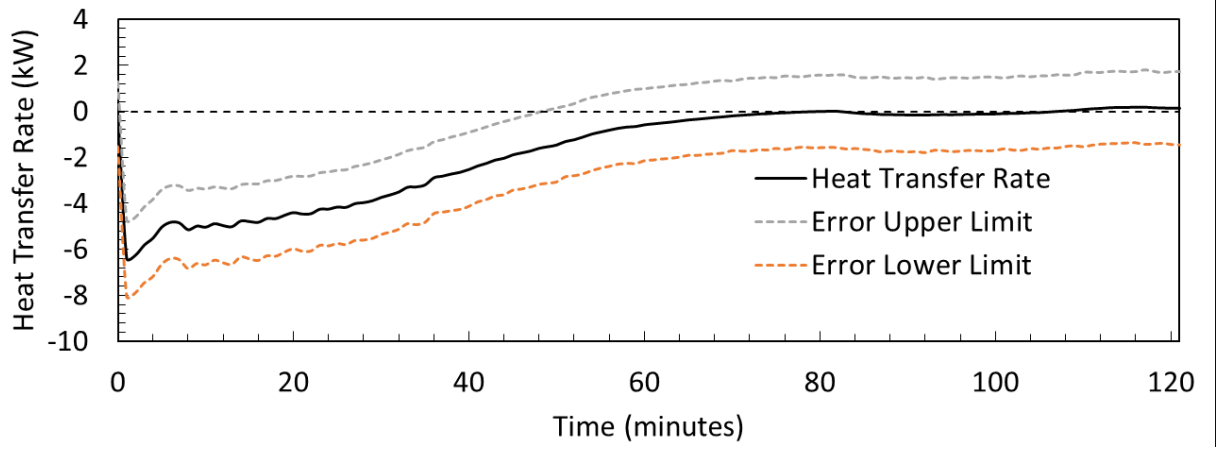

Figure 4.14 Instantaneous Heat Transfer Rate during the Discharging cycle with Error Limits

The experimental energy storage for the test is presented with error limits in Figures 4.15 and 4.16 for the charging and discharging cycles respectively. Notice that although the error limits are quite large, the experimental energy capacity is similar to the theoretical value for both charging and discharging.

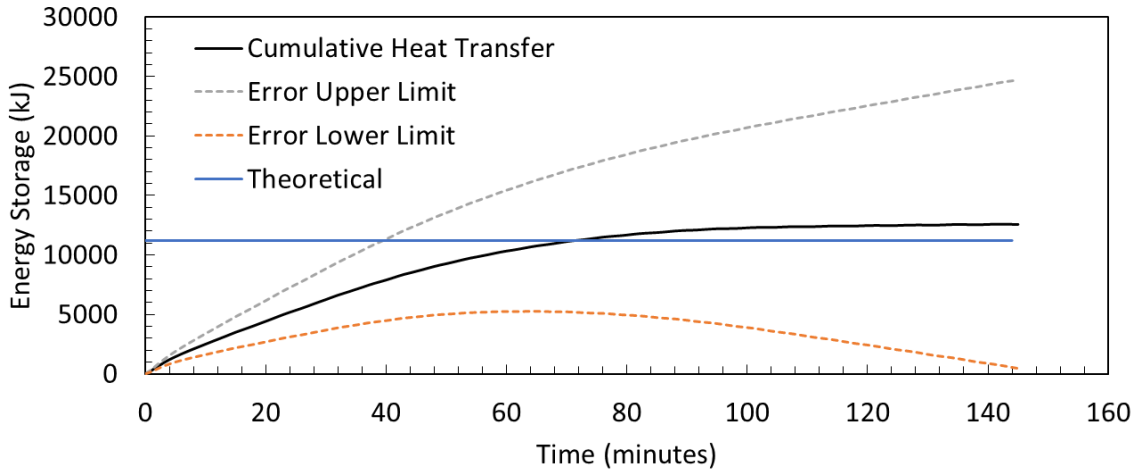

Figure 4.15 Cumulative Heat Transfer with Error Limits and Theoretical Value during Charging

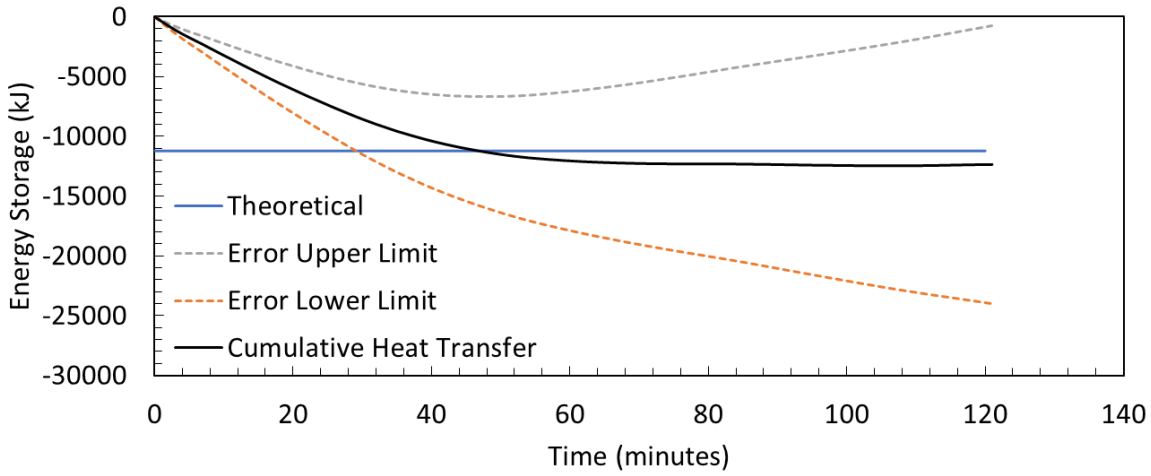

Figure 4.16 Cumulative Heat Transfer with Error Limits during Discharging

Thus far, the experimental energy storage has been calculated using average values for velocity and temperature. By looking and the temperature difference of the various thermocouples, it was seen that the measurements read were not uniform. This indicates that heat transfer was not uniform but varied through various areas of the box. It was also demonstrated from the velocity profile in Figure 4.5 that the velocity varied as well. Therefore, the PCM box cross section was divided into 8 sections shown in Figure 4.17.

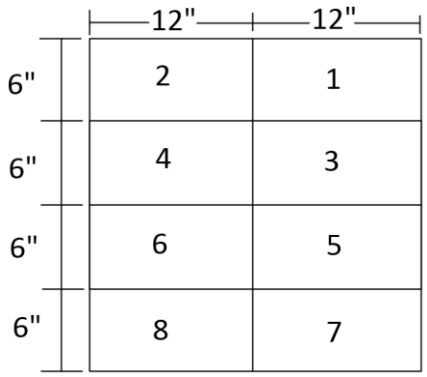

Figure 4.17 PCM Box Cross-Section Divided into 8 Evenly Divided Sections

The instantaneous heat transfer rate and cumulative heat transfer rate were calculated for each section. Every section contained one of the 8 inlet and outlet thermocouples which was used for the temperature measurement within their respective sections.

The energy storage from both the average based method and section based method were compared, see Figure 4.18. It was observed that the two methods produced the same energy storage with insignificant differences. Thus, the average method was used for all further calculations as it was simpler to implement.

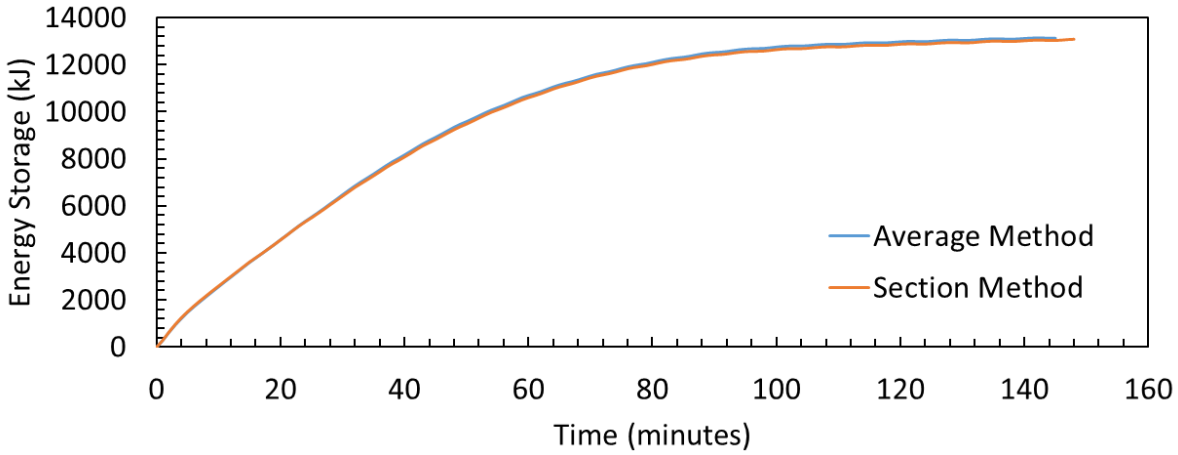

Figure 4.18 Energy Storage Capacity Comparison between the Average and Section Methods

This chapter demonstrated the characterization of the experimental setup. This was done by determining the velocity profile at the inlet of the PCM plates, discussing the theory and uncertainty behind the instantaneous heat transfer rate and energy storage calculations and an

analysis of a single full cycle test verify that all recorded and calculated values were within error limitations. The following chapter will discuss experimental results of the PCM characterization under AHU application conditions.

5 Chapter: Experimental Results

Experiments were conducted to characterize the amount of heat transferred across a PCM air heat exchanger under varying inlet conditions, i.e., the HTF flow rates, the initial temperatures of the PCM and the HTF inlet temperatures for both charging and discharging. The experimental settings for the characterization tests are displayed in Table 5-1.

Table 5-1 Tests Performed for Characterization of PCM TES for AHU Applications with Flat Plate Geometry

Test	Flow Rate (CFM)	Initial Temperature (°C)	Inlet Temperature (°C)
Variations in HTF Flow Rates – Charging	600, 800 , 1000	30	62
Variations in HTF Flow Rates - Discharging	600, 800, 1000	62	30
Variations in Initial Temperature - Charging	1000	18, 24, 30, 36	54
Variations in Initial Temperature - Discharging	1000	46, 54, 62	30
Variations in HTF Inlet Temperature - Charging	1000	30	46, 54, 62
Variations in HTF Inlet Temperature - Discharging	1000	54	18, 24, 30, 36

5.1 Variations in HTF Flow Rates

In order to properly incorporate the PCM TES into an AHU and achieve proper control of the heat transfer rates, it is important to understand how the heat transfer rates of the PCM vary with the volumetric flow rate of the HTF. Three tests were performed using the full cycle test procedure with an initial temperature setting of 30˚C, a heating temperature setting of 62˚C, a cooling temperature setting of 30˚C and varying flow rate settings for each test of 600 CFM (1019 m^3/h), 800 CFM (1359 m^3/h) and 1000 CFM (1699 m^3/h). The inlet and outlet temperature difference of the PCM, instantaneous heat transfer rate and cumulative heat transfer for all three

volumetric flow rates were plotted in Figures 5.1 to 5.3 for the charging cycle and Figures 5.4 to 5.6 for the discharging cycle.

As shown in Figure 5.1 and 5.4, the magnitude of temperature difference increases as the flow rates decrease for both charging and discharging for any given point in time. This occurs because as the flow rates decrease, the fluid travels slower through the storage unit allowing more heat to be transferred to a single air particle than would occur if the air particle were moving faster through the unit. This in turn changes the particles initial temperature based on the length of time to travel across the unit creating a larger temperature difference between the inlet and outlet for lower flow rates.

As shown in Figure 5.2 and 5.5, the increase in all three volumetric flow rates lead to higher heat transfer rates for the first 40 minutes. After this period, however lower heat transfer rates are observed for higher volumetric flow rates. This observation indicates that the tests at the lower volumetric flow rate charged and discharged slower than at higher volumetric flow rates. This was because of the abundance of air particles passing through the unit at higher temperatures. When the air particles were moving slower, they had more time to dissipate their heat at the beginning of the unit decreasing particle temperature resulting in a reduced heat transfer rate between the particle and the PCM for the rest of the unit. The faster the air particles passed through the unit, the less time they had to transfer heat and stayed at higher temperatures throughout the entire unit resulting in faster energy storage as seen in Figures 5.3 and 5.6.

The higher heat transfer rate as previously mentioned led to faster charging and discharging times for higher flow rates. Based on when the heat transfer rate first achieved a value of zero, the charge time for flow rates of 1000 CFM (1699 m^3/h), 800 CFM (1359 m^3/h) and 600 CFM (1019 m^3/h) were approximately 86 min, 102 min and 120 min, respectfully and the discharge

times were 108 min, 122 min and 150 min, respectfully. The completion times were a bit longer during the discharge cycle as the data contained significantly less oscillation and can be considered a more accurate result. Ultimately, heat transfer rates between 3 and 4 kW were maintained for approximately 40 minutes for each flow rate, decreasing linearly after that to reach a value of 0 once the system was fully charged or discharged.

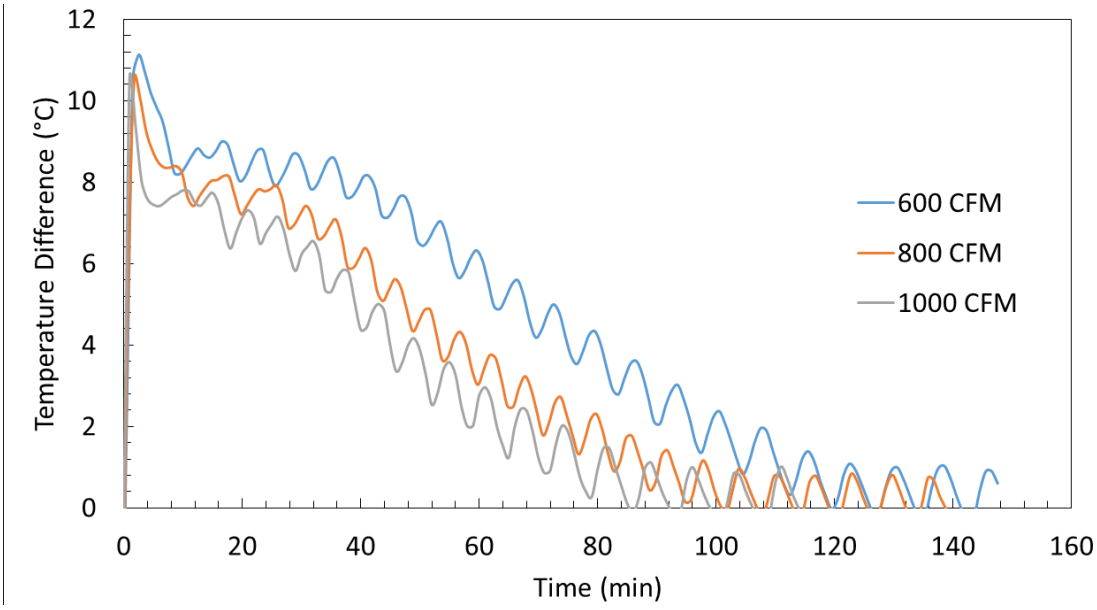

Figure 5.1 Inlet and Outlet Temperature Difference from Three Varying Volumetric Flow Rates during Charging with Initial Temperature Setting of 30˚C and HTF Heating Temperature Setting of 62˚C

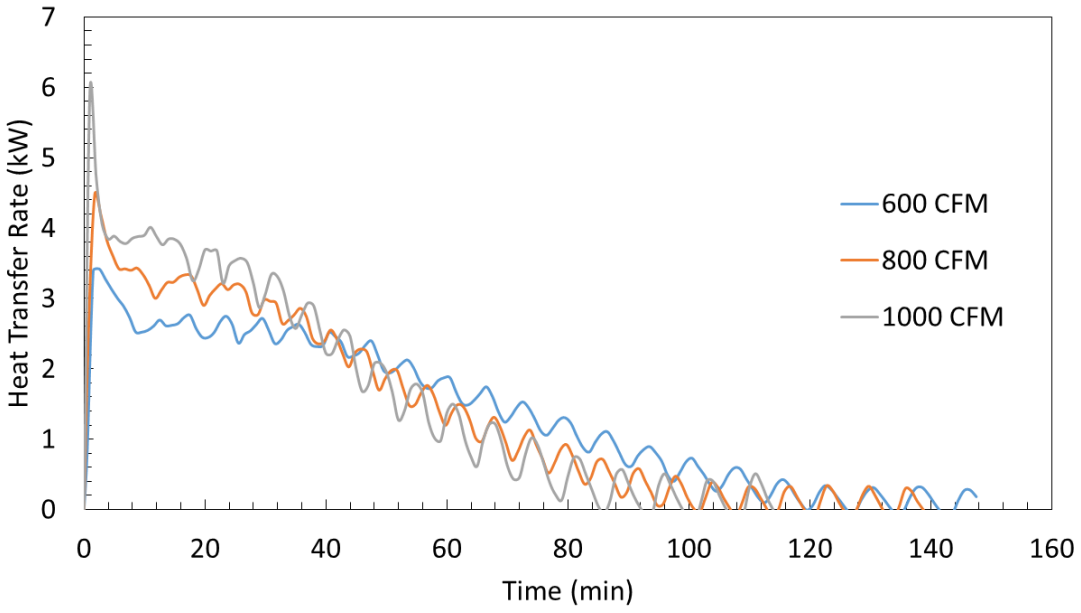

Figure 5.2 Instantaneous Heat Transfer Rate from Three Varying Volumetric Flow Rates during Charging with Initial Temperature Setting of 30˚C and HTF Heating Temperature Setting of 62˚C

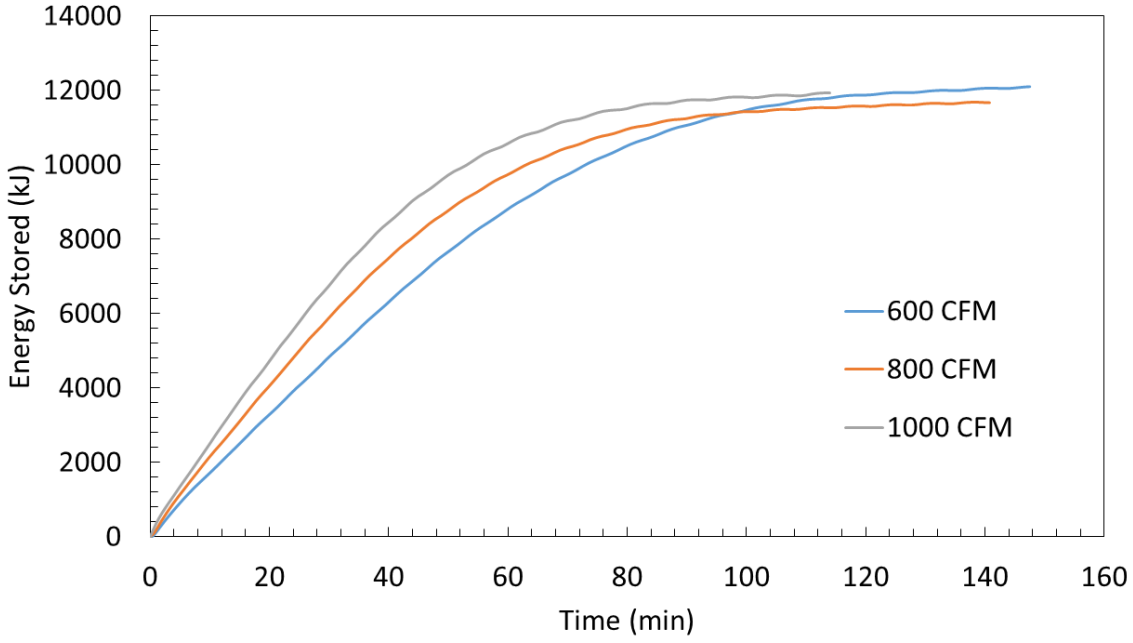

Figure 5.3 Cumulative Heat Transfer from Three Varying Flow Rates during Charging with Initial Temperature Setting of 30˚C and HTF Heating Temperature Setting of 62˚C

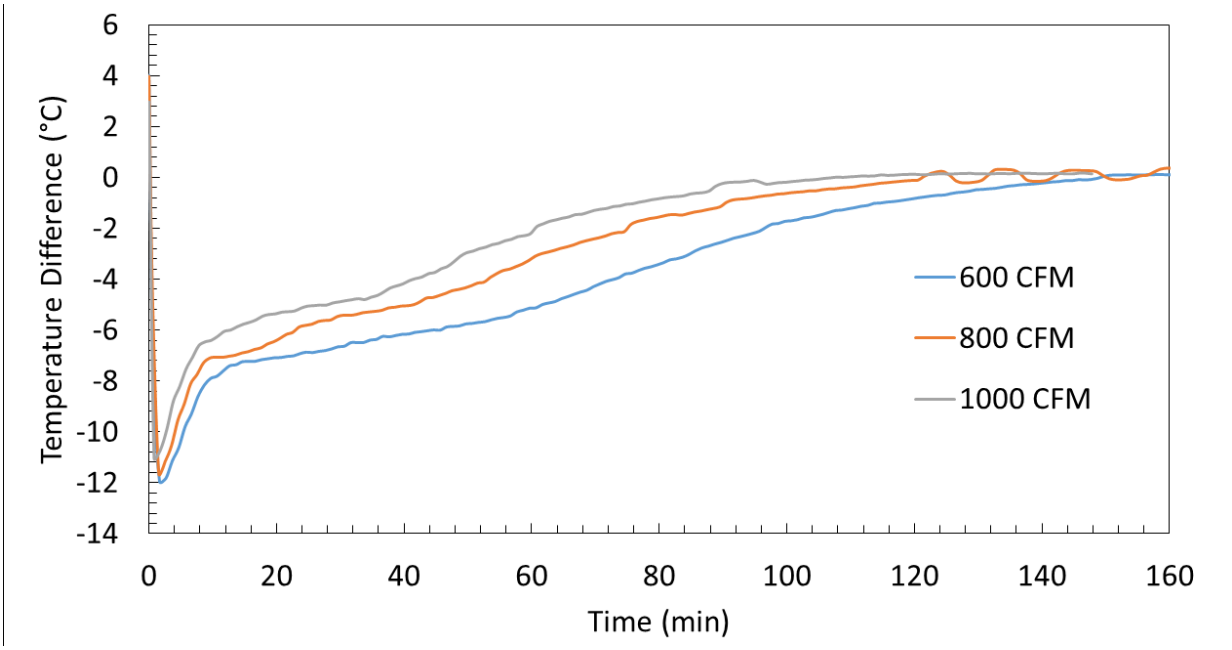

Figure 5.4 Inlet and Outlet Temperature Difference from Three Varying Volumetric Flow Rates during Discharging with Initial Temperature Setting of 62˚C and HTF Cooling Temperature Setting of 30˚C

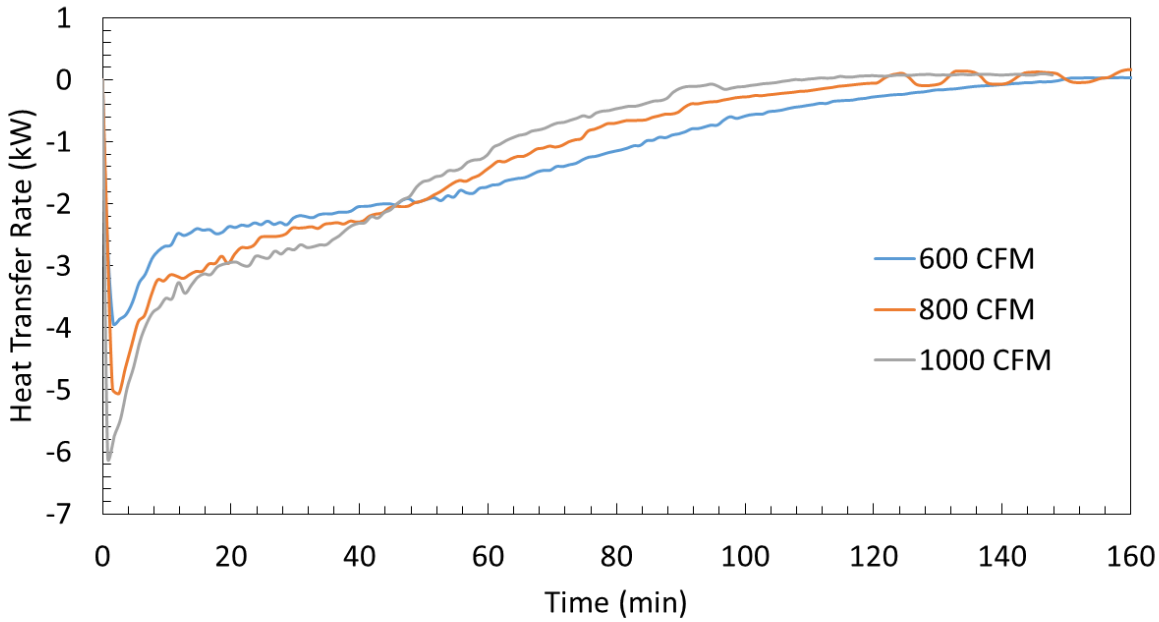

Figure 5.5 Instantaneous Heat Transfer Rate from Three Varying Flow Rates during Discharging with Initial Temperature Setting of 62˚C and HTF Cooling Temperature Setting of 30˚C

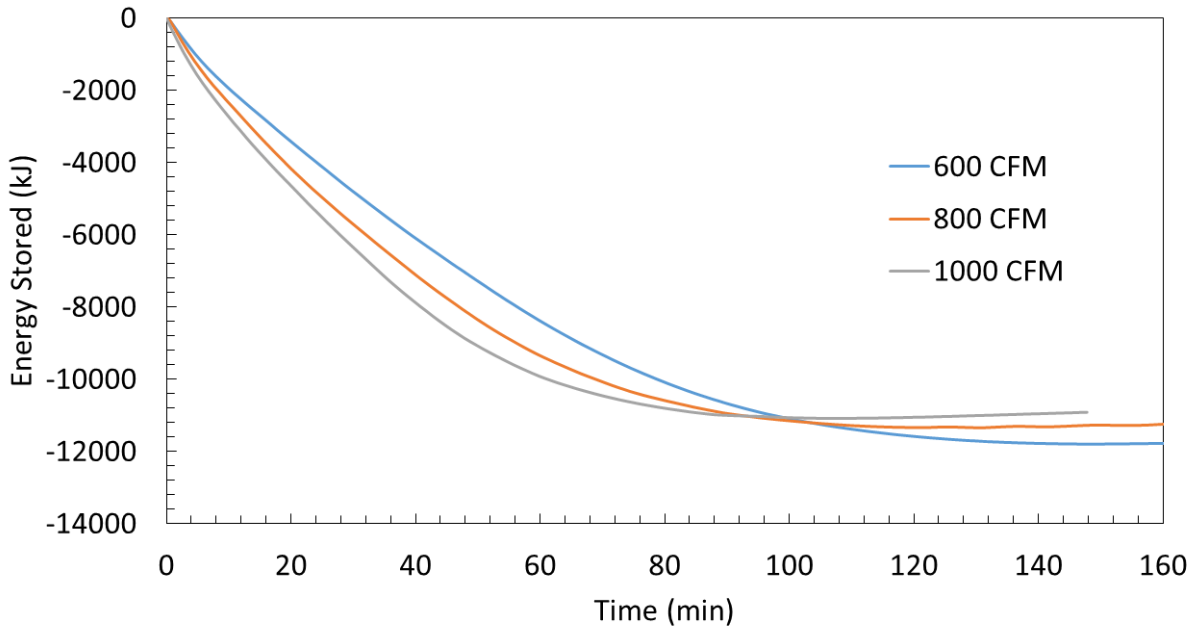

Figure 5.6 Cumulative Heat Transfer from Three Varying Volumetric Flow Rates during Discharging with Initial Temperature Setting of 62˚C and HTF Cooling Temperature Setting of 30˚C

5.2 Variations in Initial Temperatures

The effects of varying initial temperature of the PCM were further investigated by performing several tests. The charging cycle was performed four times with a volumetric flow rate setting of 1000 CFM (1699 m³/h), a heating temperature setting of 54˚C and varying initial temperature settings of 18˚C, 24˚C, 30˚C and 36˚C. The discharging cycle was performed three times with a flow rate setting of 1000 CFM (1699 m³/h), a cooling temperature setting of 30˚C and varying heating temperature settings (which was considered the initial temperature for the discharge cycle) of 46˚C, 54˚C, 62˚C. The inlet and outlet temperature difference, instantaneous heat transfer rate and cumulative heat transfer are plotted in Figures 5.7 to 5.9 for the charging cycle and Figures 5.10 to 5.12 for the discharging cycle.

It was observed from Figures 5.7 and 5.10 that the initial temperature of the PCM strongly affects the magnitude of the temperature difference. It was also observed from Figures 5.8 and

5.11 that there was a spike in the instantaneous heat transfer rate near the start of both the charging and discharging cycles. The latter was due to the large temperature difference between the melting temperature of the PCM and the initial temperature of the PCM. Once the initial spike subsided, it was found that all tests had approximately the same values with a temperature difference of about 5° C and an instantaneous heat transfer rate of about 3 kW. Therefore, the initial temperature affected the temperature difference and the overall heat transfer rate for the first few minutes of the cycle, whether charging or discharging. Based on this observation, it was theorized that the duration of the spike was the time required for the aluminum case and PCM extremities to achieve the melting temperature after which point the material can start to either store or dissipate latent heat. For instance, at an initial temperature of 36°C with only an 8°C temperature difference from the melting temperature, there is almost no visible initial spike whereas at an initial temperature of 18°C with a 26°C temperature difference from the melting temperature of 44°C, there is a significant spike of approximately 7°C. The instantaneous heat transfer rate followed the same trend as the temperature difference since it was the only variable from Eq. (4.1) that was varied.

It was observed from the energy storage graphs (Figure 5.9 and Figure 5.12) that an increase in total energy capacity occurred as the temperature difference between the melting temperature and initial temperature of the PCM became greater. For instance, at an initial temperature of 18 °C and 36 °C during the charging cycle resulted in 12400 kJ and 10700 kJ, respectively, which is a difference in energy storage capacity of 1700 kJ and an initial temperature of 46°C and 62°C during the discharging cycle resulted in a dissipation of 9400 kJ and 11000 kJ, respectively, which is a difference in storage capacity of 1600 kJ. This slight increase in energy capacity was cause due to sensible heat transfer. A material stores sensible energy as a change in

temperature thus a greater initial temperature from the inlet temperature would result in an increase in sensible heat storage capacity.

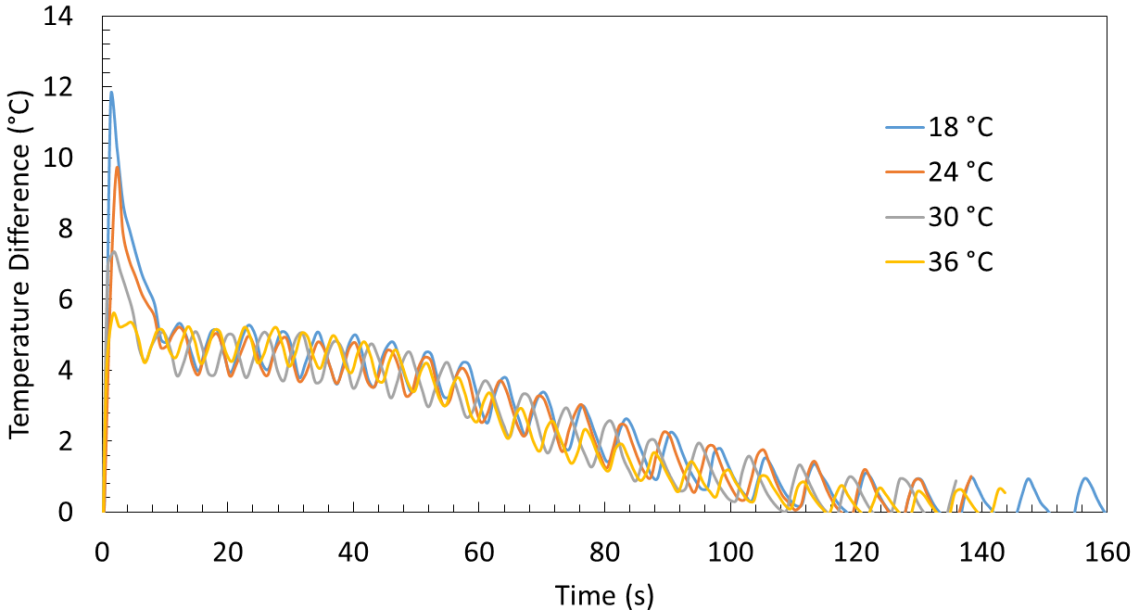

Figure 5.7 Inlet and Outlet Temperature Difference for Four Initial Temperature Values during Charging with Volumetric Flow Rate Setting of 1000 CFM (1699 m³/h) and HTF Heating Temperature Setting of 54˚C

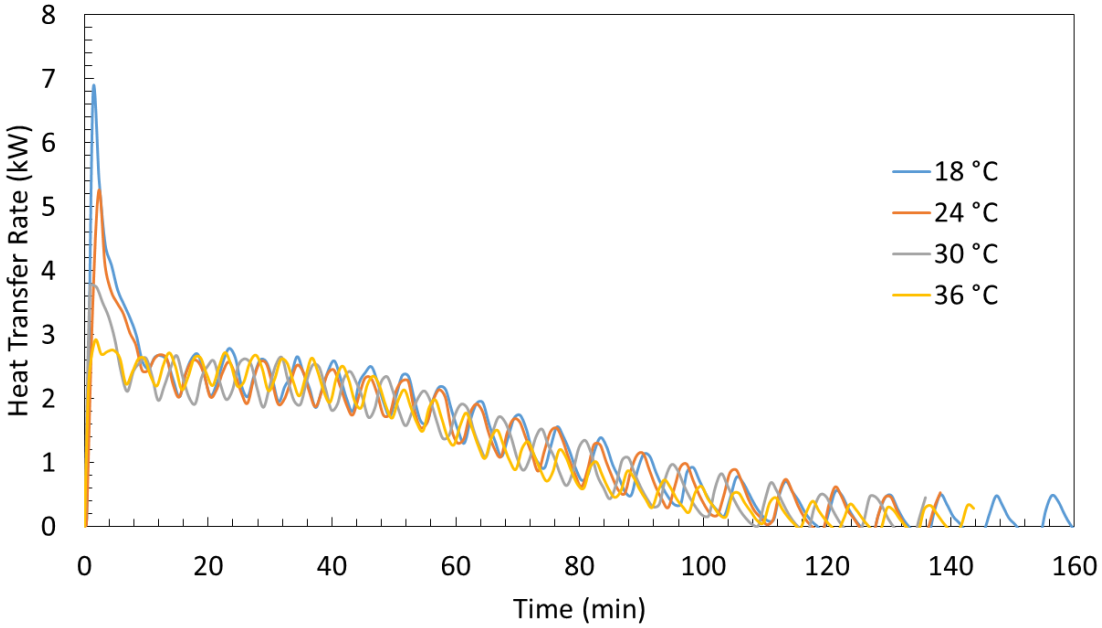

Figure 5.8 Heat Transfer Rate for Four Initial Temperature Values during Charging with Volumetric Flow Rate Setting of 1000 CFM (1699 m³/h) and HTF Heating Temperature Setting of 54˚C

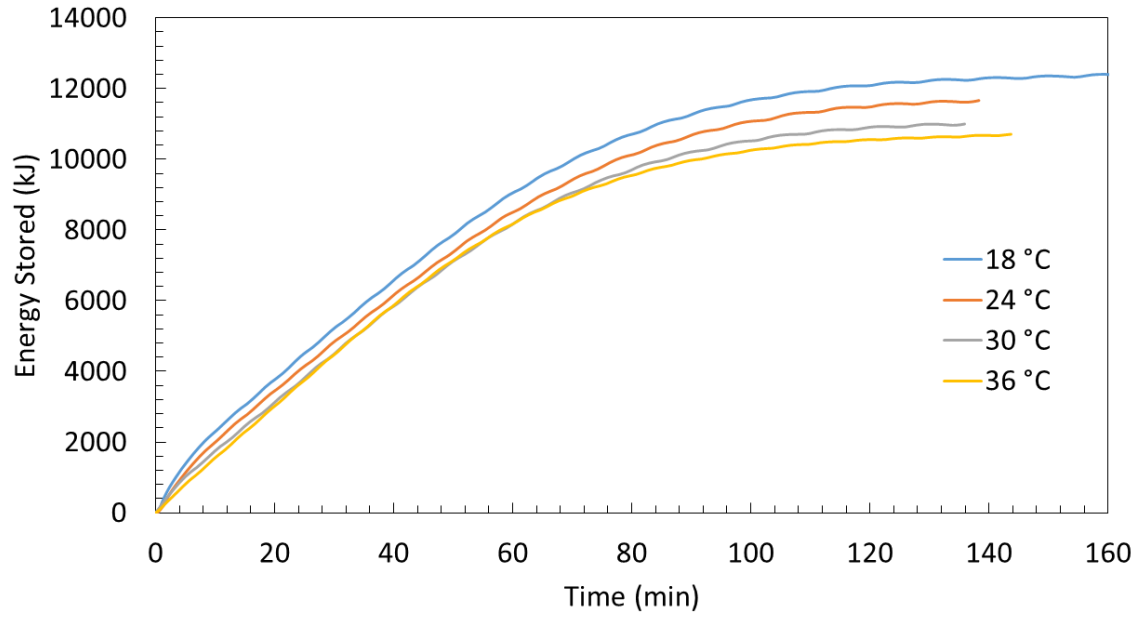

Figure 5.9 Cumulative Heat Transfer for Four Initial Temperature Values during Charging with Volumetric Flow Rate Setting of 1000 CFM (1699 m³/h) and HTF Heating Temperature Setting of 54˚C

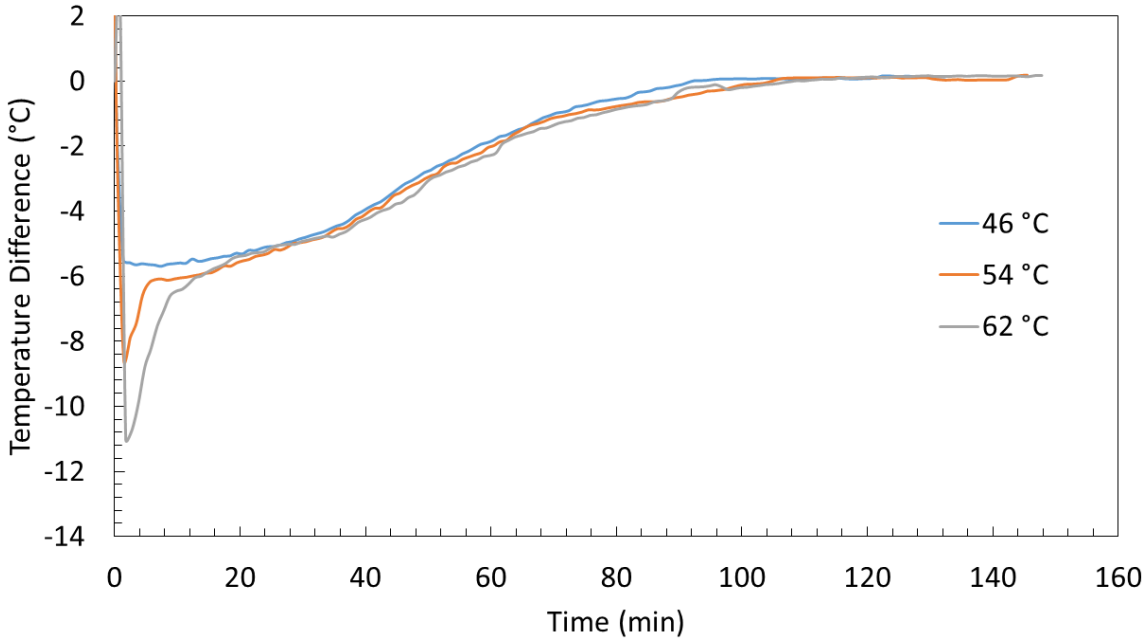

Figure 5.10 Inlet and Outlet Temperature Difference for Four Initial Temperature Values during Discharging with Volumetric Flow Rate Setting of 1000 CFM (1699 m³/h) and HTF Cooling Temperature Setting of 30˚C

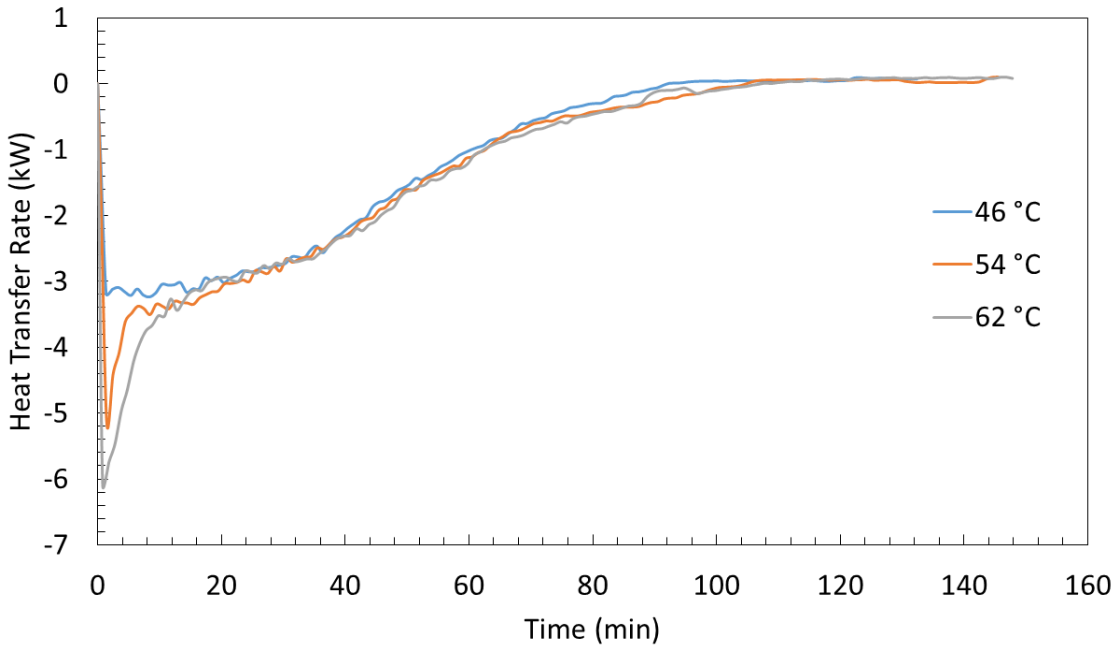

Figure 5.11 Heat Transfer Rate for Four Initial Temperature Values during Discharging with Volumetric Flow Rate Setting of 1000 CFM (1699 m³/h) and HTF Cooling Temperature Setting of 30˚C

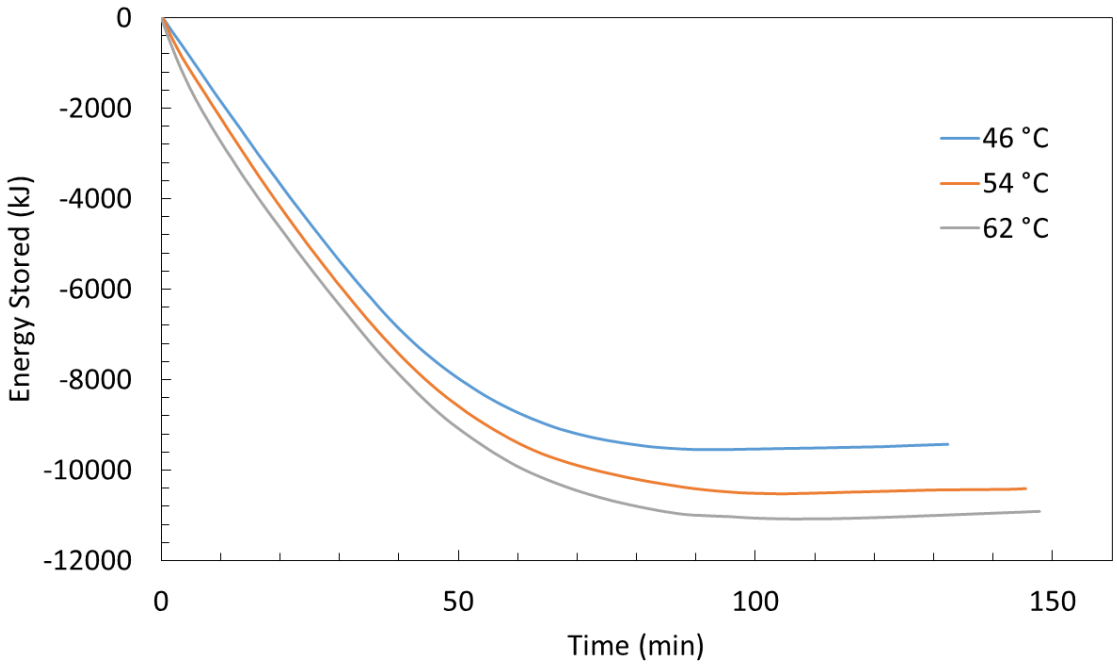

Figure 5.12 Cumulative Heat Transfer for Four Initial Temperature Values during Discharging with Volumetric Flow Rate Setting of 1000 CFM (1699 m³/h) and HTF Cooling Temperature Setting of 30˚C

5.3 Variations in HTF Inlet Temperatures

It was also important to determine the effects of the HTF inlet temperature on the PCM system's performance. Several tests were performed and compared to determine the effect of this parameter. The charging cycle was performed three times with a flow rate setting of 1000 CFM (1699 m^3/h), an initial temperature setting of 30˚C and varying heating temperature settings of 46˚C, 54˚C and 62˚C. The discharging cycle was performed four times with a flow rate setting of 1000 CFM (1699 m^3/h), a heating temperature setting of 54˚C and varying cooling temperature settings of 18˚C, 24˚C, 30˚C and 36˚C. The inlet and outlet temperature difference, instantaneous heat transfer rate and cumulative heat transfer are plotted in Figures 5.13 to 5.15 for the charging cycle and Figures 5.16 to 5.18 for the discharging cycle. Note that the discharging test at an inlet temperature of 24˚C had a momentary raise in inlet temperature due to a malfunction in laboratory equipment resulting in a spike in temperature difference and heat transfer rate seen in Figures 5.16 and 5.17 at 25 minutes.

It was observed in Figures 5.13 and 5.16 that a large temperature difference between the inlet temperature and melting temperature of the PCM resulted in a large temperature difference between the inlet and outlet of the PCM box and also shorter completion times. The completion time was recorded as the time at which the temperature difference first achieved a value of 0°C. A comparison of inlet temperatures and completion times can be seen in Table 5-2.

Table 5-2 Inlet Temperature vs Completion Time

Inlet Temperature (°C)	Inlet and Melting Temperature Difference (°C)	Completion Time (min)
Charging Cycle		
46	2	232
54	10	116
62	18	86
Discharging Cycle		
18	26	67
24	20	87
30	14	105
36	8	173

The instantaneous heat transfer rate was observed in Figures 5.14 and 5.17 to follow the same trend as the temperature difference in Figures 5.13 and 5.16. This was expected as the instantaneous heat transfer rate, as given in Eq (4.1), is only significantly dependent on temperature difference if the flow rate is held constant as in these tests. A larger temperature difference between the HTF and the PCM, as measured by the inlet and outlet temperature sensors of the PCM box, will result in a faster change in temperature of the PCM. All the PCM will not achieve the melting temperature at the same time but rater in layers of material particles with the outer particle layer achieving the melting temperature first. As discussed in the literature review, the melting of the PCM during charging introduces heat transfer by convection which eventually becomes the main mode of heat transfer instead of conduction. Thus, the faster the PCM achieves the melting temperature, the faster it will melt which will result in increased heat transfer by convection. The cycle would be slightly different for the discharging cycle where literature has shown convection to contribute little to the solidification phase. In this case, lower inlet temperatures will cause the PCM's first particle layer to achieve the melting temperature first having the greatest temperature difference between the HTF and PCM. As the first particle layer increases in temperature it will increase the temperature difference to the next particle layer until the entire PCM achieves the

melting temperature. This would trigger the solidification phase throughout the PCM increasing heat transfer rate to the HTF. The higher heat transfer rates for both charging and discharging result in greater temperature changes from the PCM to the HTF and thus a greater difference between the measurements of inlet and outlet temperatures.

It was observed in Figures 5.15 and 5.18 that an increase in total energy capacity occurred as the temperature difference between the melting temperature and inlet temperature of the PCM became greater. This is a similar observation to that of variations in initial temperature of the PCM made in Subsection 5.2. For instance, at an inlet temperature of 62 °C and 46°C during the charging cycle resulted in 12000 kJ and 10000 kJ respectively, which is a difference in energy storage capacity of 2000 kJ. The inlet temperature of 36°C and 18°C during the discharging cycle resulted in a dissipation of 9400 kJ and 11700 kJ, respectively, which is a difference in storage capacity of 2300 kJ.

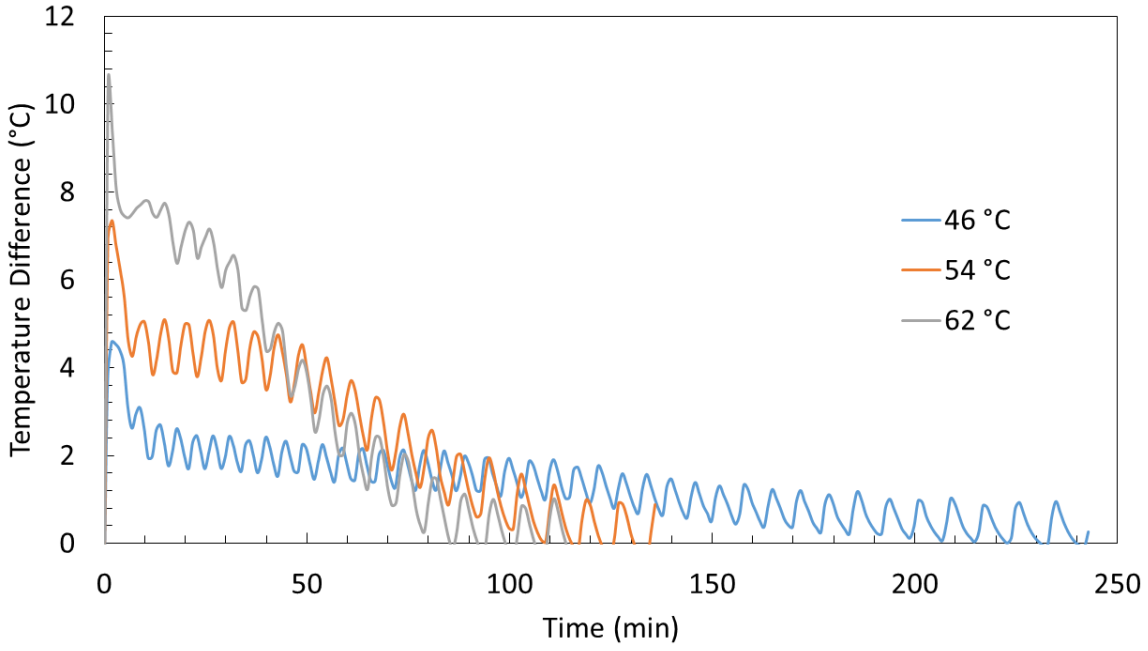

Figure 5.13 Inlet and Outlet Temperature Difference for Three HTF Heating Temperatures during Charging with a Flow Rate Setting of 1000 CFM (1699 m³/h) and an Initial Temperature Setting of 30˚C

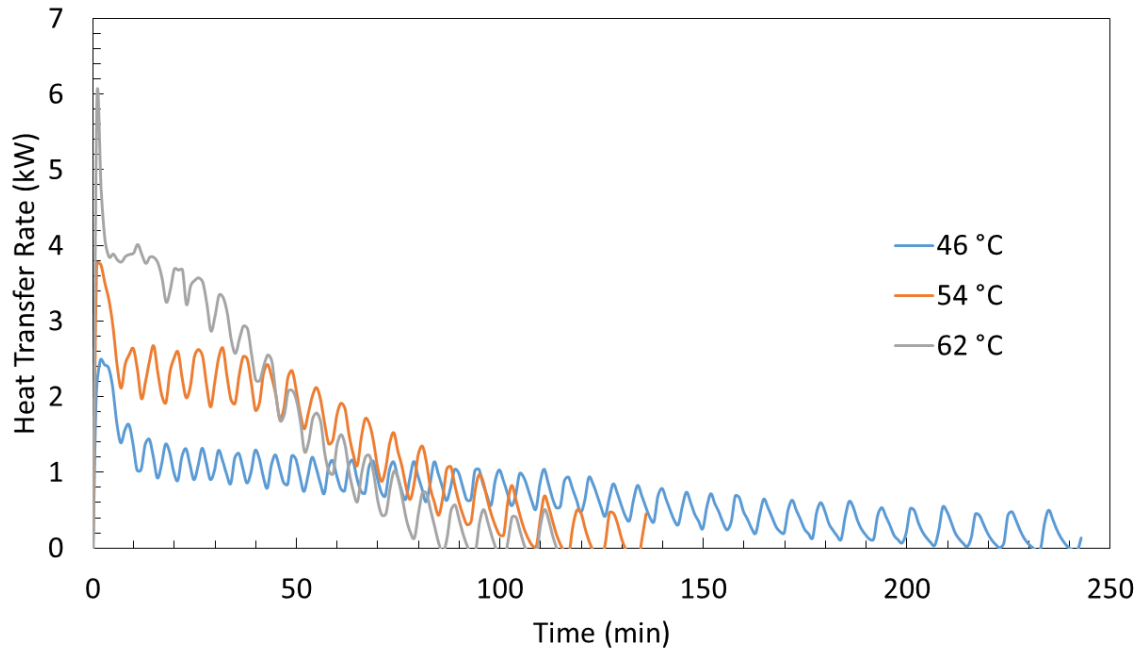

Figure 5.14 Instantaneous Heat Transfer Rate for Three HTF Heating Temperatures during Charging with a Flow Rate Setting of 1000 CFM (1699 m³/h) and an Initial Temperature Setting of 30˚C

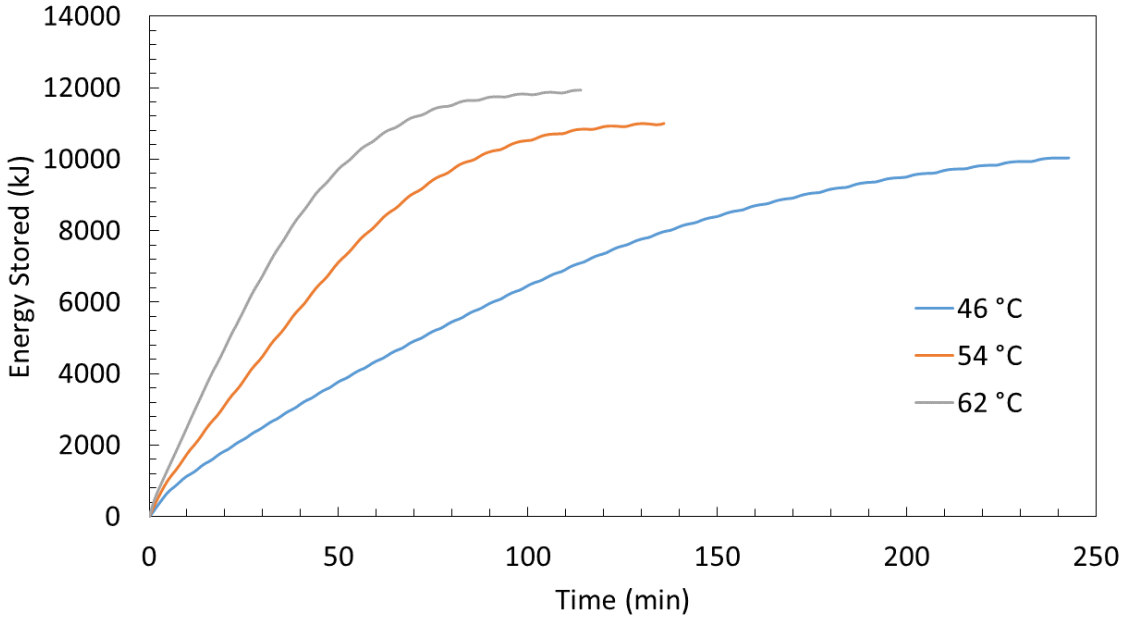

Figure 5.15 Cumulative Heat Transfer for Three HTF Heating Temperatures during Charging with a Flow Rate Setting of 1000 CFM (1699 m³/h) and an Initial Temperature Setting of 30˚C

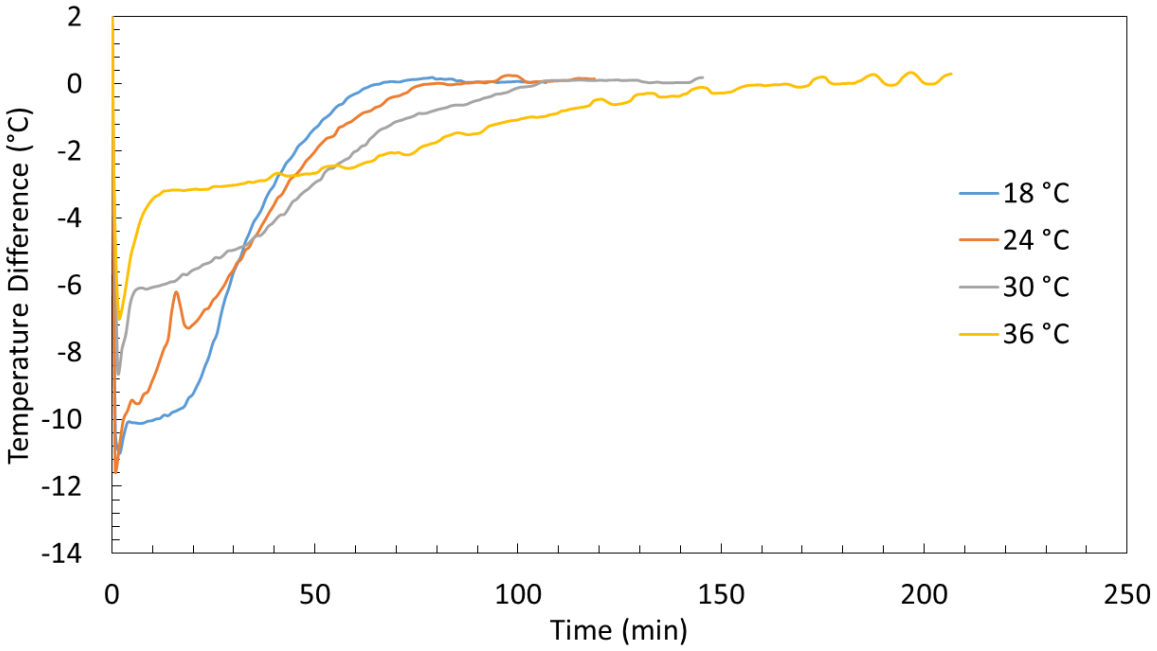

Figure 5.16 Inlet and Outlet Temperature Difference for Four HTF Heating Temperatures during Charging with a Flow Rate Setting of 1000 CFM (1699 m³/h) and an Initial Temperature Setting of 54˚C

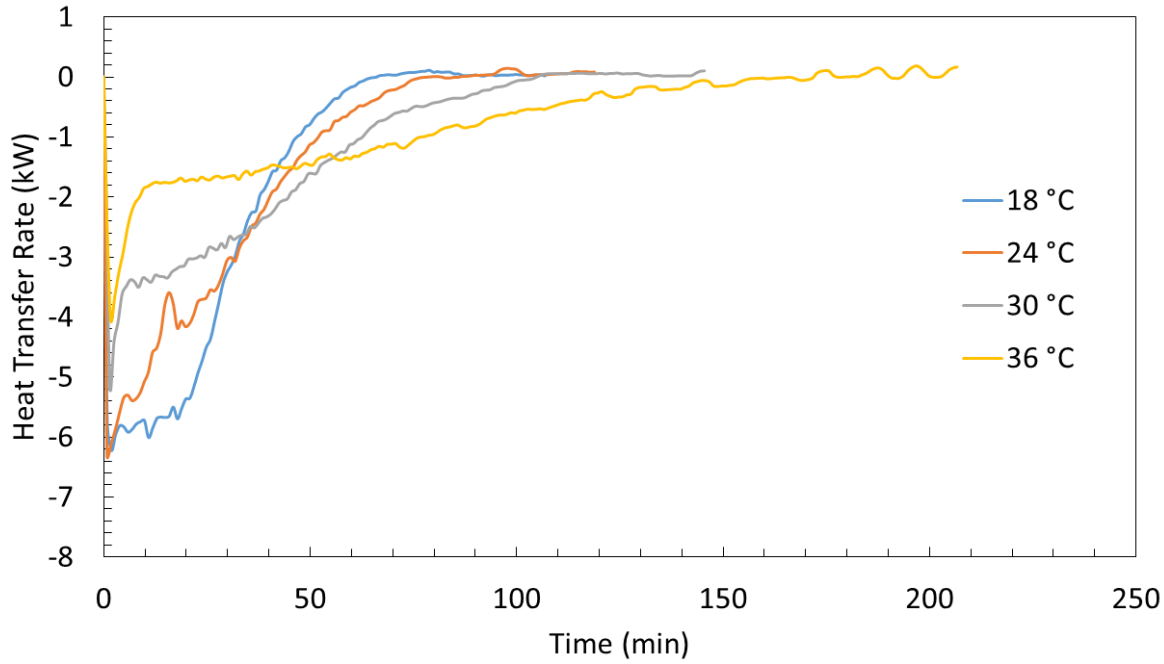

Figure 5.17 Instantaneous Heat Transfer Rate for Four HTF Heating Temperatures during Charging with a Flow Rate Setting of 1000 CFM (1699 m³/h) and an Initial Temperature Setting of 54˚C

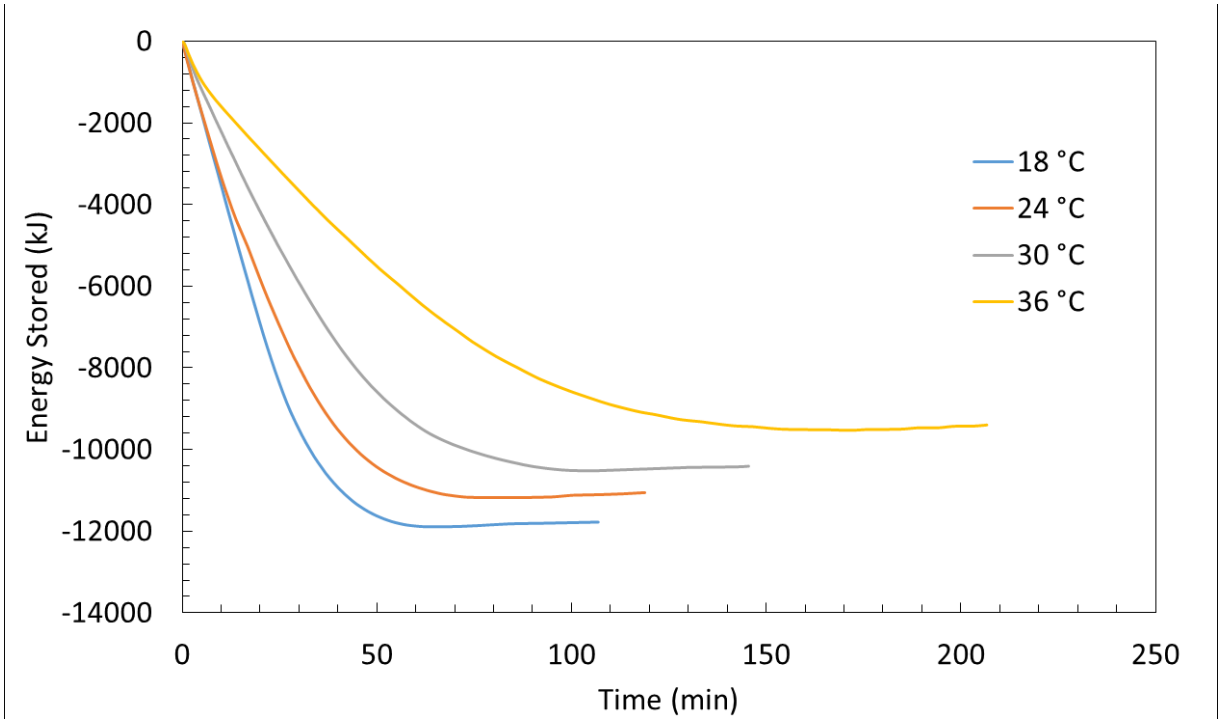

Figure 5.18 Cumulative Heat Transfer for Four HTF Heating Temperatures during Charging with a Flow Rate Setting of 1000 CFM (1699 m³/h) and an Initial Temperature Setting of 54˚C

This chapter described the characterization procedure of the PCM with AHU conditions. This characterization was done by varying three variables; the HTF flow rate, the initial temperature of the PCM and the HTF inlet temperature. The process provided information on heat transfer rates, energy capacity and completion time. The next chapter explains how this information was used in the creation of an empirical model of the PCM TES.

6 Chapter: Modelling Approach

Simulations using the TRNSYS software were conducted to determine how the integration of a PCM TES into an AHU would affect the amount of heat required from the AHU's heater. TRNSYS is a transient systems simulation software specializing mainly in thermal and electrical energy components. The program for each individual component such as a heater, solar collector, fan, etc. is stored in a module called a 'Type' and every different Type is assigned a unique number. The Type has a set of parameter and inputs which are used in transient calculations to display a set of outputs. In order to be able to incorporate the PCM TES into the TRNSYS AHU, the simulation of a TRNSYS 'Type' first needed to be created. The new Type created will be henceforth referred to as the PCM TES Type.

6.1 Phase Change Material Thermal Energy Storage Type

The need to create the PCM TES Type was to determine the heat transferred to the HTF at a specified temperature (an 'input' to the TRNSYS Type) and the new temperature of the HTF (an 'output' of the TRNSYS Type) based on the heat transfer rate during the current time interval. The PCM TES Type was programmed using a FORTRAN compiler. The full FORTRAN code can be viewed in Appendix L. This section will briefly describe the variables and an overview of the Type.

The variables of the PCM TES Type are shown in Table 6-1. The unit parameters, Cunit and Dunit, were used to retrieve the stored experimental data. This process will be discussed further in the subsection. The melting temperature of the desired PCM could be entered as a parameter at the beginning of the simulation. The desired PCM was required to have similar properties to RT44HC to produce valid results. The unit number was used to identify a unit if multiple PCM TES Types were used in the same simulation. The TotalUnitNumber parameter was

used to determine the total number of PCM TES Types used in a single simulation. The final parameter was used to specify the hour of the day when conversion from discharging to charging was desirable.

Table 6-1 PCM TES Type Variables

Parameters	Inputs	Outputs
Cunit	Tcharge	EnergyStorage
Dunit	Tdischarge	HeatTransfer
Tmelt	Hour	Mode
UnitNumber	ControlSignal	FlowOutput
TotalUnitNumber	FlowCharge	
HourChange	FlowDischarge	

The input variables consisted of the inlet temperature of the HTF used during the charging cycle, the inlet temperature of the HTF used during the discharging cycle, the hour of the day provided by Type 21 (an integer control signal used to indicate when the AHU was in operation), and the mass flow rate of air entering the Type when charging and discharging. The output variables consisted of the current amount of energy stored during the specified time interval, the heat transfer rate to the HTF, the mode that was used to communicate to the other Types whether the PCM TES Type was charging or discharging, and the output temperature of the HTF. Recall from Figure 3.8 that a temperature conversion was used between the experimental and application values with the experimental values having a PCM with a higher melting temperature than would be used in application. Thus, all temperature values read from the simulation were converted to higher values adding the difference in PCM melting temperature inserted in the parameters to the 44˚C melting temperature of the PCM used during experimentation. The mode was also used as an internal variable in the Type to initiate charging if set to 1 and discharging if set to 0. The time of day was used to trigger the mode variable depending on the desired control sequence. If the

AHU was not in operation, as indicated by the control signal, the PCM Type would neither charge nor discharge.

The TES PCM Type's main feature utilizes InterpolateData, a built-in FORTRAN utility subroutine [65]. This subroutine would retrieve and interpolate experimental data from a performance map using up to six independent variables. The PCM TES Type used two separate performance maps, one for the charging cycle and the other for the discharging cycle. Both maps had four independent variables; current amount of energy stored, inlet HTF temperature, the initial temperature of the PCM when the cycle began and the volumetric flow rate. The values used for each independent variable is shown in Table 6-2. The single dependent variable read from both maps was the instantaneous heat transfer rate. Note that the energy stored variable shows the range with the intervals over which a value was recorded for the performance map starting with zero.

Table 6-2 Values of Independent Variables used in the Performance Maps

Independent Variables	Charging Cycle	Discharging Cycle
Energy Stored (kJ)	0:14000 [500 intervals]	0:-14000 [500 intervals]
Inlet HTF Temperature (˚C)	46, 54, 62	18, 24, 30, 36
Initial Temperature (˚C)	18, 24, 30, 36	46, 54,62
Volumetric Flow Rate (CFM)	600, 800, 1000	600, 800, 1000

The experimental data was acquired by performing 36 tests using the full cycle test procedure implementing the independent variables from Table 6-2 while recording data every minute. The instantaneous heat transfer rate and energy stored were calculated and graphed with the rate of heat transfer on the y-axis and energy stored on the x-axis. As previously noted, there were considerable oscillations in temperature readings due to the PID controller, particularly during the charging cycle. In order for the subroutine to read the performance maps, the oscillations needed to be reduced. This was accomplished by adding a trend line to the heat transfer versus energy graphs with high linear regression values close to 1. The equation of the trend lines were

obtained and used to calculate the heat transfer values from the corresponding amount of the energy stored in 500 kJ intervals. A section of the performance maps is demonstrated graphically in Figure 6.1 for the charging cycle and in Figure 6.2 for the discharging cycle.

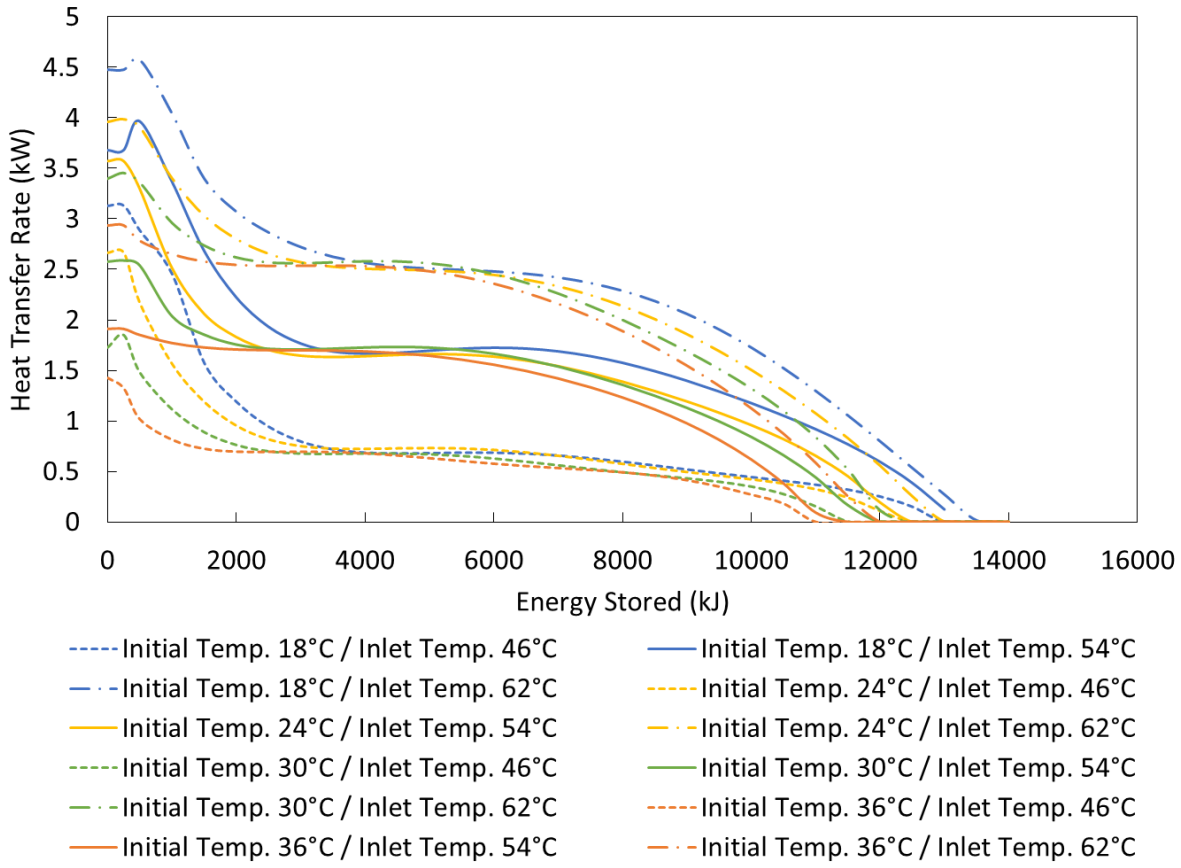

Figure 6.1 Section of the Charging Performance Map using 600 CFM (1019 m³/h) Flow Rate.

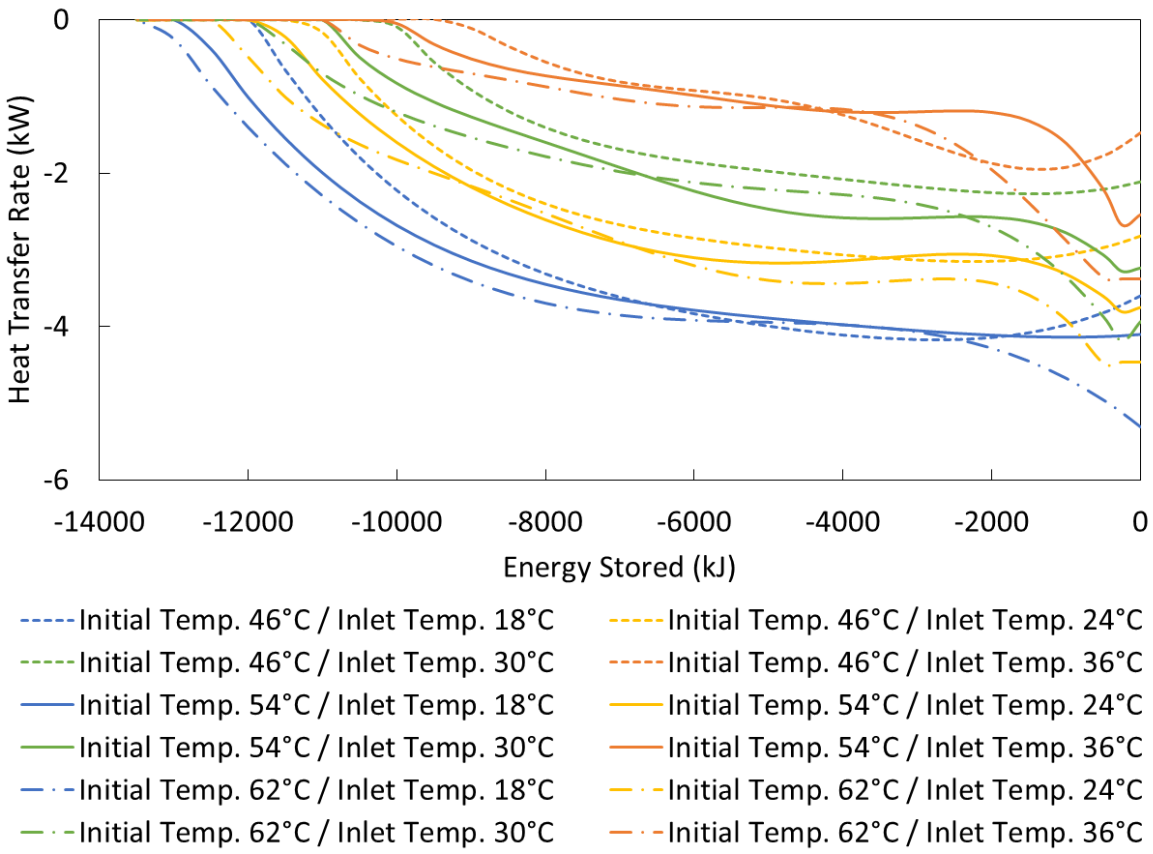

Figure 6.2 Section of the Discharging Performance Map using 600 CFM (1019 m³/h) Flow Rate.

The key independent variable for retrieving data from the performance maps was the energy storage value. Both the inlet HTF temperature and the inlet flow rate were provided by the simulation and the initial temperature was stored at the end of the previous iteration and remained constant until the mode changed. The Type initiated in the discharge cycle with the PCM being fully charged. The energy stored began with a value of 0 kJ indicating the PCM was at maximum capacity for the corresponding initial temperature. The subroutine would interpolate the performance map with the indicated variables and output rate of heat transfer. The rate of heat transfer was then used to calculate the addition energy dissipated (or stored for the charging cycle) for the given time interval. This value would be used to determine a new value for total energy stored that would be used as the energy stored value during the next interval. When the mode

changed, the energy stored value would be reset to 0. The same method was used to obtain heat transfer values during the charging cycle as well. Note that the energy stored values are positive for the charging cycle but negative for the discharging cycle indicating energy dissipation from the storage material.

The PCM TES Type has several limitations that originate from the experimental limitations. These limitations did not prevent the usage of the Type for its main purpose of determining the effect that a PCM TES flat plate design would have when integrated into an AHU. They might however present a challenge if the Type were attempted to be used for another application in a different study. These limitations are as follows:

1. The PCM TES Type can only be used with the flat plate design with the geometry described and used during experimentation;
2. The volumetric flow rates are limited between 600 to 1000 CFM (1019 to 1699 m^3/h) ;
3. The inlet HTF temperatures are limited based on the parameter value of the PCM melting temperature set before running the simulation. The inlet temperature must result in a temperature difference from the PCM melting temperature of 8 to 26˚C for charging and 2 to 18˚C for discharging;
4. The Type is limited to use melting temperatures of PCM with similar properties to RT44HC;
5. The Type will not take into consideration whether the previous cycle was fully charged or discharged. The cycle will start with the assumption that the previous cycle was fully charged or discharged.

6.2 Type Validation

The PCM TES Type was validated by comparing experimental data to results obtained from the TRNSYS simulations using the Type. The experimental data were obtained by running one charging cycle and one discharging cycle that varied the inlet temperature over the test temperature range; 62°C to 46°C for charging and 36°C to 18°C for discharging. The air flow rate was also varied over the range, once during charging and again for discharging. The TRNSYS data was obtain by using the temperatures and flow rates used during the experiment. The comparison for heat transfer rate and energy stored can be seen in Figure 6.3 and Figure **6.4** for charging and in Figure 6.5 and Figure **6.6** for discharging.

In general, there is good agreement between the experimental data and the simulation data. It is noted that after the 3000 s mark in Figure 6.3 that the inlet temperature and air flow rate were constant and the oscillation seen was caused by the PID controller. The TRNSYS Type does not follow the oscillations as accurately because as mentioned previously the oscillations were smoothed out when the performance maps were created. This is less apparent during discharging where oscillations from the PID controller are less frequent.

The difference between the TRNSYS and experimental energy storage values becomes greater over time as seen in Figure 6.6. This was due to the error accumulation in the energy storage calculation as discussed in Subsection 4.2. There was some discrepancy observed between the heat transfer rate results in the discharge cycle in Figure 6.5. Regrettably the programming of the laboratory cold water lines was changed before the validation test could be performed. This impacted the heat transfer rate in the chilled water thermacoil. While the initial inlet temperature was achieved, once the dampers opened the inlet temperature overshot the setpoint value becoming warmer than desired before gradually cooling to the desired temperature where it would remain

for the remaining duration of the validation test. Even with the discrepancy, the heat transfer rate results follow a similar trend particularly near the end of the test.

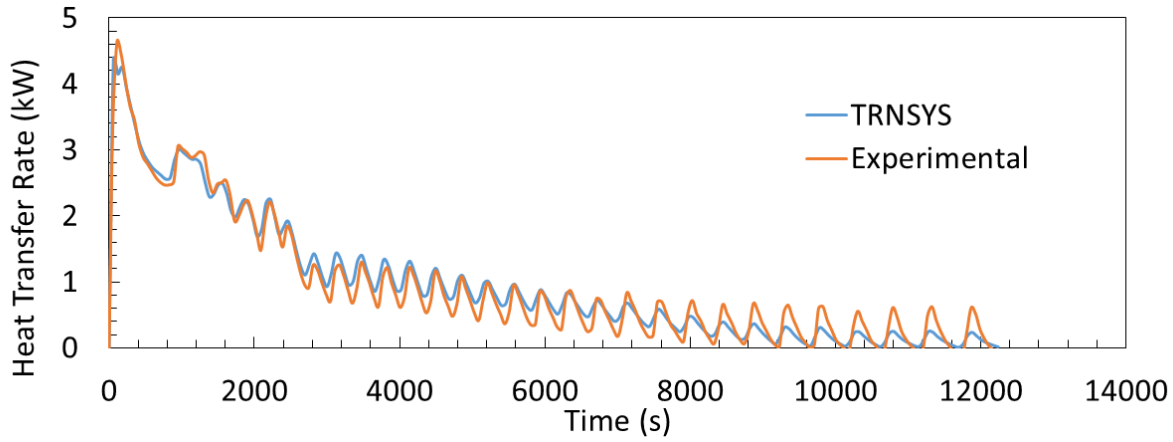

Figure 6.3 Comparison of TRNSYS Type and Experimental Heat Transfer Rate of Charging Cycle with Initial Temperature Setting of 18°C, Flow Rate of 600 CFM (1019 m³/h), Heating Setting of 62°C with Varying Inlet Temperature and Flow Rate throughout Test

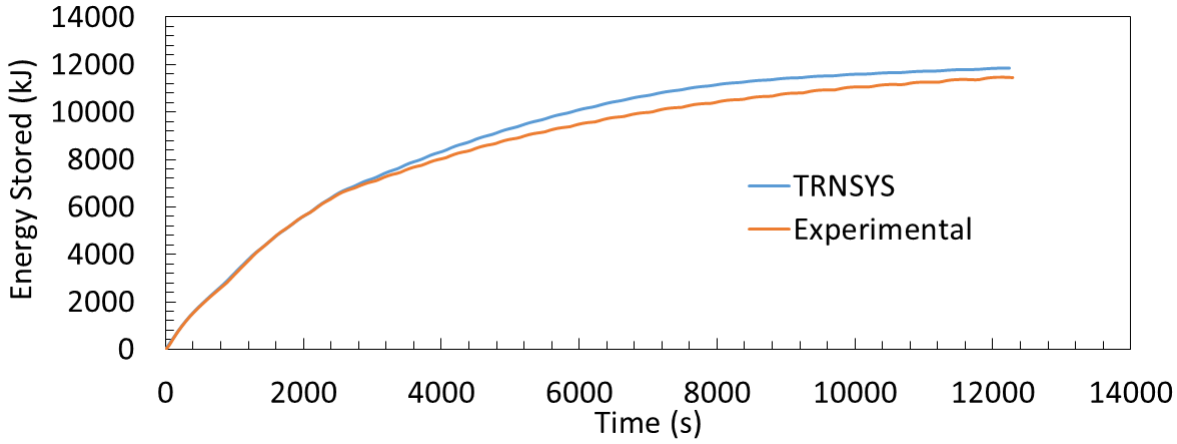

Figure 6.4 Comparison of TRNSYS Type and Experimental Energy Storage of Charging Cycle with Initial Temperature Setting of 18°C, Flow Rate of 600 CFM (1019 m³/h), Heating Setting of 62°C with Varying Inlet Temperature and Flow Rate throughout Test

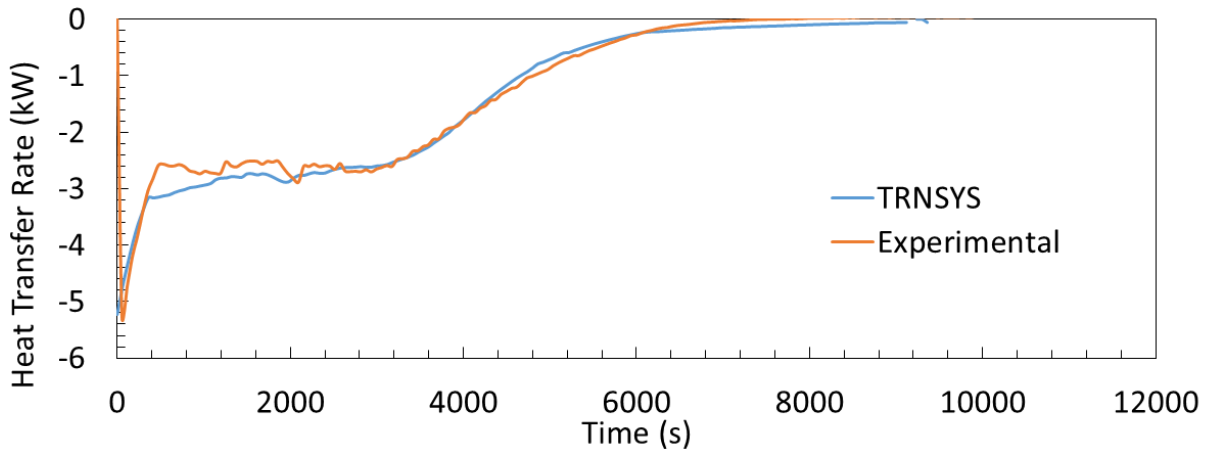

Figure 6.5 Comparison of TRNSYS Type and Experimental Heat Transfer Rate of Discharging Cycle with Initial Temperature Setting of 62°C, Flow Rate of 1000 CFM (1699 m³/h), Cooling Setting of 36°C with Varying Inlet Temperature and Flow Rate throughout Test

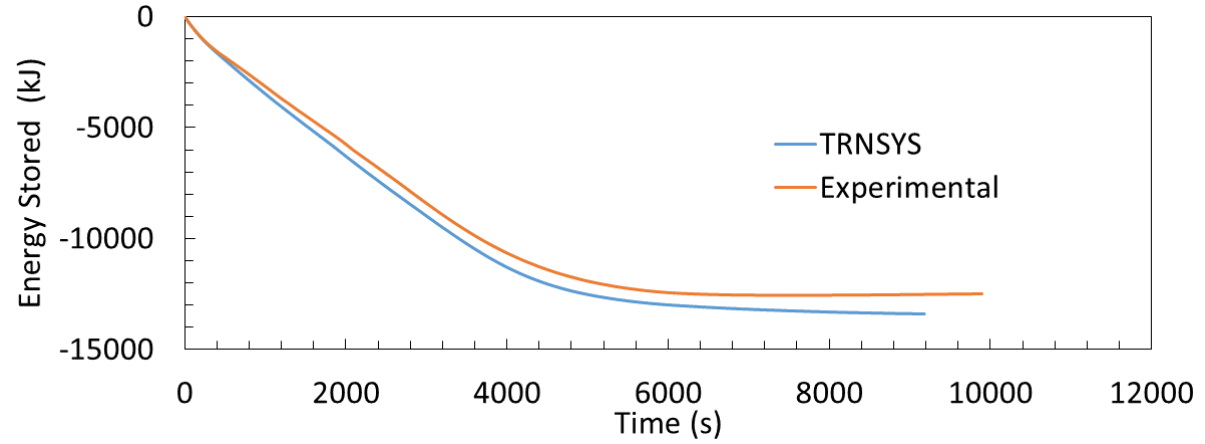

Figure 6.6 Comparison of TRNSYS Type and Experimental Energy Storage of Discharging Cycle with Initial Temperature Setting of 62C, Flow Rate of 1000 CFM (1699 m³/h), Heating Setting of 36C with Varying Inlet Temperature and Flow Rate throughout Test

6.3 Base Air Handling Unit

The base model was constructed to model the original AHU in order to compare its performance with an AHU with an integrated PCM TES unit. The most important factors when analyzing the AHU for improvements were the rate of heat transfer and the power required of the AHU heater. Note that in this instance, "power" refers to the thermal energy required to heat the

air and not the electrical power to operate the other components of the AHU such as the fan or the dampers. The base AHU used the building data and several Type components to simulate the same supply temperature as the real AHU. The building AHU data were provided on 15 minute intervals for most days through the months of January to March 2015. The information included the maximum volumetric flow rate of the fan, the variable control signal of the fan, the mixed air temperature, the supply air temperature, the return air temperature and the outdoor air temperature. It should be noted that the building AHU that was used for this analysis was not the only heat contributor for the building. There was a second identical large AHU and two smaller AHUs. This study did not focus on the temperature of the building overall but rather on the heater heat transfer rates of the chosen AHU. For this reason, the supply temperature is assumed to be the desired temperature of the building and the building will be considered successfully heated if the outlet air flow rate and temperature from the simulation matches the building data.

6.3.1 TRNSYS Simulation Component Layout

The simulation for the base AHU was created in TRNSYS. The AHU was modelled as four major components including the fan, inlet damper, outlet damper and heater. This was done so that the PCM TES type could be installed between various components depending on the desired configuration and the AHU would still be able to operate using the inputs from the building data. A schematic of the TRNSYS layout for the base AHU simulation is shown in Figure 6.7 with the TRNSYS interface schematic layout shown in Appendix M.1. The TRNSYS components used were Type 646 (an air diverting valve for Damper 1), Type 648 (an air mixing valve for Damper 2) and Type 6 (a heater designed to add heat to a flow stream to achieve a setpoint temperature). A calculator was used to output the mass flow rate of the AHU using the flow signal and return temperature of the building data. The heat transfer rate of the heat was set to a high limit so that

heating demands would be met at all times of the simulation. The heater was not used to replicate the building AHU heater but rather to provide a heat rate required base line for simulation comparison.

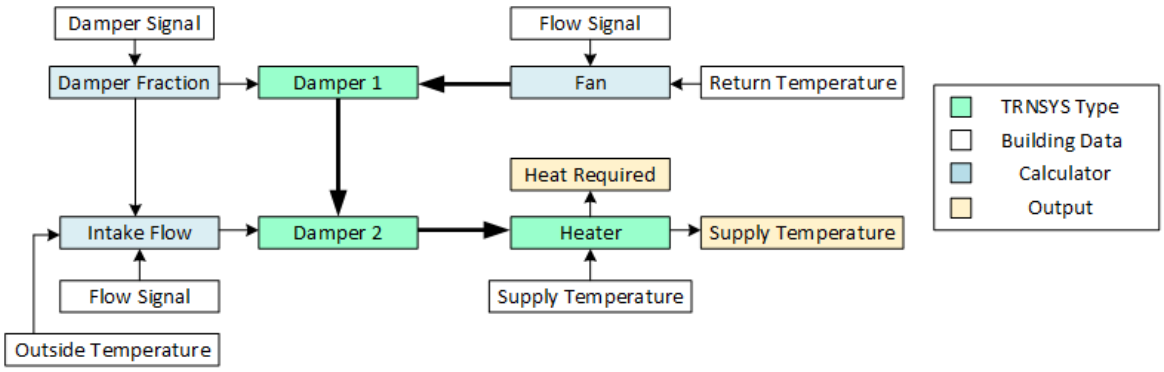

Figure 6.7 Schematic Layout of Base AHU Simulation

Obtaining the proper flow rate for each component was an important part of this study. The volumetric flow rate of the fan at the inlet of the AHU was the only indication of flow provided by the building data. For this simulation to function properly, it was necessary to determine the flow rate through both dampers. A new data set called damper signal was determined by calculating the percentage of intake and exhaust air flow to the AHU by using the fan flow rate, the mix temperature from the return air mixing with the intake air, the outdoor temperature and the return temperature with the assumption that the exhaust and intake flow rates would be the same as specified in the controls manual, see Appendix N for full calculations.

6.3.2 Data Analysis of Base Air Handling Unit

In order to demonstrate that the AHU functioned properly when separated into components, the mix and supply temperatures of the TRNSY AHU were compared. The mix temperature was not read directly from the data set but was calculated from the damper components thus it was important to verify that the proper mix temperature was achieved. Figure 6.8 shows good agreement between mix temperatures, with the building data being slightly higher by

approximately 0.4 °C. The supply temperature of the building data was used as the setpoint of the heater. The supply temperatures are compared to ensure that the heater was able to provide the required heat transfer rate to achieve the setpoint temperature. Figure 6.8 shows that the supply temperatures are identical, thus the TRNSYS Type heater was adequate for the simulation.

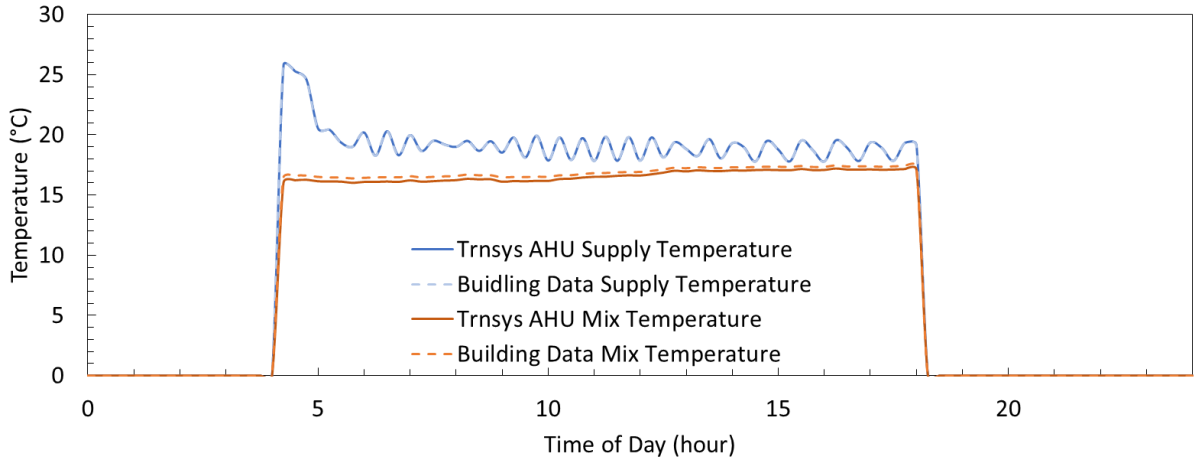

Figure 6.8 Supply and Mix Temperature Comparison between TRNSYS AHU and Building Data

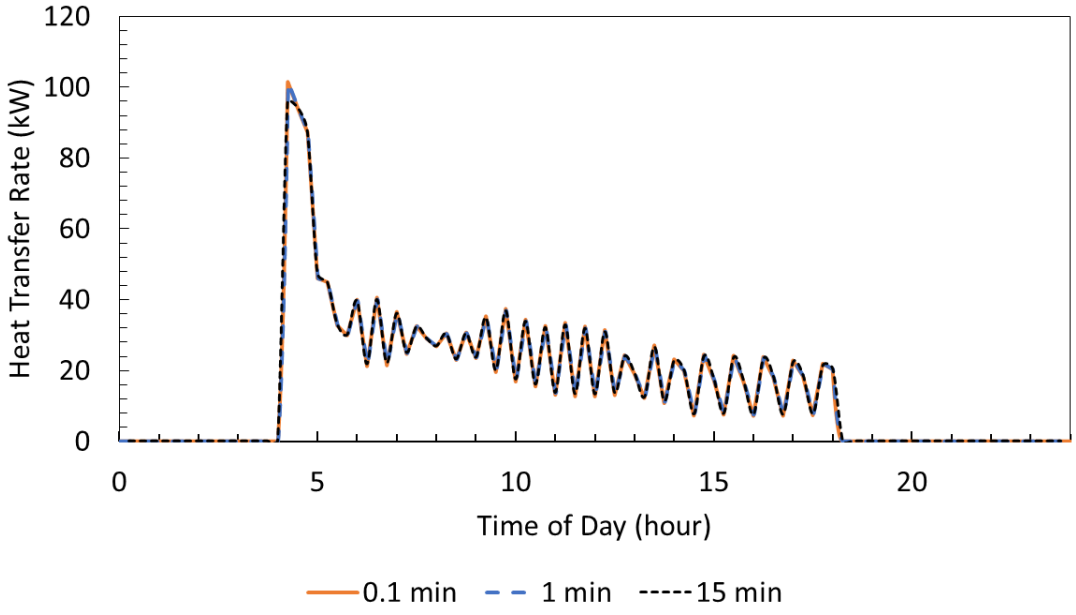

Figure 6.9 Comparison between Simulation Time Intervals for Base AHU

The simulation time step was determined by comparing rate of heat transfer results for the simulation heater at three different time steps: 15 minutes, 1 minute and 0.1 minute. A smaller

time step would produce more accurate results however it would also take more computation time. Figure 6.9 demonstrates that all three time steps give similar results overlapping in most areas, except at the beginning of the rate of heat transfer where the 15 minute time step was not as detailed as the others. For this reason, a simulation time step of 1 minute was chosen for all simulations in this study.

6.4 Air Handling Unit with Integrated PCM TES using Method 1

The TRNSYS program was also used to simulate an AHU with the PCM TES using the Integration Method 1 of Strategic Heating previously discussed in Section 1.4.1. Recall that this method charged the storage unit during the day (when outdoor temperatures are higher thus requiring less energy from the heater) and discharged during the early morning to the outdoor intake air in an attempt to reduce the sharp power peak produced upon start-up of the AHU.

6.4.1 PCM TES Type Configurations

The AHU subroutine in TRNSYS modelled a commercial building's scale AHU and the PCM TES Type was developed based on laboratory scale experiments. That is, to resolve the scale difference, multiple PCM TES units were implemented in parallel. The number of PCM TES units used was dictated by the exhaust flow entering the storage units. It was determined that the simulations would require four PCM TES units to meet the flow rate limitation of the Type. The flow rate was split evenly between each unit. This scenario was implemented in TRNSYS using one PCM TES Type for one set of parallel units. The flow was assumed to enter and exit in the same manner for each unit which would result in comparable outlet temperatures. Thus, the inlet mass flow rate was divided by four and the outlet flow rate of the PCM TES Type was multiplied by four.

The total mass and heat transfer rate was varied by placing the PCM TES units in series. This was implemented by using the outlet mass flow rate and temperature from the previous PCM TES Type as inlet values to the next unit in the series. Several simulations were performed to determine the optimal number of PCM TES units for the application.

6.4.2 TRNSYS Simulation Component Layout

The simulation study of the air handling unit with integrated PCM TES with Method 1 used the major components from the base AHU simulation. The additional components including the placement of the PMC TES Type are discussed in the following section. The additional components include two new calculators (Flow Division and Mixing Flows), two new Types (PCM TES Type and Type 21), one new building data input (control signal) and one new recorded output (heat transfer of storage unit). The schematic of the component layout for the strategic heating PCM TES incorporation into AHU simulation is seen in Figure 6.10, see Appendix M.2 for image of layout in TRNSYS.

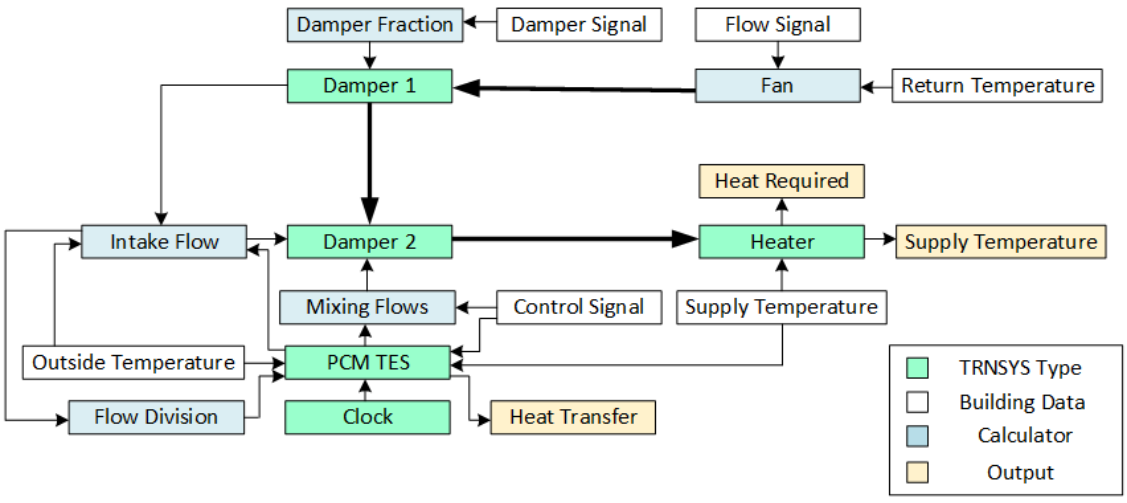

Figure 6.10 Schematic Layout of Strategic Heating PCM TES Incorporation into AHU Simulation

The additional calculators used with the PCM TES Type were called Flow Division and Mixing Flows. The Flow Division calculator calculated the flow rate for charging and discharging independently creating outputs that would be connected to the charge flow and discharge flow inlets of the PCM TES Type. For discharging the Flow Division calculator would obtain the value of the exhaust mass flow rate and divide by four for the four parallel storage units being represented by a single PCM TES Type. For charging, the Flow Division calculator was set to a permeant mass flow rate of 0.375 kg/s to provide a lower flow rate than the exhaust flow rate to achieve slower charging. The Mixing Flows calculator performed the opposite function of Flow Division. It would input the output flow rate and temperature of the PCM TES Type. Note that there was only one set of data and that charging and discharging cycles were not distinguished. There was also a new building data file added called Control Signal. This data file provided a '0' whenever the AHU was not operational and a '1' when the AHU was operating. The Control Signal data file was used as an input to the PCM TES Type as well as to the Mixing Flows calculator.

The PCM TES Type used Type 21 would receive the hour of the day. The strategic heating strategy used the supply air from the outlet of the heater with the lowest flow rate setting within the limitations of the PCM TES Type as the input during charging and output to the mix air stream to be reheated by the heater. During discharging, the outside temperature and intake flow were used as inputs to the PCM TES Type and output once again to the mix air stream before passing through the heater for any additional heating to achieve the setpoint temperature. Some modifications were made to Damper 2 which was changed to incorporate three intake streams to create the mix stream, one for the return air, one for the outdoor air and one for the additional air from the storage unit. Both the return air and storage unit air streams would flow continually in accordance with the strategy but the outdoor air was set to zero during discharge, as all the intake

air would pass through the storage unit instead. This was achieved by modifying the Intake Flow calculator with the additional input of the output mode of the PCM TES Type which would multiply the flow by zero when in the discharge cycle and by one during charging.

This chapter gave an overview of the empirical model of the PCM TES. This model utilized the data collected from the PCM characterization discussed in Chapter 5. The limitations of the PCM TES Type were outlined. A validation was presented by comparing experimental data to simulation data. Both the base AHU model and AHU model with PCM TES integrated using Method 1 of Strategic Heating were presented and discussed. The next chapter will display and analyses the results from various simulations using these models.

7 Chapter: TRNSYS Simulation Results

The TRNSYS simulation software was used to analyze the Integration Method 1 of Strategic Heating. This chapter will present and discuss the results of several simulations. Simulations were first run using only one PCM TES Type over the duration of a single day. Simulations were then run to examine the behavior of the PCM with different melting temperatures. After, simulations were run with various configurations of PCM TES units in series which were then compared to determine the optimum configuration for the application. Finally, simulations using the optimum melting temperature and configuration were performed over the duration of multiple days.

7.1 Results over a Single Day

The Integration Method 1 of Strategic Heating simulation was first performed with one PCM TES Type to study how the AHU would interact with the PCM TES for the duration of a single day. Recall that one PCM TES Type represents four storage units in parallel. The building data used were from February 4th, 2015 and had outdoor temperatures varying between -6.2°C to -12.5°C during hours of operation. The initial temperature of the PCM for the discharge cycle was set to 19°C which represents the final charging temperature from the previous day. The Hour Change parameter was set to 8 AM. As the start of operation was at 4 AM, the discharge cycle lasted for a duration of 4 hours. The unit number and total unit number parameters were set to '1' as there was only one PCM TES Type for this simulation. Finally, the melting temperature parameter was set to 11°C indicating that RT11HC would be the potential PCM used for this integration method. This PCM was chosen as the discharging was needed to be short to minimize the peak and the charging cycle could last the rest of the day. Thus, a melting point closer to the charge temperature was desirable. Recall that there were three PCM that had similar properties to

the PCM used during experimentation, RT18HC, RT11HC and RT5HC. Unfortunately, RT18HC was eliminated as an option as the input charging temperature would have exceeded the limitations of the PCM TES Type outlined in Subsection 6.1. Note that all the following graphs will show the 24 hours of a single day. The AHU began operating at 4:00 AM and ended operating at 6:00 PM. Data was only plotted during the hours of operation.

Figure 7.1 shows the various mass flow rates that exist at different locations of the AHU, see Figure 1.3, including the fan output (or return flow from the building), the flow recirculated, the mixed flow, the exhaust flow, the intake flow, the PCM TES outlet flow and the supply flow to the building. It was observed that the mixed mass flow rate, shown in green, increased from the addition of the PCM TES mass flow outlet, shown in black, during the charging cycle. Although an increase was observed in the mixed mass flow rate, the supply mass flow rate remained comparable to the mass flow rate of the fan output, keeping the pressure difference inside the building constant. This was due to 0.375 kg/s of air being redirected from the supply flow rate to the PCM TES units. Once the air passed through the PCM TES units it would re-enter the AHU and become a part of the mixed mass flow rate. The recirculated mass flow rate was observed to follow the same trend as the fan mass flow rate only at lower flow rate values, as a percentage of the original flow has been exhausted to the outside. Another observation was that the intake mass flow rate was identical to the exhaust mass flow rate as specified in the control program of the AHU to prevent any pressure changes inside the building. The value of the PCM TES outlet mass flow rate was observed to be identical to the value of the exhaust mass flow rate during the first four hours of operation as it was replacing the intake stream, which has been closed, to heat the outdoor air during the discharging cycle. It was important to keep the mass flow rate in the PCM TES equal to the mass flow rate at the exhaust during the discharging cycle to prevent pressure

differences in the building. Once the PCM TES Type changed from the discharging to charging mode at 8 AM, the intake valves were opened and a flow rate value was observed. The inlet mass flow rate to the PCM TES was set to a constant value and was no longer programmed to copy the exhaust mass flow rate.

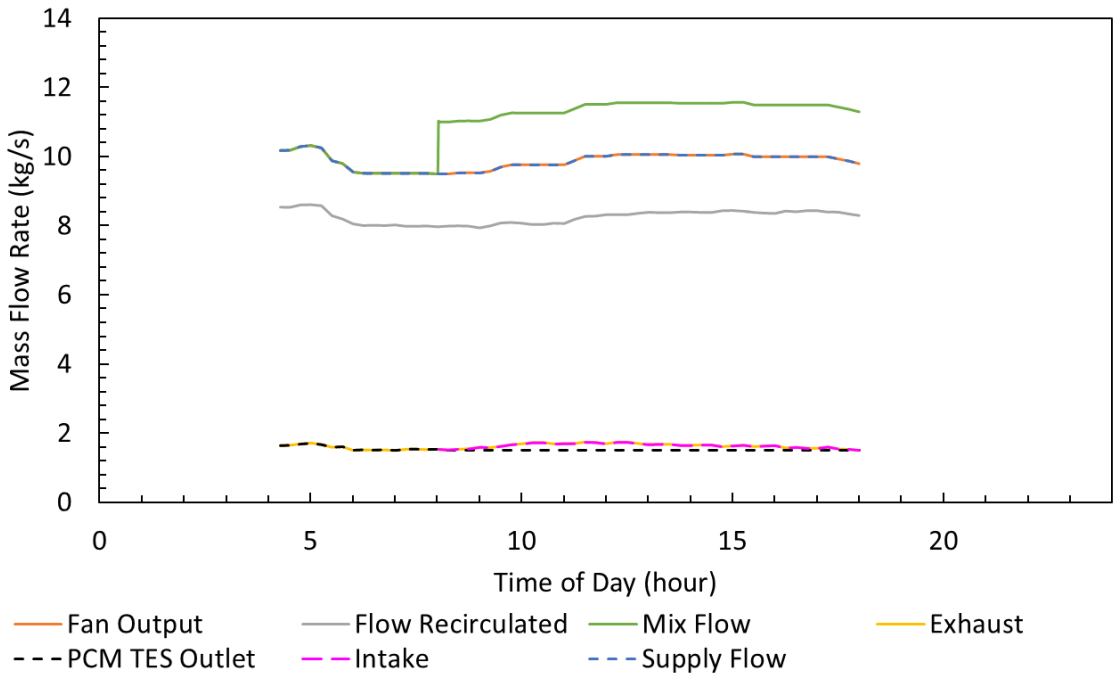

Figure 7.1 Mass Flow Rates through the AHU using One PCM TES Type for a Single Day

It was important to determine whether the flow rate limitations of the PCM TES Type outlined at the end of Subsection 6.1 were not exceeded. A conversion was required as the PCM TES inlet flow rate parameter was in units of mass flow rate and the limitations were in units of volumetric flow rate. The inlet temperature was used to calculate density for the conversion. The volumetric flow rates for the discharging and charging cycles are shown in Figure 7.2 with the lower limitation of 600 CFM (1019 m^3/h) included. All volumetric flow rates were observed to be within the PCM TES Type limitations.

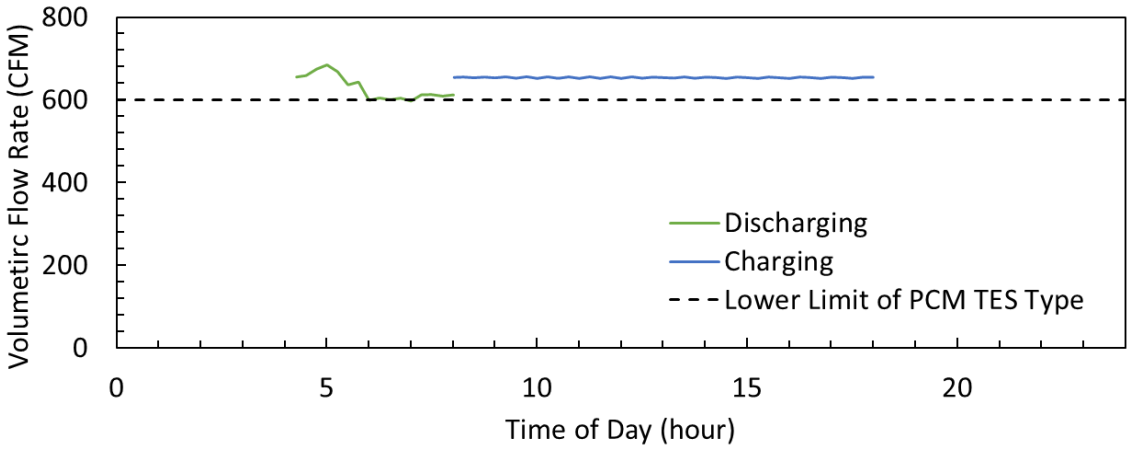

Figure 7.2 Volumetric Flow Rate through a Single PCM TES Type

A comparison between the mixed temperatures of the current simulation (an AHU with four parallel PCM TES units) with the mixed temperature of the base AHU is shown in Figure 7.3. It was observed that during discharging, the PCM TES was successful in raising the air temperature before entering the heater for the first hour by several degrees. At the very beginning of the charging cycle, the mixed temperature was observed to be below the base AHU mixed temperature. This was due to the large amount of heat initially stored in the PCM TES reducing the temperature of the HTF. As the cycle progresses, the storage units transfer less and less heat until the maximum capacity was obtained. After approximately two hours of charging, the mixed temperature was observed to be slightly higher than the base AHU. This is because unlike in the base AHU, a third stream from the PCM TES was added to the mixed air which previously only consisted of the recirculation and intake air. This third stream, taking air from the supply stream, was warmer than the other two and would thus rise the overall temperature when added.

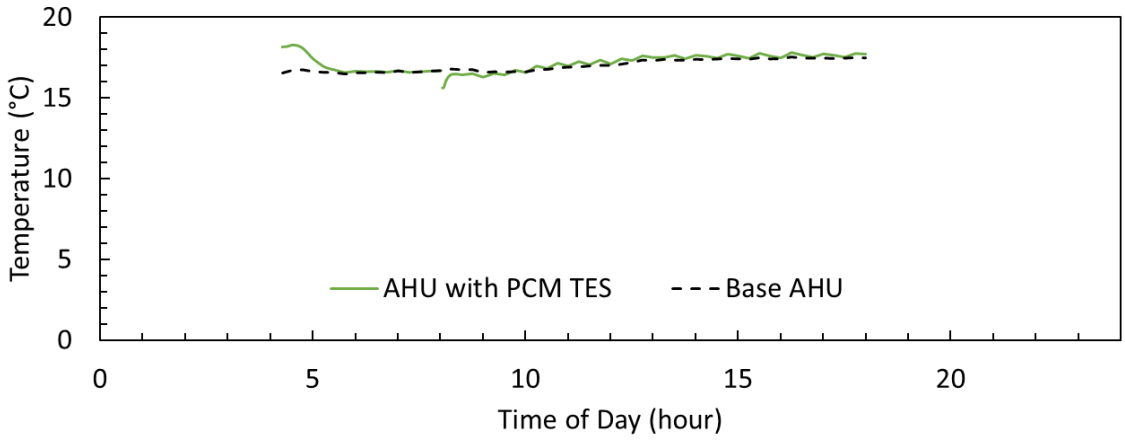

Figure 7.3 Mixed Temperature Comparison of AHU with One PCM TES Type from the Base AHU

Figure 7.4 shows the various temperatures that exist at different locations of the AHU, including the return temperature (air from the building), the outside temperature, the mixed temperature, the PCM TES outlet temperature and the supply temperature (air to the building). The return, supply and outside temperature would not have changed from the base AHU, but were included for perspective. The outdoor temperature was observed to be coldest in the early morning with a low of -12.5°C and gradually increased throughout the day to a high of -6.2°C before decreasing in the evening. At the beginning of the discharge cycle, the outdoor air was preheated by the storage units by approximately 10°C. This difference was maintained for a few minutes where the temperature of the PCM TES output was observed to decrease considerably until it attained an equivalent value as the outdoor temperature. During the charge cycle the inlet air to the PCM TES was a portion of the supply air. At the start of the cycle it was observed that the PCM TES outlet temperature was significantly lower than the supply due to the initial energy storage and warming of the cold air temperature from the discharge cycle. After the first few minutes of the charging cycle there was a 5°C temperature difference between the inlet and outlet of the PCM TES which gradually reduced until charging was complete and the PCM TES outlet temperature was the same as the supply temperature.

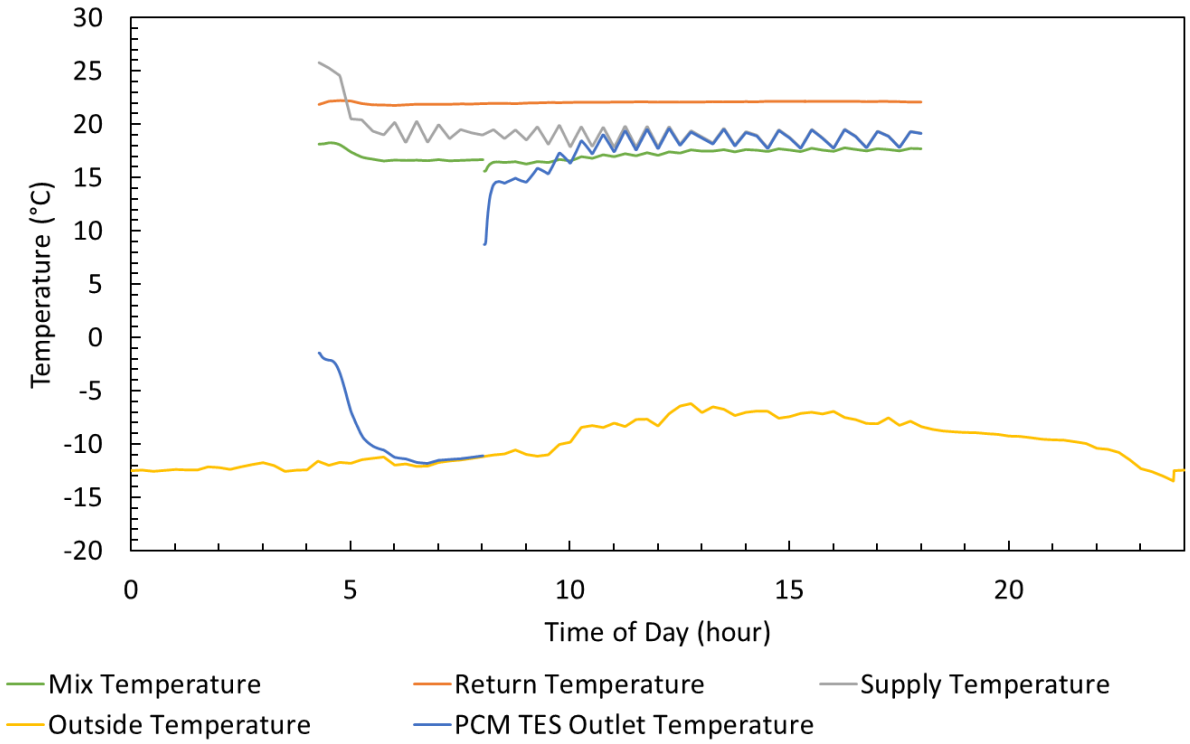

Figure 7.4 Temperatures through the AHU using One PCM TES Type

The heat transfer rate and energy storage of a single PCM TES unit are shown in Figure 7.5. As there were four units in parallel for this simulation, the total heat transfer rate would be the heat transfer rate demonstrated in Figure 7.5 multiplied by four. A sharp increase in heat transfer rate of approximately 4 kW was observed during discharging or 16 kW in total when considering all four units. This sharp increase was desirable to reduce the peak power upon start-up. The rate of heat transfer during charging was observed to be more gradual with an initial spike of 4 kW to approximately 2 kW for 1.5 hours or 16 kW and 8 kW respectively in total when considering all four units. It would, however, be desirable to have a smaller heat transfer rate over a longer period of time as there were hours of the day left available for charging that were not being utilized.

The power required from the heater from the first simulation was compared to that of the base AHU heater. Figure 7.6 shows the difference in the required rate of heat transfer between the two simulations. It was observed that the peak power required was successfully reduced by 16 kW

with the addition of PCM TES units which coincides with the heat transfer rate observation of the PCM TES Type from Figure 7.5. A small peak in required power was observed to pass above the original demand from the base AHU during the charging cycle. This was expected due to the higher inlet flow rates to the heater compared to the inlet flow rate values of the heater of base AHU and from lower mixed air temperatures at the start of the cycle caused by heat storage to the PCM.

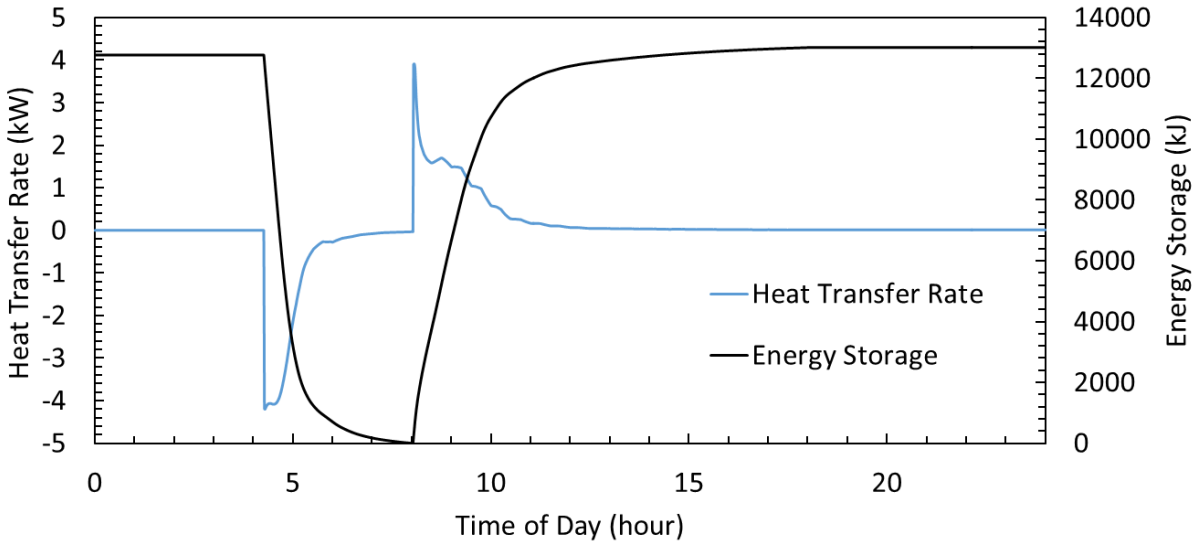

Figure 7.5 Heat Transfer Rate and Energy Storage of a Single PCM TES Unit

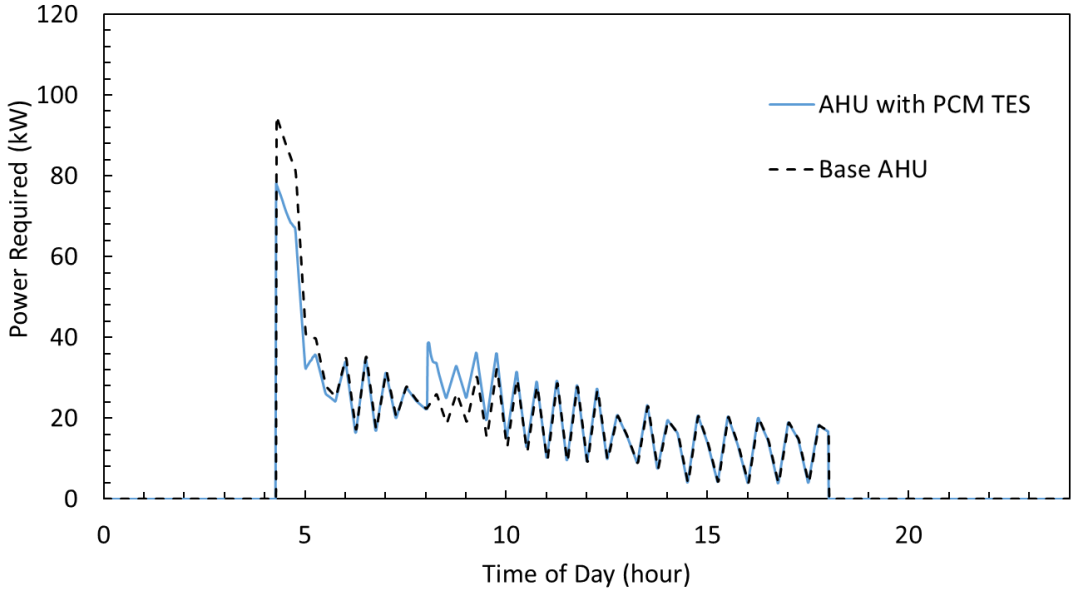

Figure 7.6 Heat Required from Heater Comparison of AHU with Four Parallel PCM TES Units from the Base AHU

7.2 Variations in Melting Temperature

Using PCM with similar properties with different melting temperature would have an effect on the heat transfer rates of the PCM TES. The following will demonstrate whether the effect would be relevant for the current application. The PCMs for this comparison would all theoretically have the same properties as the PCM used during experimentation with different melting temperatures. The melting temperatures were chosen to demonstrate the range that could be used for this application while remaining within the limitations of the PCM TES Type. These simulations were performed with one PCM TES Type or four PCM TES units in parallel using building data again from February 4th, 2015 with the hour change parameter set to 8 AM.

The heat transfer rate comparison of a single PCM TES Type of PCM with varying melting temperatures of 5°C, 9°C and 13°C can be seen in Figure 7.7. It was observed during the discharging cycle that the PCM with the higher melting temperature had a higher heat transfer rate for a longer duration but reduced rate of heat transfer more quickly after approximately an hour of entering the cycle than the lower melting temperatures. This occurred because the PCM with the higher melting temperature had a greater temperature difference to the cold inlet temperatures of the outdoor air. As previously discussed in detail in Subsection 5.3, a larger difference between the inlet and melting temperatures will cause higher heat transfer rates with shorter completion times. During the charging cycle it was observed that all melting temperatures experience the same spike in heat transfer rate at the beginning of charging. Afterwards the PCM with the lower melting temperature maintained a heat transfer rate of approximately 2.5 kW for 1 hour whereas the PCM with the higher melting temperature maintained a heat transfer rate of approximately 1.4 kW for 2 hours. The higher melting temperature had a longer overall completion time. In this case the PCM with the higher melting temperature had a smaller temperature difference to the inlet

temperature which was at room temperature and would thus experience smaller values of heater transfer with a longer completion time.

Figure 7.8 shows a comparison of the power required from the AHU heater of a single PCM TES Type of PCM with varying melting temperatures of 5°C, 9°C and 13°C. It was observed that the peak in power was reduced by approximately 4 kW by using the PCM with the higher melting temperature of 13°C compared to using the PCM with the lower melting temperature of 5°C. It was noted however that at the very tip of the peak, all of the PCMs with varying melting temperatures resulted in approximately the same value in power required from the heater. After 8 AM, the lower melting temperature of 5°C was observed to require slightly more power from the heater for one hour. While the lower peak value and smaller power requirements over a longer duration for charging are both desirable, the differences in power required from the heater are so small that any of these three PCMs could have been used for the application.

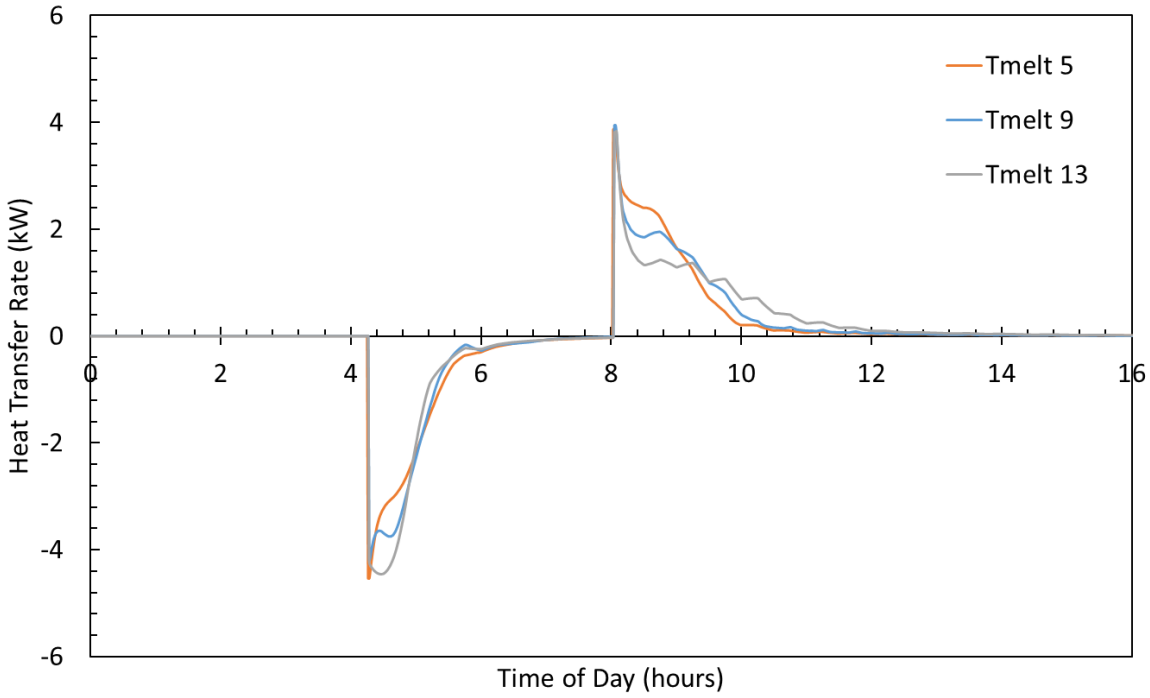

Figure 7.7 Rate of Heat Transfer Rate Comparison of a Single PCM TES Type of PCM with Varying Melting Temperatures of 5 °C, 9 °C and 13 °C

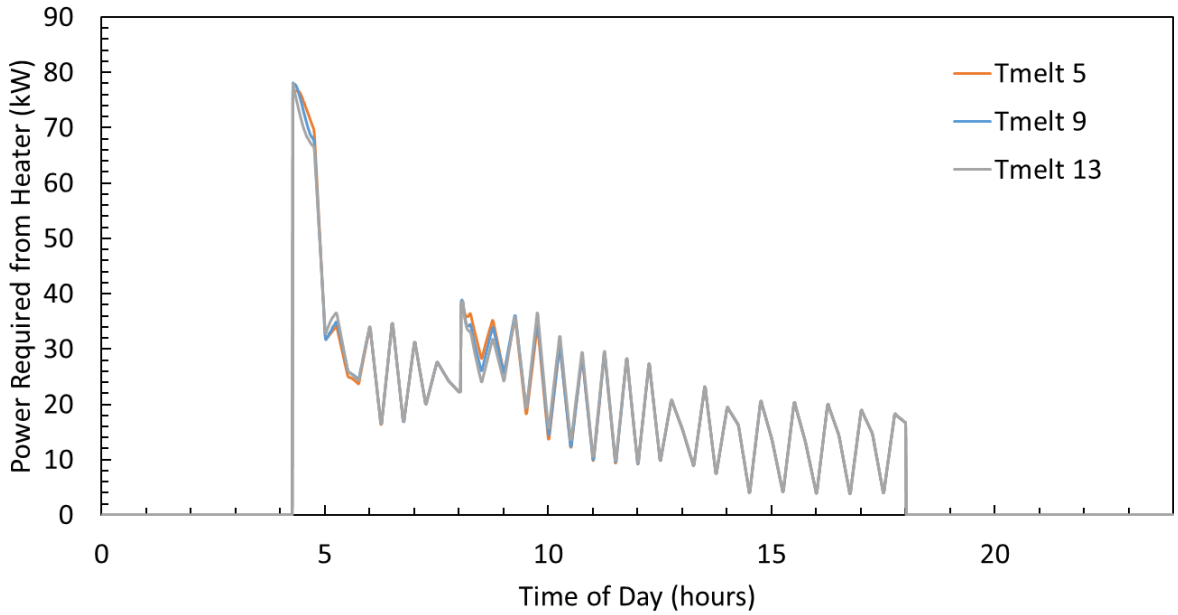

Figure 7.8 Power Required From Heater Comparison of a Single PCM TES Type of PCM with Varying Melting Temperatures of 5 °C, 9 °C and 13 °C

7.3 Optimal PCM TES Configuration

It was determined that four PCM TES units in parallel were required to meet the flow rate demand of the commercial building's AHU. The following will determine the optimal number of PCM TES units in series required for Incorporation Method 1: Strategic Heating. Three simulations were performed starting with one PCM TES Type, then two PCM TES Types in series and finally three PCM TES Types in series. When placing the PCM TES Types in series, the flow rate and temperature outlet of the previous PCM TES Type became the inlet values for the next PCM TES Type in the series. The simulations were done using a melting temperature of 11 °C for all PCM TES Types, the hour change parameter was set to 8 AM and the building data used was February 4th, 2015.

The heat transfer rate for three PCM TES units in series is shown in Figure 7.9. Note that the overall heat transfer rate of the storage system can be achieved by multiplying each of the three units in the series by four to include the four units in parallel. It was observed that the first unit in

the series would achieve the largest value of heat transfer rate in the beginning followed by the second unit with the third producing the smallest value of heat transfer rate. This was because the temperature entering the subsequent units would be decreased (or increased for discharging) as energy was stored in the PCM of the previous unit. As the PCM of the previous units reached capacity their heat transfer rate would decrease and the next unit would receive higher temperatures increasing the heat transferred until its capacity was attained. Thus, the first unit would reach energy capacity first with the third unit taking the longest to charge.

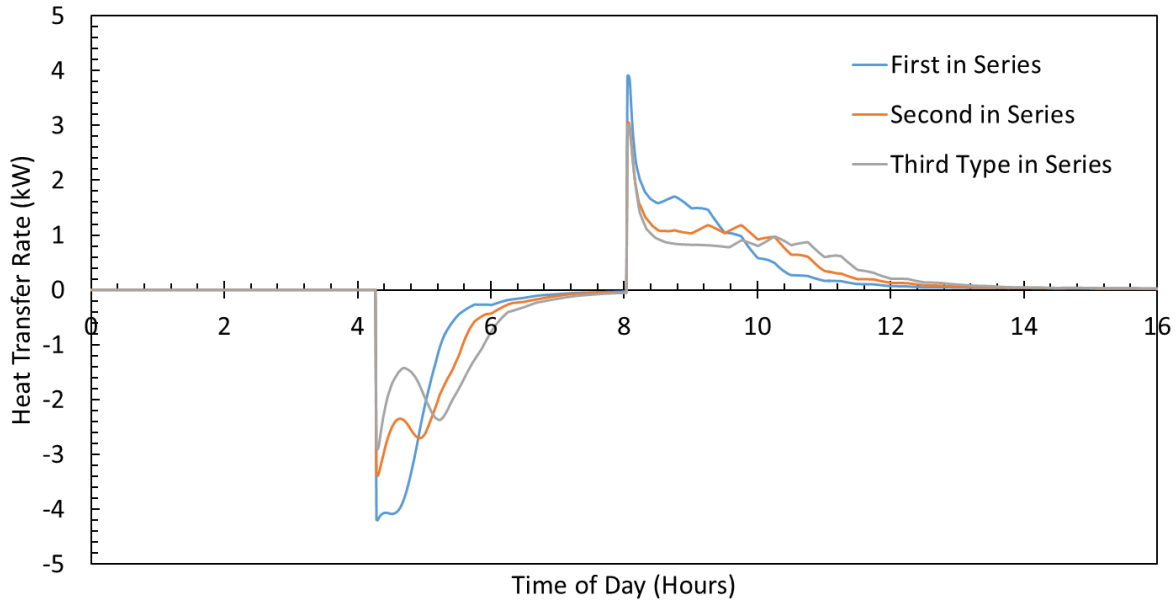

Figure 7.9 Heat Transfer Rate of Three PCM TES Units in Series

A comparison of the power required from the AHU heater with one, two, three PCM TES Types in series and the base AHU is shown in Figure 7.10. It was observed that all three simulations were successful in decreasing the peak power at the start of operation. As previously determined in Subsection 7.1, the peak power was reduced by 16 kW with one PCM TES Type which represents a 20% reduction. With two PCM TES Types in series, the peak power was reduced by 30 kW which represents a 32% reduction. Finally, with three PCM TES Types in series, the peak power was reduced by 40 kW which represents 42% reduction. Unfortunately, the

additional power required for the charging cycle created a second peak in power. This secondary peak increased by 16 kW, 28 kW, and 40 kW with one, two and three PCM TES Types in series, respectively. With three units, the initial peak in power was significantly reduced however the second peak in power increased to slightly higher than the initial peak. Thus, it would be advisable to use two PCM TES Types in series as there was a significant reduction in power required by the AHU heater and the secondary peak did not surpass the original peak.

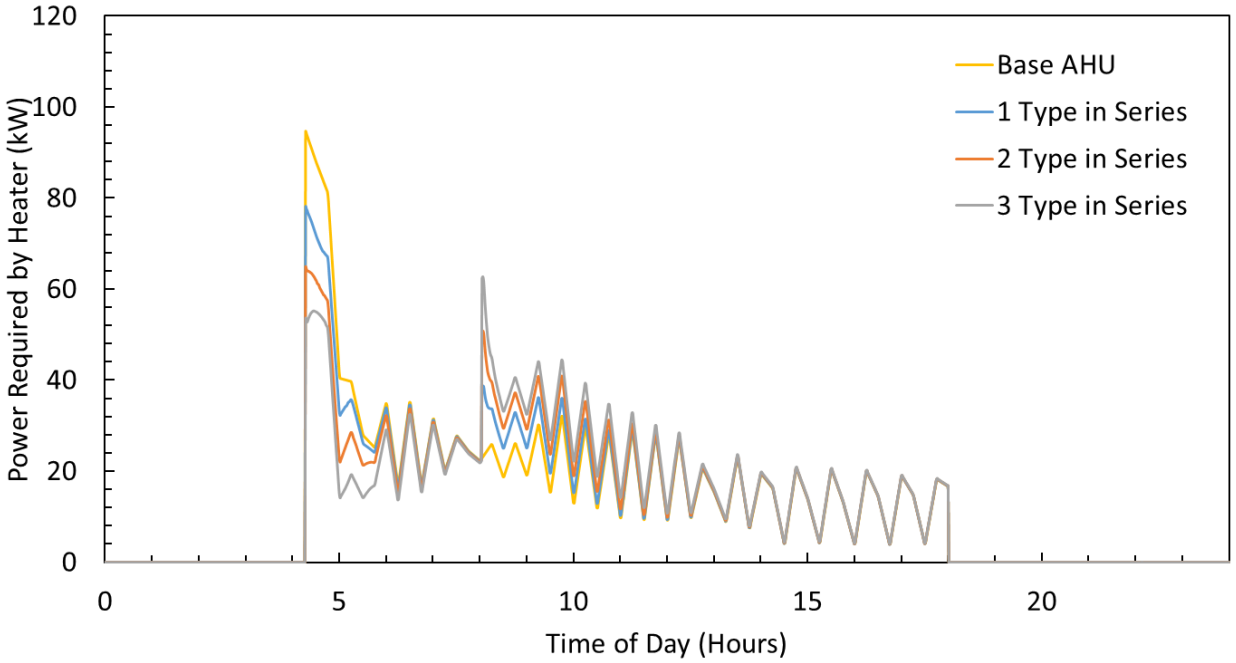

Figure 7.10 Power Required from AHU Heater for Simulations with One, Two and Three PCM TES Types and the Base AHU

Overall the Integration Method 1: Strategic Heating was successful in reducing the initial peak power of the heater but it was unable to completely smooth out the power over the entire duration of operation. Instead, a second peak was created from the charging cycle which was undesirable.

7.4 Results for Multiple Days

A simulation was performed for Integration Method 1: Strategic Heating over multiple days. The simulation consisted of four PCM TES units in parallel with two units in series for a total of eight PCM TES units represented by two PCM TES Types in series. The simulation ran for 96 hours or 4 days which used building data from February 4, 2015, February 10, 2015, March 12, 2015 and March 13, 2015, see Table 7-1 for minimum and maximum outdoor temperatures. These days were selected as their outdoor temperatures functioned within the limitations of the PCM TES Type. Unfortunately, there were not four consecutive days available within the limitations. The melting temperature parameter was set to 11°C and the hour change parameter was set to 8 AM.

Table 7-1 Minimum and Maximum Outdoor Temperatures

Date	Min. Outdoor Temperature (°C)	Max. Outdoor Temperature (°C)
February 4, 2015	-12.5	-6.2
February 10, 2015	-13.5	-6.5
March 12, 2015	-10.0	-4.5
March 13, 2015	-11.0	-2.0

Figure 7.11 illustrates the temperatures throughout the various stages of the AHU over multiple days including the return temperature (air from the building), the outside temperature, the mixed temperature, the PCM TES outlet temperature and the supply temperature (air to the building). All observed trends from the single day analysis were observed to occur throughout each day. It was noted that the two February days had colder outdoor temperatures overall than the two March days. This resulted in a smaller temperature difference between inlet and melting temperatures during discharging for the March days.

Figure 7.12 illustrates the mass flow rates throughout the various stages of the AHU over multiple days including the fan output (or return flow from the building), the flow recirculated, the mixed flow, the exhaust flow, the intake flow, the PCM TES outlet flow and the supply flow to

the building. The mass flow rate trends made from the single day analysis occurred throughout each day. It was observed that the two February days followed similar trends which were slightly varied from the two March days. The overall mass flow rate represented by the fan output was lower in March than in February particularly in early morning. The other notable difference was that the exhaust flow rate and the intake flow rate increased throughout the day for the two days in March. This occurred as the AHU was programming to increase the intake of outdoor air in relation to any increase in outdoor temperature.

Figure 7.13 shows the volumetric flow rate entering one of the first PCM TES units in series with the lower limitation of the PCM TES Type displayed. It was observed that all of the four days selected fall within the limitations. It was noted that the volumetric flow rates for discharging were considerably different for each day. The volumetric flow rate is a function of both mass flow rate and temperature. The mass flow rates and the outdoor temperatures were different each morning which resulted in varying volumetric flow rates during discharging. The volumetric flow rate during charging was only a function of the supply temperature as the mass flow rate was set to a fix value. The volumetric flow rate during charging was observed as a constant value for each day as observed from Figure 7.11, the supply temperature only fluctuates between a few degrees throughout the charging time period.

Figure 7.14 shows the heat transfer rate of two single units in series over multiple days. The overall trends for each day were again similar. It was noted that the magnitude of the initial peak of the first PCM TES unit in series directly correlated with the outdoor temperature. It was observed that a lower outdoor temperature at the start of the discharge cycle would result in a greater peak in heat transfer rate and a higher outdoor temperature would result in a smaller peak in heat transfer rate. It was also observed that the smallest peak in heat transfer rate observed on

March 12, occurred for a longer duration in comparison to the greatest peak in heat transfer rate of the coldest morning observed on February 10th. A smaller heat transfer rate would result in slower energy storage leaving more room for energy storage in the PCM over a longer period of time.

Figure 7.6 shows the difference in required power from the AHU heater between the simulation of two PCM TES Types in series and the base AHU heater over multiple days. It was observed that on February 10th (the day with the coldest outdoor temperature during discharging), the greatest reduction in peak power occurred at approximately 30 kW. It was also observed that on March 12th (the day with the warmer outdoor temperature during discharging), the smallest reduction in peak power occurred at approximately 20 kW.

It can be concluded that power savings using the PCM TES units has greater benefits in colder temperatures. This correlation is desirable as colder temperatures demand more power from the AHU heater creating a larger need for rapid dissipation of heat from the storage units to increase the temperature of the outdoor air entering the system. Overall the system was successful in reducing peak power of the heater over multiple days while successfully charging and discharging.

This chapter presented simulation results for a PCM TES integrated into an AHU, using the Integration Method 1: Strategic Heating. The air flow rate and air temperature, at various points in the AHU, were presented first for a single day and afterwards over multiple days. A comparison of PCM with variations in melting temperature was made. The optimal number of PCM TES units in series was determined. Finally, the power required from the heater of all models with PCM TES integration for both a single day and multiple days, were compared to the power required from the heater of the base model to demonstrate the reduction of the peak power at start-up.

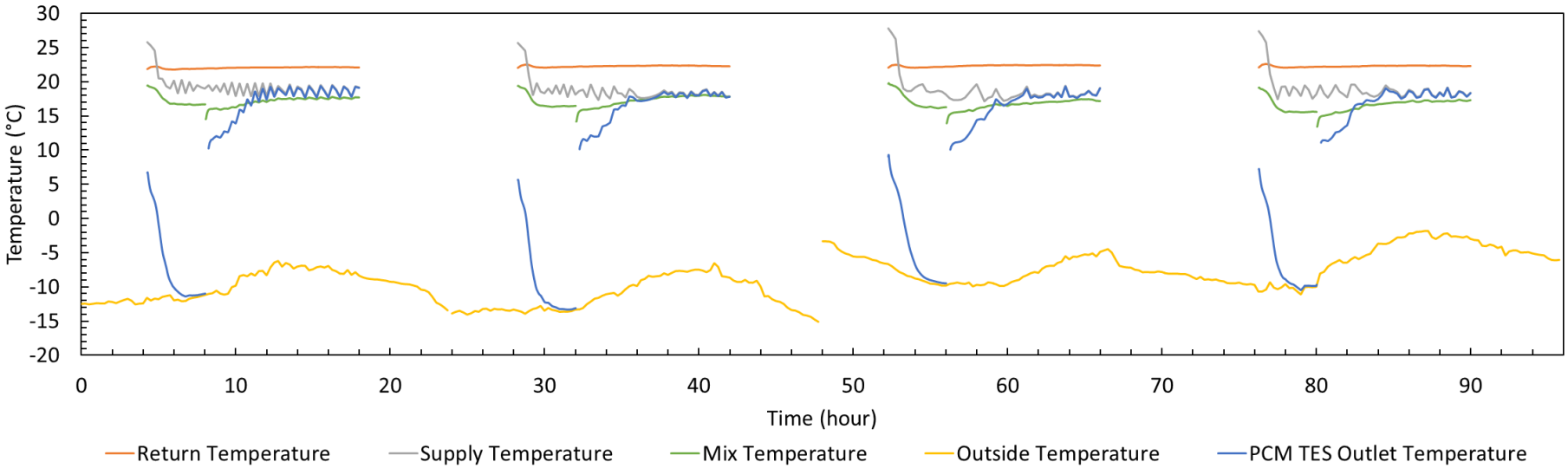

Figure 7.11 Temperatures through the AHU using Two PCM TES Types in Series over Multiple Days

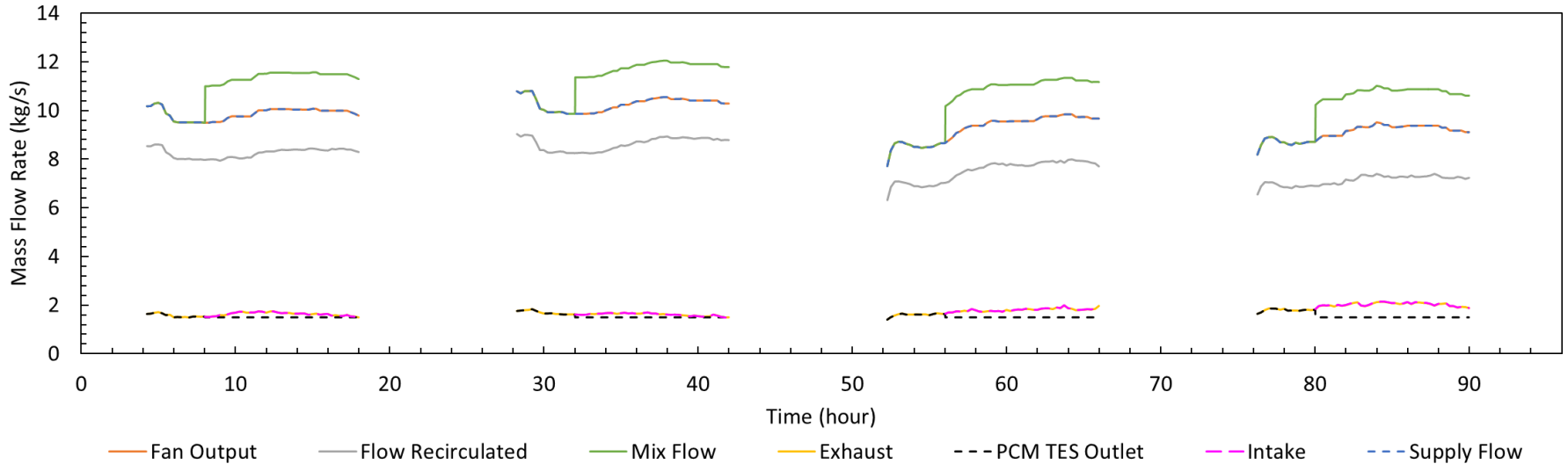

Figure 7.12 Mass flow rates through the AHU using Two PCM TES Types in Series over Multiple Days

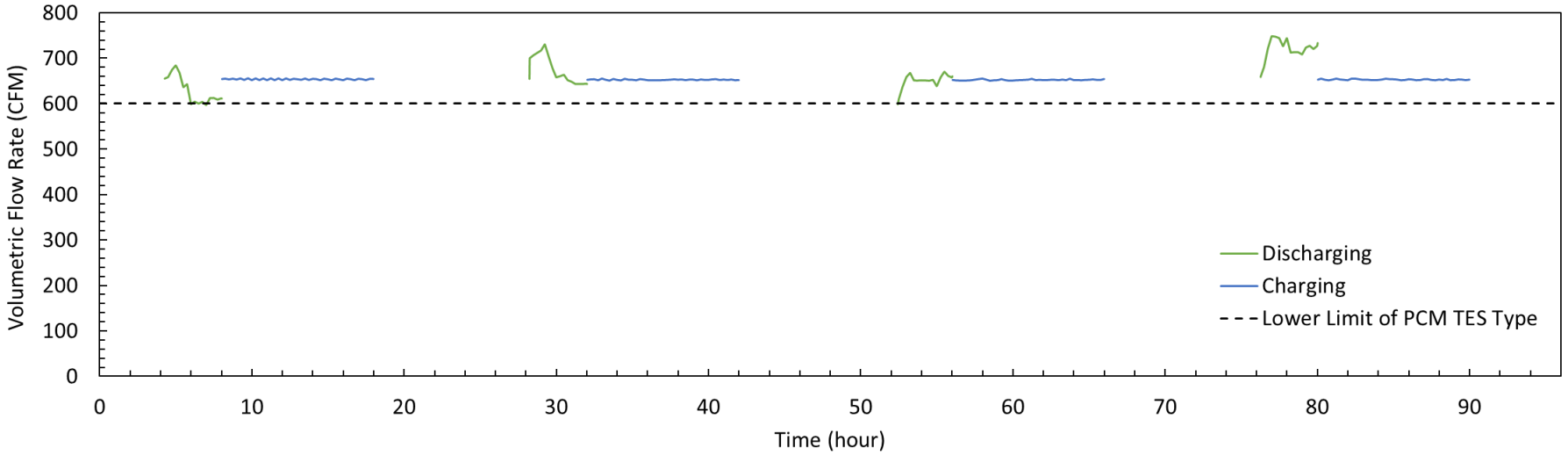

Figure 7.13 Volumetric Flow Rate through the AHU using Two PCM TES Types in Series over Multiple Days

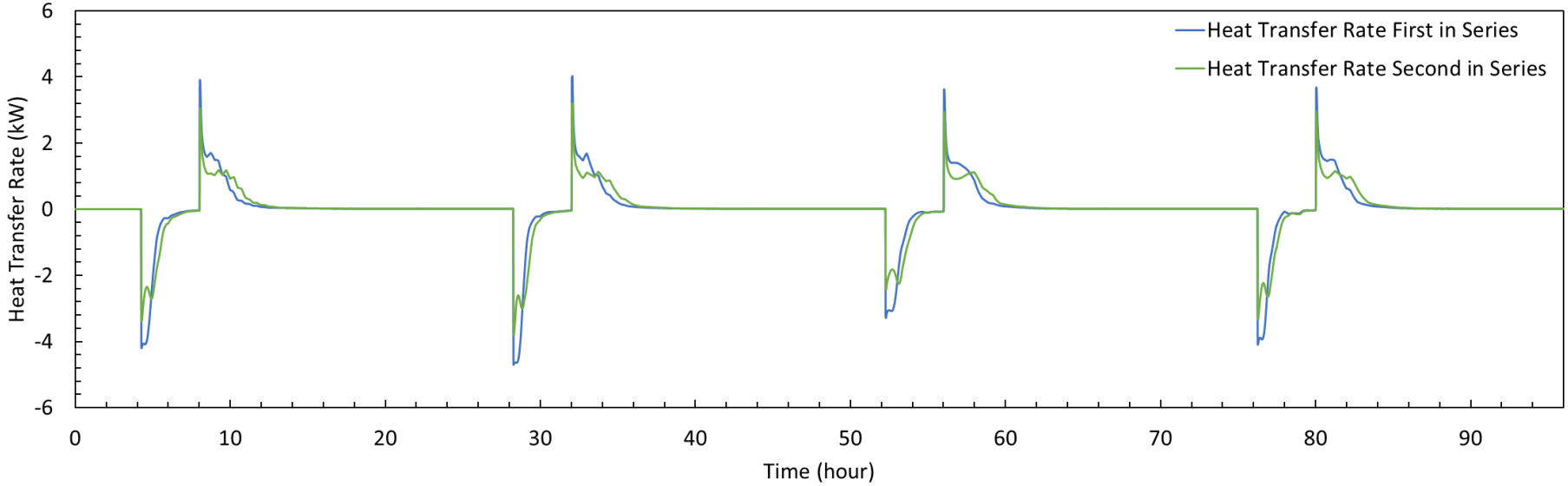

Figure 7.14 Heat Transfer Rate of Two Single PCM TES Units in Series over Multiple Days

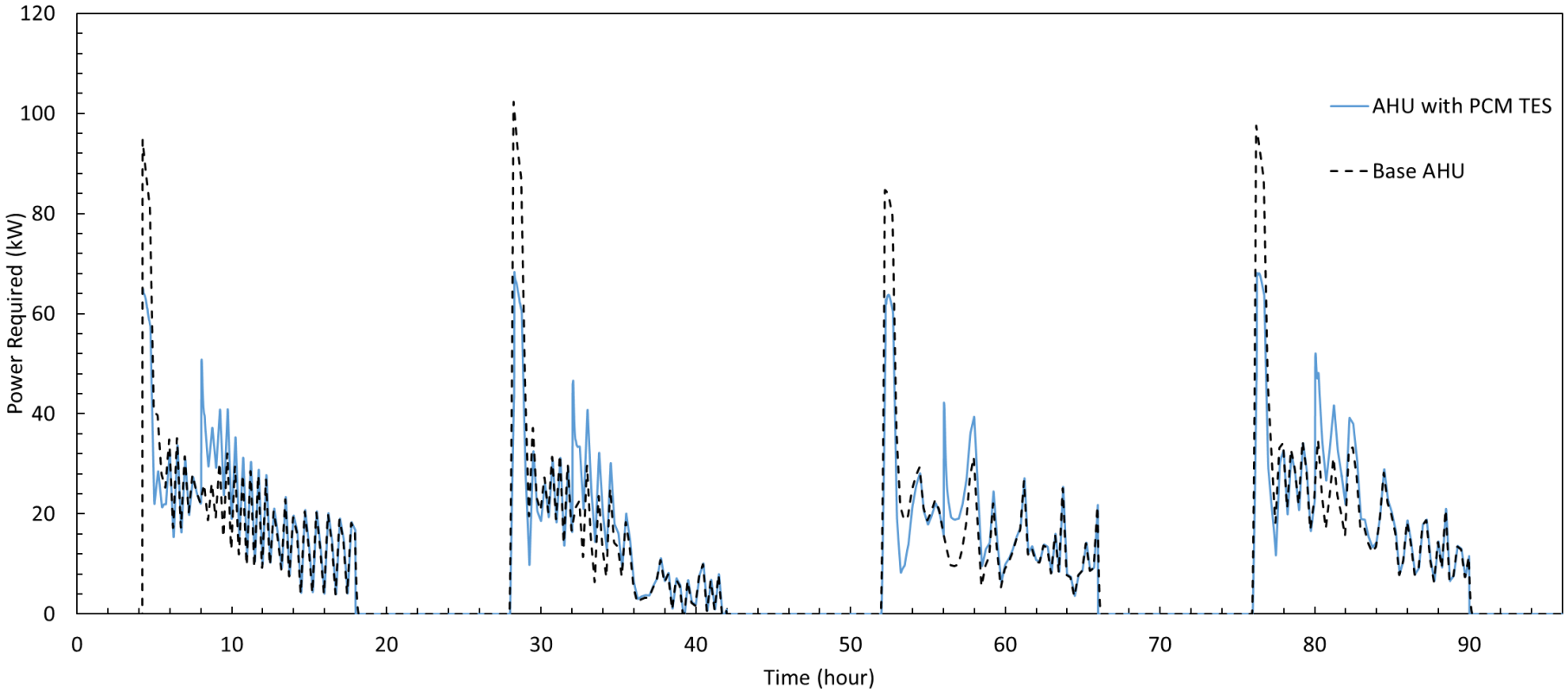

Figure 7.15 Power Required from Heater Comparison of AHU with Two PCM TES Types in Series from the Base AHU

8 Chapter: Conclusions and Future Work

8.1 Conclusions

There is a need to advance technologies that will reduce energy consumption and GHG emissions, and improve the affordability of energy. Space heating accounts for approximately half of the total energy consumption in the commercial building sector in Canada in 2013 and is one area where small improvements could have large benefits. The integration of PCM TES into AHUs is one advancement that has the potential to achieve these goals. This thesis focused on the characterization of PCM for the described application and preliminary TRNSYS simulations of the PCM TES integrated into an AHU using Integration Method 1: Strategic Heating for demonstration. The characterization of the PCM was achieved through the design, construction and characterization of an air-loop. The experimental data from the PCM characterization was used to create an empirical model of a PCM TES in TRNSYS called the PCM TES Type. This new Type was used in TRNSYS simulations to demonstrate a basic understanding of how the AHU would react to the integration of a PCM TES system.

The air-loop was created to test the characterization of the PCM for the application and geometry of this project. The air-loop was also created with flexibility to allow the performance of the PCM to be characterized for different geometries and applications for future projects. The experimental setup of the air-loop was characterized to ensure proper function and determine accuracy of results. The velocity profile was determined at the inlet of the PCM plates within the PCM box. It was found that the velocity profile was symmetrical from side to side but the velocity had higher values at the bottom of the box than at the top. The analysis of a single full cycle test concluded that the volumetric flow rate, the instantaneous heat transfer rate and the energy stored values were all within their respective error limits for both charging and discharging cycles. It was

found that the inlet temperatures from the eight inlet thermocouples had slightly higher values from the bottom readings than the top due to transient values. The outlet temperature from the eight outlet thermocouples had differences in values that could not be easily explained and require further experimentation, see next subsection for suggested future work.

The PCM characterization was done experimentally with the air-loop. Three variables were varied for the characterization: HTF flow rates, initial temperature of the PCM and HTF inlet temperature. The variation in HTF flow rates resulted in faster completion times for both the charging and discharging cycles for higher values in HTF flow rates. It was found that for all flow rate variations, heat transfer rates were maintained between 3 and 4 kW for the first 40 min of the cycle after which they would gradually decrease with higher HTF flow rates decreasing at a faster rate. The variation in initial temperature of the PCM resulted in a spike in temperature at the start of both the charging and discharging cycles. It was concluded that the larger the temperature difference between the initial temperature of the PCM and the melting temperature of the PCM would result in a greater temperature difference in the HTF between the inlet and outlet of the PCM at the start of the cycle. After the spike subsided, the HTF temperature difference and the heat transfer rates of all variation in initial temperature tests would have the same values. Thus, it was concluded that a decrease in initial temperature for charging and an increase during discharging will lead to a larger spike in the temperature difference of the HTF. Variations in initial temperature will have no further noticeable effect on these values once the spike has subsided. This initial spike did however impact the energy capacity of the PCM, storing additional energy in the form of sensible heat. The variation in HTF inlet temperature resulted in a large HTF inlet and outlet temperature difference and shorter completion time for larger temperature difference between the HTF inlet temperature and the melting temperature. It was found that for all HTF inlet

temperature variations, heat transfer rates were maintained between 1.5 and 4 kW after the initial spike. The heat transfer rates were maintained for a longer time period for lower HTF inlet temperatures during charging and higher HTF inlet temperatures during discharging where after the heat transfer rate would decrease. It is concluded that the difference in energy capacity between variations in HTF inlet temperature is in part due to additional storage through sensible heat but mostly due to the mechanisms of conduction and convection that effect the melting and solidification process of the material. The overall characterization of the PCM resulted with a decent range of heat transfer rates, energy capacity values and completion times to be utilized for the integration of a PCM TES into an AHU.

The next step was to verify whether this range in values would be adequate for the application. To achieve this, the information from the PCM characterization was used to create an empirical model of a PCM TES in TRNSYS called the PCM TES Type. The PCM TES Type had limitations set by the experimental range of the test equipment. These limitations needed to be observed to obtain reliable results. A validation was performed comparing the experimental results to simulation results using the PCM TES Type with tests that covered the experimental range of HTF flow rates and HTF inlet temperature. The experimental and simulations results were found to be in good agreement. A base AHU model was created in TRNSYS and validated using data from an existing AHU operating in a commercial building. Data from this model were used to verify whether any improvements were made by implementing a PCM TES.

In the introduction, three PCM TES integration methods were presented. The goal of the TRNSYS simulation in this thesis was to give an example of how the PCM TES integration could be simulated and to present some preliminary results. Integration Method 1: Strategic Heating was selected for simulation and analysis. This method was selected as it addressed the energy peak

problem of the existing AHU used for this project. It was concluded that a PCM with a melting temperature of 13°C would be the better option for this method when compared to PCM with melting temperatures of 9°C and 5°C. The PCM with a melting temperature of 13°C was determined to reduce the heat required from the AHU heater by 4 kW over the PCM with a melting temperature of 5°C. This reduction was notable however it was not significant in comparison to the total heat required during the initial start-up spike. It was concluded that two PCM TES units in series was the optimal configuration for the geometry used. It was found that three units in series significantly reduced the peak from a value of approximately 100 kW to 55 kW but resulted in the creation in a second higher peak in required heat of approximately 65 kW from the AHU heater at the start of the charging cycle. By using only two PCM TES units in series, there was still a significant reduction to the initial heat requirement peak from a value of approximately 100 kW to 65 kW while keeping the secondary peak at a lower value of approximately 50 kW. The optimal configuration and PCM with most suitable melting temperature were used in a simulation that ran for the duration of four consecutive days. The simulation was determined to be successful producing expected results for each day. It was found that Integration Method 1: Strategic Heating had greater benefits in heat requirements from the heater on days with colder outdoor temperatures.

In conclusion, the integration of a PCM TES Type into a commercial building's AHU using Integration Method 1 was successful in reducing the large peak requirement of the AHU heater at the start of operations. Reducing the peak would in many cases reduce the cost of energy for a commercial building. Improvement in energy affordability was but one of the goals for this application. The other integration methods have the potential to improve energy consumption and would need to be evaluated in future work using the foundation outlined in this thesis.

8.2 Future Work

The objective of this thesis was to conduct a preliminary feasibility study of a PCM TES and characterize its heat transfer rates when integrated in an air handling unit. This section describes the next steps of the project.

Modifications to the air-loop could be implemented to achieve an improved uniform air flow from top to bottom. One suggestion for improvement would be to add a contraction cone to the inlet of the PCM box and a diffuser cone at the outlet. This will reduce flow separation caused by the 90° elbow. It would also be advisable to add a honeycomb structure between the elbow and the contraction cone to increase turbulence in the flow.

Further experimentation should be conducted to achieve an explanation for the temperature variations outlined in Subsection 4.3 (FiguresFigure 4.9 andFigure 4.10) between the eight outlet thermocouples. One suggestion would be to add additional thermocouples to the PCM aluminum cases in several locations. This would give a better understanding of how the temperatures are changing in the PCM system. Also, it would be of interest to determine whether the PCM cases have identical heat transfer rates with the HTF or if there are discrepancies between the cases.

The limitations of the PCM TES Type should also be improved to include a larger range of outdoor temperatures. The current range would not be able to accurately analyze other potential integration methods. This limitation improvement can be achieved by adding a chiller to the cold water line of the experimental setup. The additional result can be added to the empirical model.

Next, various integration methods should be simulated and analyzed to obtain a full understanding of the best methods for this application. This would include Integration Method 2: Peak Shaving and Integration Method 3: Heat Recovery, proposed in the Introduction. The simulations would be achieved by modifying the base model layout from Figure 6.7 to create new

layouts with the same methodology to that shown in Subsection 6.4.2 for Integration Method 1: Strategic Heating.

Finally, a full scale PCM TES prototype should be constructed based on the PCM characterization results from Chapter 5. The integration method chosen should be based on the future TRNSYS simulations. The PCM TES prototype would be placed in an existing commercial building for testing to verify accuracy of simulation results and feasibility of retrofitting existing equipment.

References

[1] EIA-0484(2016), "International Energy Outlook 2016," U.S. Energy Information Administration, Washington D.C., 2016.

[2] M. Hamit-Hagger, "Greenhouse gas emissions, energy consumption and economic growth: A panel co-integration analysis from Canadian industrial sector perspective," *Energy Economics,* vol. 34, pp. 358-364, 2012.

[3] T.F. Stocker, D. Qin, G.K Plattner, M.M.B Tignor, P.M. Midgley, "Climate Change 2013 The Physical Science Basis," Intergovernmental Panel on Climate Change 2013, Cambridge University Press, New York, 2013.

[4] K. Pielichowska, K. Pielichowski, "Phase change materials for thermal enrgy storage," *Progress in Materials Science,* vol. 65, pp. 61-123, 2014.

[5] Natural Resources Canada, "Energy Efficiency Trends in Canada 1991 to 2013," Minister of Natural Resources, 2016.

[6] A. Joseph, M. Kabbara, D. Groulx, P. Allred, M.A. White, "Characterization and real-time testing of phase-change materials for solar thermal energy storage," *International Journal of Energy Research,* vol. 40, pp. 61-70, 2016.

[7] T.M. Letcher, "Chapter 13: Phase Change Materials," in *Storing Energy with Special Reference to Renewable Energy Sources*, MA, USA, Elsevier Inc, 2016.

[8] American Society of Heating, Refrigeration and Air-Conditioning Engineers, Inc, "Building Air Distribution," in *2004 ASHRAE Handbook: Heating, Ventilation, and Air-Conditioning Systems and Equipment*, Atlanta USA, ASHRAE, 2004, pp. 2.1-2.14.

[9] F. McQuiston, J. Parker, J. Spitler, "Air-Conditioning Systems," in *Heating, Ventilating, and Air Conditioning Analysis and Design*, Hoboken, NJ, John Wiley & Sons, 2005, pp. 22-48.

[10] Greenheck, "Heat Recovery Ventilatior Model PVe," Greenheck Fan Corp., Schofield, 2017.

[11] P. Promoppatum, S. Yao, T. Hutz, D. Agee, "Experimental and numerical investigation of the cross-flow PCM heat exchanger for the energy saving of building HVAC," *Energy and Buildings,* vol. 138, pp. 468-478, 2017.

[12] S. Wert, C.A. Cruickshank, D. Groulx, "Energy Analysis of the ---- Building," Carleton University, Ottawa, 2016.

[13] J.R. Turnpenny, D.W. Etheridge, D.A. Reay, "Novel ventilation cooling system for reducing air conditioning in buildings," *Applied Thermal Engineering,* vol. 20, pp. 1019-1037, 2000.

[14] F. Haghighat, "Annex 23: Energy storage in buildings of the future - Applying Energy Storage in Ultra-low Energy Buildings," iea Eneragy Technology Network, 2013.

[15] D. Snow, Plant Enegineer's Reference Book, Oxford: Butterworth Heinmann, 1991.

[16] J. Turnpenny, "Novel ventilation system for reducing air conditioning in buildings. Part II: testing of prototype," *Applied Thermal Engineering,* vol. 21, no. 12, pp. 1203-1217, 2001.

[17] T.L. Bergman, A.S. Lavine, F.P. Incropera, D.P. Dewitt, Fundamentals of heat and mass transfer, Seventh Edition, USA: John Wiley & Sons Inc, 2011.

[18] L. Fan, J.M. Khodadadi, "Thermal conductivity enhancement of phase change materials for thermal energy storage: A review," *Renewable and Sustainable Energy Reviews,* vol. 15, pp. 24-46, 2011.

[19] A. Sasfari, R. Saidur, F.A. Sulaiman, Y.Xu, J. Dong, "A review on supercooling of Phase Change Materials in thermal energy storage sysems," *Renewable and Sustainable Energy Reviews,* vol. 70, pp. 905-919, 2017.

[20] C. Amaral, R. Vicente, P.A.A.P. Marques, A. Barros-Timmons, "Phase change materials and carbon nanostructures for thermal energy storage: A literature review," *Renewable and Sustainable Energy Reviews,* no. 79, pp. 1212-1228, 2017.

[21] D. Zhou, C.Y. Zhao, Y. Tian, "Review on thermal energy storage with phase change materials (PCMs) in building applications," *Applied Energy,* no. 92, pp. 593-605, 2012.

[22] P. Tatsidyodoung, N. Le Pierrès, L. Luo, "A review of potential materials for thermal energy storage in building applications," *Renewable and Sustainable Energy Reviews,* no. 18, pp. 327-349, 2013.

[23] A.S. Fleischer, "Types of PCMs and Their Selection," in *Thermal Energy Storage Using Phase Change Materials Fundamentals and Applications*, Vilanova, PA, Springer, 2015, pp. 37-47.

[24] S.A. Nada, W.G. Alshaer, "Comprehensive parametric study of using carbon foam structures saturated with PCMs in thermal management of electronic systems," *Energy Conversion and Management,* vol. 105, pp. 93-102, 2015.

[25] H. Jamil, M. Alam, J. Sanjayan, J. Wilson, "Investigation of PCM as retrofitting option to enhance occupant thermal comfort in a modern residential building," *Energy and Buildings,* vol. 133, pp. 217-229, 2016.

[26] S. Ali Memon, "Phase change materials integrated in building walls: A state of the art review," *Renewable and Sustainable Energy Reviews,* vol. 31, pp. 870-906, 2014.

[27] M.C. Browne, E. Boyd. S.J.McCormack, "Investigation of the corrosive properties of phase change materials in contact with metals and plastic," *Renewable Energy,* vol. 108, pp. 555-568, 2017.

[28] R.A. Taylor, N. Tsafnat, A. Washer, "Experimental characterisation of sub-cooling in hydrated salt phase change materials," *Applied Thermal Engineering,* vol. 93, pp. 935-938, 2016.

[29] "A.I. Fernandez, C. Barreneche, M. Belusko, M. Segarra, F. Bruno," *Considerations for the use of metal alloys as phase change materials for high temperature applications,* vol. 171, pp. 275-281, 2017.

[30] S.S Narayanan, A. Kardam, V. Kumar, N. Bhardwaj, D. Madhwal, P. Shukla, A.Kumar, A. Verma, V.K. Jain, "Development of sunlight-driven eutectic phase change material nanocomposite for applications in solar water heating," *Resource-Efficient Technologies,* 2017.

[31] A. Lazaro, P. Dolado, J.M. Marin, and B. Zelba, "PCM-air heat exchangers for free-cooling applications in buildings: Experimental results of two real-scale prototypes," *Energy Convers. Manag.,* vol. 50, no. 3, pp. 439-443, 2009.

[32] A. El-Sawi, F. Haghighat, and R. Yang, "Centralized latent heat thermal energy storage system: Nodel development and validation," *Energy Buildings,* vol. 65, pp. 260-271, 2013.

[33] M. Kabbara, D. Groulx, A. Joseph, "Experimental investigations of a latent heat energy storage unit using finned tubes," *Applied Thermal Engineering,* vol. 101, pp. 601-611, 2016.

[34] R.E. Murray, D. Groulx, "Experimental study of the phase change and energy characteristics inside a cylindrical latenet heat energy storage system: Part 1 consecutive charging and discharging," *Renewable Energy,* vol. 62, pp. 571-581, 2014.

[35] A. Joseph, M. Kabbara, D. Groulx, P. Allred, M.A. White, "Characterization and real-time testing of phase-change materials for solar thermal energy storage," *International Journal of Energy Research,* vol. 40, pp. 61-70, 2016.

[36] B. Zelba, J.M. Marin, L.F. Cabeza, H. Mehling, "Free-cooling of buildings with phase change materials," *Int. J. Refrig.,* vol. 27, no. 8, pp. 839-849, 2004.

[37] C. Arkar, "Efficiency of free cooling using latent heat storage integrated into the ventilationsystem of a low energy building," *International Journal of Refrigeration,* vol. 30, no. 1, pp. 134-143, 2007.

[38] C. Liu, D. Groulx, "Experimental study of the phase change heat transfer inside a horizontal cylindrical latent heat energy storage system," *International Journal of Thermal Sciences,* vol. 82, pp. 100-110, 2014.

[39] R.E. Murray, D. Groulx, "Experimental study of the phase change and energy characteristics inside a cylindrical latent heat energy storage system: Part 2 simultaneous charging and discharging," *Renewable Energy,* vol. 63, pp. 724-734, 2014.

[40] V. Palomba, V. Brancato, A. Frazzica, "Experimental investigation of a latent heat storage for solar cooling applications," *Applied Energy,* vol. 199, pp. 347-358, 2017.

[41] M. Dadollahi, M.Mehropooya, "Modeling and investigation of high temperature phase change materials (PCM) in different storage tank configurations," *Journal of Cleaner Production,* p. In Press, 2017.

[42] C. Arkar, S. Medved, "Influence of accuracy of thermal property data of a phase change material on the result of a numerical model of a packed bed latent heat storage with spheres," *Thermochimica Acta,* vol. 438, no. 1-2, pp. 192-201, 2005.

[43] K. Nagano, S. Takeda, T. Mochida, K. Shimakura, "Thermal characteristics of a direct heat exchange system between granules with phase change material and air," *Applied Thermal Engineering,* vol. 24, pp. 2131-2144, 2004.

[44] N.H.S. Tay, M.Belusko, F. Bruno, "Designing a PCM storage system using the effectiveness-number of transfer units method in low energy cooling of buildings.," *Energy and buildings,* vol. 50, pp. 234-242, 2012.

[45] M. Lacroix, "Numerical simulation of a shell-and-tube latent heat thermal energy storage unit," *Solar Energy,* vol. 50, pp. 357-367, 1993.

[46] V. Antony Aroul Raj, R. Velraj, "Heat transfer and pressure drop studies on a PCM-heat exchanger module for free cooling applications," *International Journal of Thermal Sciences,* vol. 80, no. 8, pp. 1573-1582, 2011.

[47] F. Bruno, N.H.S. Tay, M. Belusko, "Minimising energy usage for domestic cooling with off-peak PCM storage," *Energy and Buildings,* vol. 76, pp. 347-353, 2014.

[48] S.M. Vakilaltojjar, W.Saman, "Analysis and modelling of a phase change storage system for air conditioning applications," *Applied Theraml Engineering,* vol. 21, no. 3, pp. 249-263, 2001.

[49] P. Dolado, A. Lazaro, J.M. Marin, and B. Zelba, "Characterization of melting and solidification in a real-scale PCM-air heat exchanger: Experimental results and empirical model," *Renewable Energy,* vol. 36, no. 11, pp. 2906-2917, 2011.

[50] E.Osterman, V.Butala,U.Stritih, "PCM thermal storage system for 'free' heating and cooling of buildings," *Energy and Buildings,* vol. 106, pp. 125-133, 2015.

[51] A.H. Mosaffa, C.A. Infante Ferreira, F. Talati, M.A. Rosen, "Thermal performance of a multiple PCM thermal storage unit for free cooling," *Energy Conversion and Management,* vol. 67, pp. 1-7, 2013.

[52] M. Iten, S. Liu, "Experimental study on the thermal performance of air-PCM unit," *Building and Environment,* vol. 105, pp. 128-139, 2016.

[53] N. Stathopoulos, M.El Mankibi, M. Santamouris, "Numerical calibration and experimental validation of a PCM-Air heat exchanger model," *Applied Thermal Engineering,* vol. 114, pp. 1064-1072, 2017.

[54] Monodraught, "Cool-phase Low energy cooling and ventilation system," 2012.

[55] H. Weinläder, "A ventilated cooling ceiling with integrated latent heat storage - Monitoring results," *Energy and Buildings,* vol. 82, pp. 65-72, 2014.

[56] S. Liu, M. Iten, A. Shukla, "Numerical study on the performance of an air - Multiple PCMs unit for free cooling and ventilation," *Energy and Buildings,* vol. 151, pp. 520-533, 2017.

[57] A.A. Rabienataj Darzi, S.M. Moosania, F.L. Tan, M. Farhadi, "Numerical investigation of free-cooling system using plate type PCM storage," *International Communications in Heat and Mass Transfer,* vol. 48, pp. 155-163, 2013.

[58] R. Brazin, J.J. Chen, B. R. Young, M.M. Farid, "Application of PCM energy storage in combination with night ventilation for space cooling," *Applied Energy,* vol. 158, pp. 412-421, 2015.

[59] N. Stathopoulos, M. El Mankibi, P. Michel, "Contribution à l'effacement énergétique: approche numérique et expérimentale pour la conception et la caractérisation d'un échangeur airMCP couplé au bâtiment," in *RIDA2D Conference*, 2012.

[60] K. Lin, "Study of an electrical heating system with ductless air supply and shape-stabilized PCM for thermal storage," *Energy Conversion and Management,* vol. 48, no. 7, pp. 2016-2024, 2007.

[61] York International, "Air Systems - Energy Series Energy Recovery Wheels," York International Corporation, USA, 2001.

[62] A. Leva, E. Zavaglio, M. Bonvini, "Dynamic modelling of desiccant wheels for the design of energy-efficient air handling units," in *Proceedings of the 19th World Congress, The International Federation of Automatic Control*, Cape Town, South Africa, 2014.

[63] G. Plavenieks, A. Lesinskis, "Case study of energy efficiency in air handling units with heat exchangers for residential application in latvia," in *4th International Scientific Conference Part I Civil Engineering 13*, Jelgava, 2013.

[64] Natural Resources Canada, "Heat Recovery Ventilators," Energy Publications Office of Energy Efficiency Natural Resources Canada, Ottawa, 2012.

[65] T.L. Bergman, A.S. Lavine, F.P. Incropera, D.P. Dewitt, "Chapter 11: Heat Exchangers," in *Fundamentals of Heat and Mass Transfer Seventh Edition*, USA, John Wiley & Sons Inc, 2011, pp. 705-765.

[66] Rubitherm, "Data Sheet RT44HC," Rubitherm Technologies GmbH, Berlin, Germany, 2016.

[67] T.L. Bergman, A.S. Lavine, F.P. Incropera, D.P. Dewitt, "Internal Flow," in *Fundamentals of Heat and Mass Transfer Seventh Edition*, USA, John Wiley & Sons, Inc., 2011, pp. 517-592.

[68] Solar Energy Laboratory, Univerity of Wisconsin-Madison, "TRNSYS Programmer's Guide," Univerity of Wisconsin-Madison, Wisconsin, 2012.

[69] Rubitherm, "Data Sheet RT5HC," Rubitherm Technologies GmbH, Berlin, Germany, 2016.

[70] Rubitherm, "Data Sheet RT11HC," Rubitherm Technologies GmbH, Berlin, Germany, 2016.

[71] Rubitherm, "Data Sheet RT18HC," Rubitherm Technologies GmbH, Berlin, Germany, 2016.

[72] R. S. Figliola, D.E. Beasley, Theory and Design for Mechanical Measurments, Fourth Edition, USA: John Wiley and Sons Inc, 2006.

[73] Onset Computer Corporation, "Accusense F900 Series Air Velocity and Air Temperature Sensors Manual Part No: MAN-DRGREE CONTROLS, DOC NO: 13040-B," 2009.

[74] GreenHeck, "Direct Drive Centrifugal Inline Fan Model:SQ-130HP-VG," GreenHeck, Brownsville, 2016.

[75] B. He, V. Martin, F. Setterwall, "Phase transition temperature ranges and storage density of paraffin wax phase change materials," *Energy,* vol. 29, pp. 1785-1804, 2004.

Appendix A PCM Box Construction

The following provides a detailed outline of how the PCM box was constructed with accompanying images. The plywood pieces were cut with the use of a table saw and a hand saw. Holes were drilled through the base plate, middle plate and top bars to hold the dowel pins. The holes were made the same size as the pins for a snug fit. The holes were drilled with precision tools. The top bars and the middle plate were drilled with a milling machine and the base plate was robotically drilled with a CNC router table. The pins were inserted with a makeshift pin holder and a soft hammer.

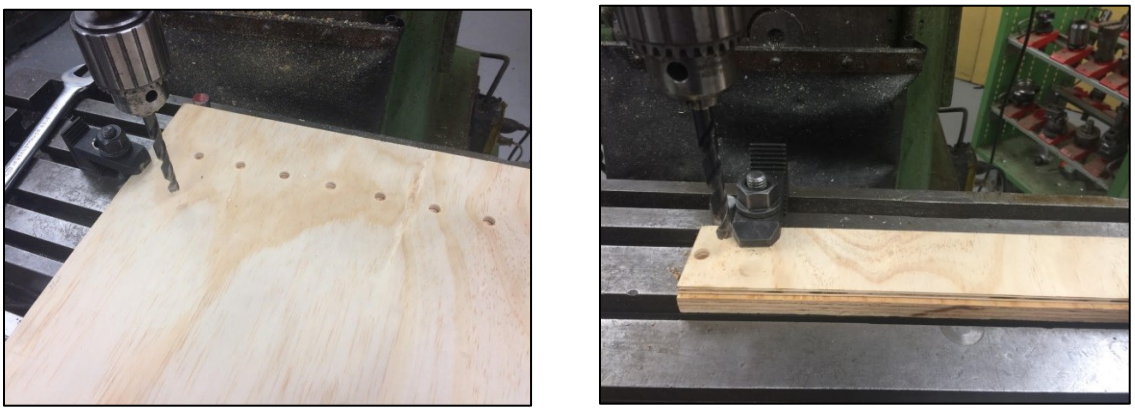

Figure A.1 Left) Holes being Drilled into the Middle Plate and Right) Holes being Drilled into the Top Bars

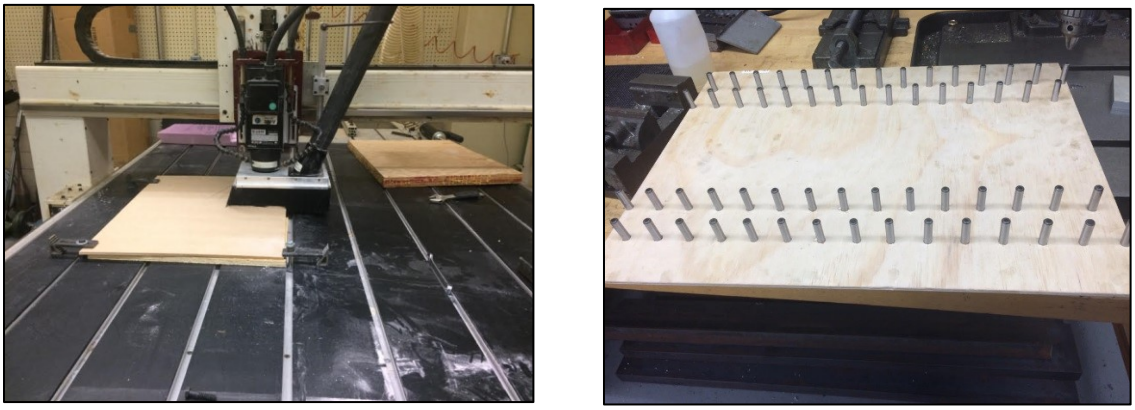

Figure A.2 Left) CNC Router Table Drilling Holes into Base Plate and Right) Middle Plate with Dowel Pins

The PCM box assembly was started by screwing the two inner side walls to the base plate with wood screws. The metal frame that would be used to connect the PCM box to the duct work of the air-loop was positioned on either end and attached with metal screws as seen in Figure A.3 right. Large metal clamps were temporarily inserted over the inner walls in order to obtain the desired width at the top of the box, see Figure A.4 left. The middle plate and top bars were installed by carefully nailing there edges into a ¾" thick piece of wood and then using a wood screw through the wood into the side walls, see Figure A.4 right.

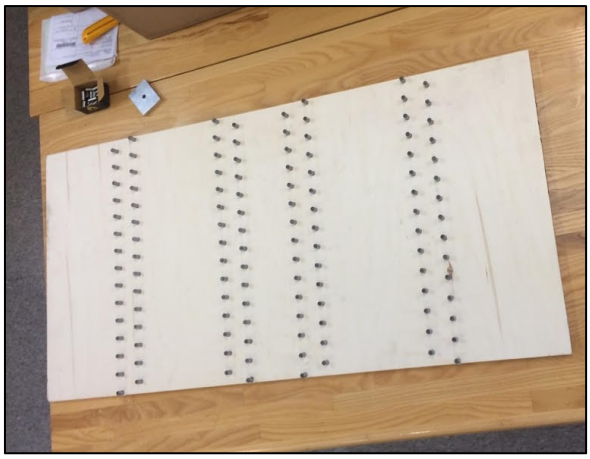

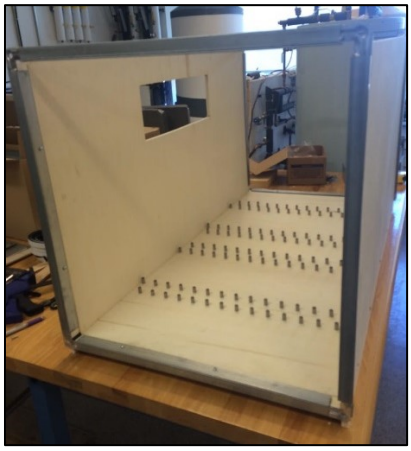

Figure A.3 Left) Base Plate with Dowel Pins inserted and Right) Inner Walls with Metal Frame Attached

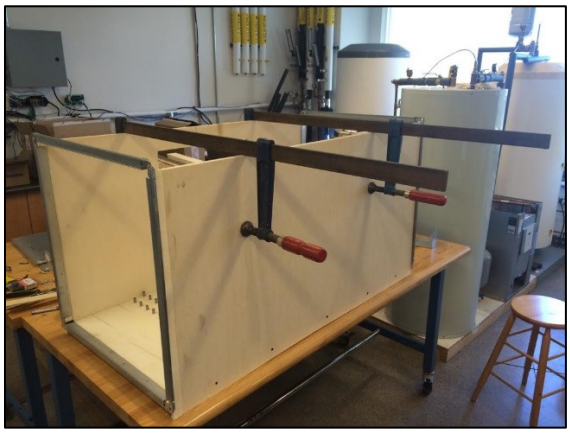

Figure A.4 Left) Large Clamps on Inner Box Walls and Right) Middle Plate Installed

With the base plate, middle plate and top bars installed, the PCM plates were inserted to verify whether they would fit properly. It was found that the middle plate needed to be

repositioned, then the PCM plates all fit into place properly, see Figure A.5 left. The insulation and bottom board were held in place by inserting several long screws into both layers and the base plate, see Figure A.5 right. Four wheels were attached to the bottom of the box with small wooden piece in between to achieve the proper box height for the metal frame to match with the air-loop duct, see Figure A.6 right.

Figure A.5 Left) the PCM Plates Properly Inserted into the PCM Box and Right) the Bottom Insulation with the Bottom Board Attached to the Inner Box.

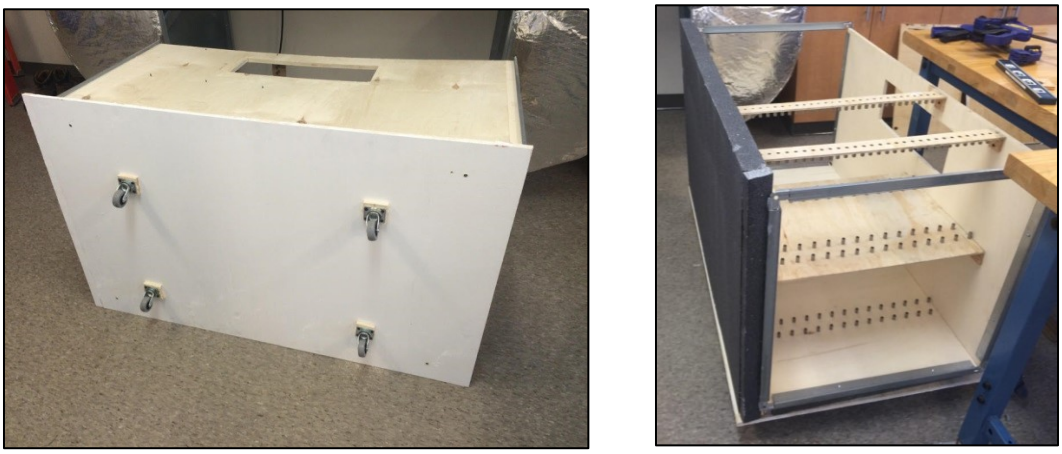

Figure A.6 Left) Four Wheels on Bottom of PCM Box and Right) Insulation Placed on the Side of PCM Box

The side insulation and outer boards were installed with the same method as the bottom. Small clamps were used to keep the layers in place as the long screws were inserted to hold

everything together, see Figure A.6 right and Figure A.7 left. Long pieces of plywood were used to cover the exposed insulation at the top (Figure A.7 right).

Figure A.7 Left) Side Wall Installed Right) Side Wall with Window Set in Place with Small Clamps

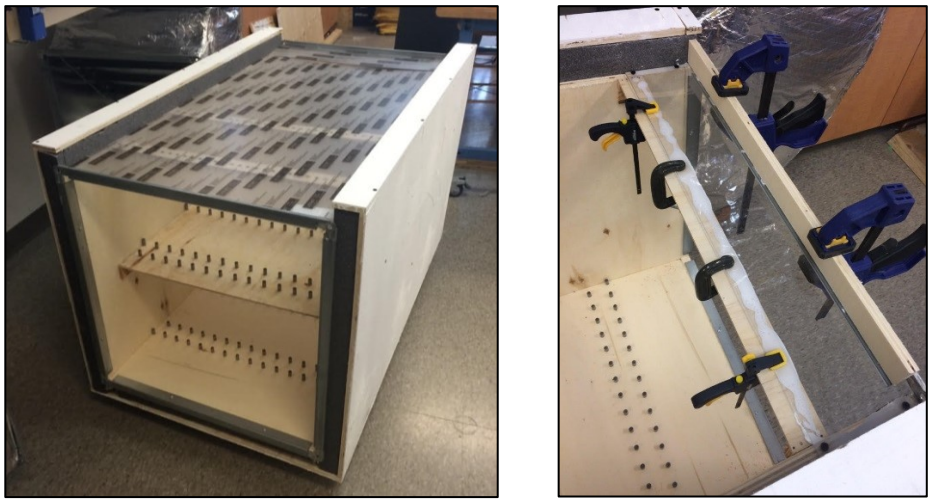

Figure A.8 Left) Completed Box Sides with Plexiglass and Right) Small Section of Plexiglass Installation

The Plexiglass was installed in two sections as the sheet acquired was not long enough to cover the entire area required. A small bar was placed at the location where the Plexiglass sections would meet to prevent air leakage and facilitate installment, see Figure A.8 right. The Plexiglass was installed with silicon along the wooden edges and the top of the metal frame. Screws were also used in multiple locations. The Plexiglass was clamped tight with multiple clamps and left overnight for the silicon to dry, see Figure A.8 right and Figure A.9 left. Plexiglass was also

installed over the small window on the side wall on the PCM box using the same method, see Figure A.9 right.

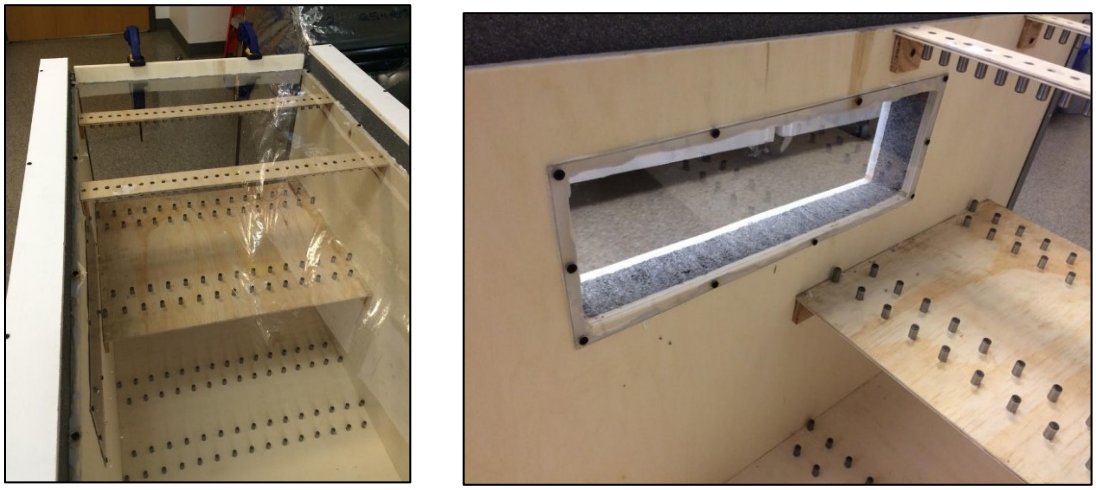

Figure A.9 Left) PCM Box with Plexiglass Installed and b) Installation of Plexiglass in Side Window

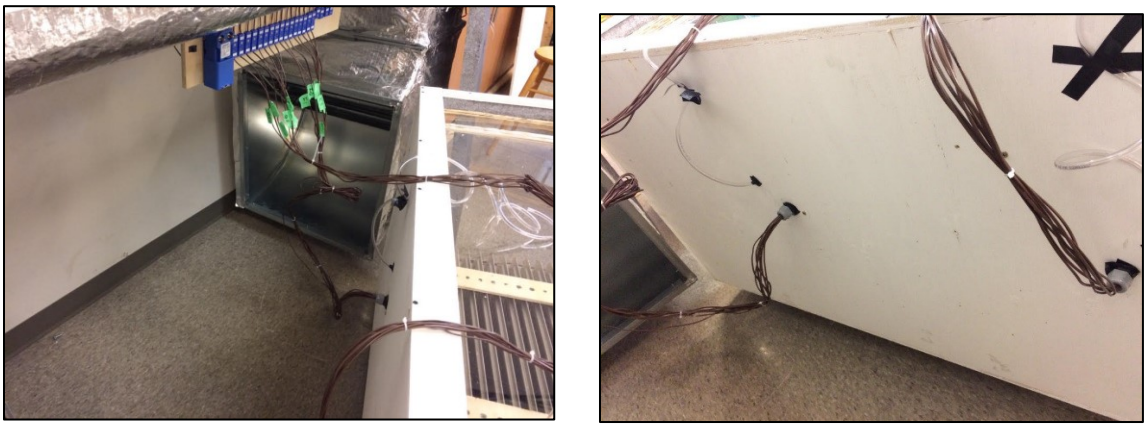

Figure A.10 Thermocouple and Pressure Tube Insertion into the Side of the PCM Box

The thermocouples and pressure tubes were installed with minimal air leakage from the PCM box in mind. On both sides of the PCM plates on the back side wall, two holes were drilled through all the layers of the box wall. In one set of holes the pressure tubes were inserted so that they would be flush with the inner wall. Electrical tape was used around the tubes to keep them in place and prevent air leakage. In the second set of holes conduit strain relief connectors were installed. The thermocouples were then threaded through the connectors which were then sealed, see Figure A.10.

Once all the insturmentation was properly positioned, the PCM box was wheeled into the opening of the air-loop. The metal frame of the box and the duct were sealed together with ducting tape along the outer perimeter, see Figure A.11 left. The completed PCM box with its Plexiglass insulation cover installed in the air-loop can be seen in Figure A.11 right.

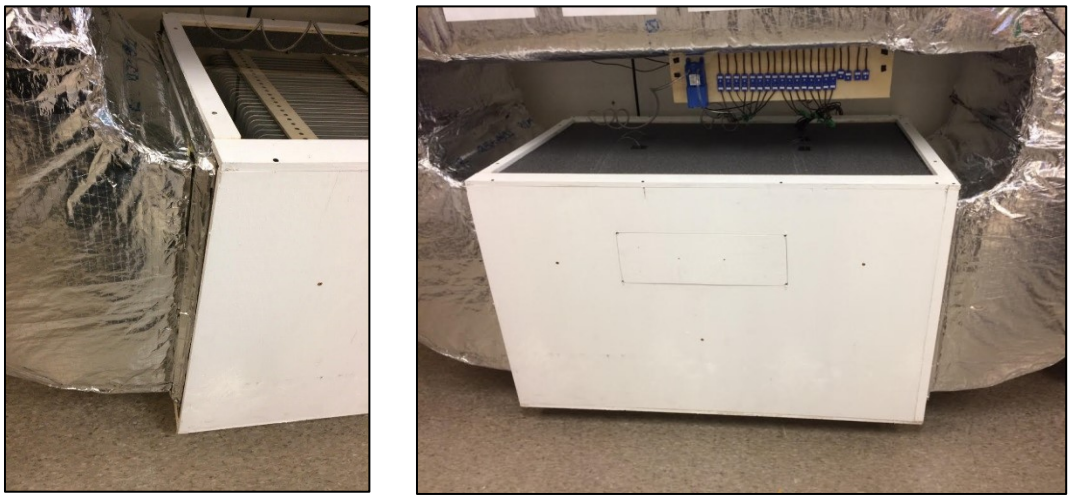

Figure A.11 Left) Ducting Tap used to Seal PCM Box to Duct and b) Completed PCM Box Installed in Air-Loop

Appendix B Rubitherm PCM Properties

Tables A-1 to A-3 show the properties of the three Rubitherm PCM that were selected as potential candidates to be used in application. All three contain similar properties to the experimental PCM, RT44HC.

Table A-1 Properties of RT5HC [69]

Property	Value
Melting area	5-6°C
Solidification area	6-5°C
Heat storage capacity with temperature range of -2°C to 13°C	250 kJ/kg
Specific heat capacity	2 kJ/kg K
Density solid	0.88 kg/l
Density liquid	0.76 kg/l
Heat conductivity	0.2 W/m-K
Volume expansion	13 %

Table A-2 Properties of RT11HC [70]

Property	Value
Melting area	10-12°C
Solidification area	12-10°C
Heat storage capacity with temperature range of 5°C to 20°C	200 kJ/kg
Specific heat capacity	2 kJ/kg K
Density solid	0.88 kg/l
Density liquid	0.77 kg/l
Heat conductivity	0.2 W/m-K
Volume expansion	12.5 %

Table A-3 Properties of RT18HC [71]

Property	Value
Melting area	17-19°C
Solidification area	19-17°C
Heat storage capacity with temperature range of 11°C to 26°C	260 kJ/kg
Specific heat capacity	2 kJ/kg K
Density solid	0.88 kg/l
Density liquid	0.77 kg/l
Heat conductivity	0.2 W/m-K
Volume expansion	12.5 %

Appendix C - Wiring Diagram

The following is the wiring diagram used to power all instrumentation and equipment of the air-loop.

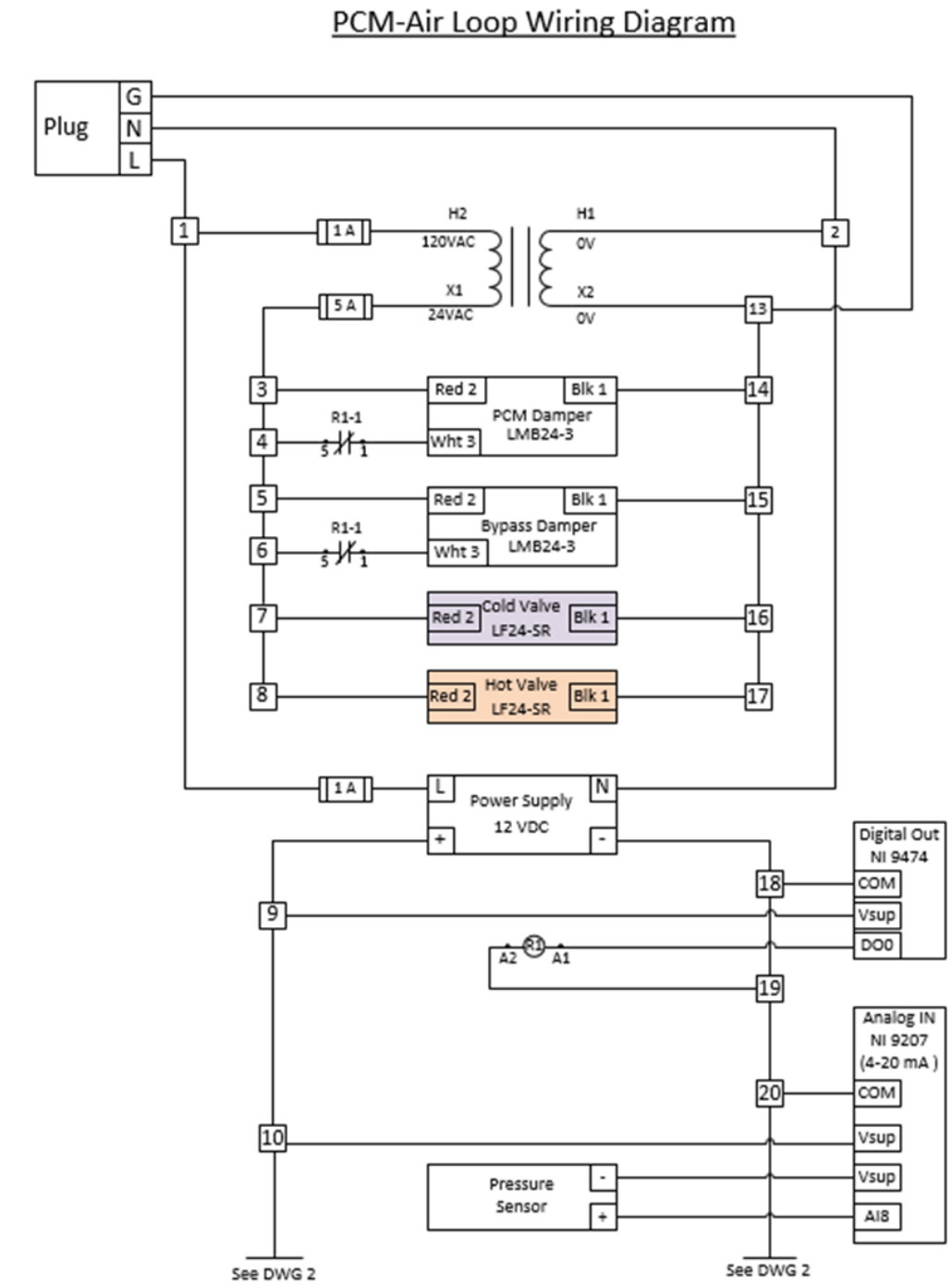

Drawing 1

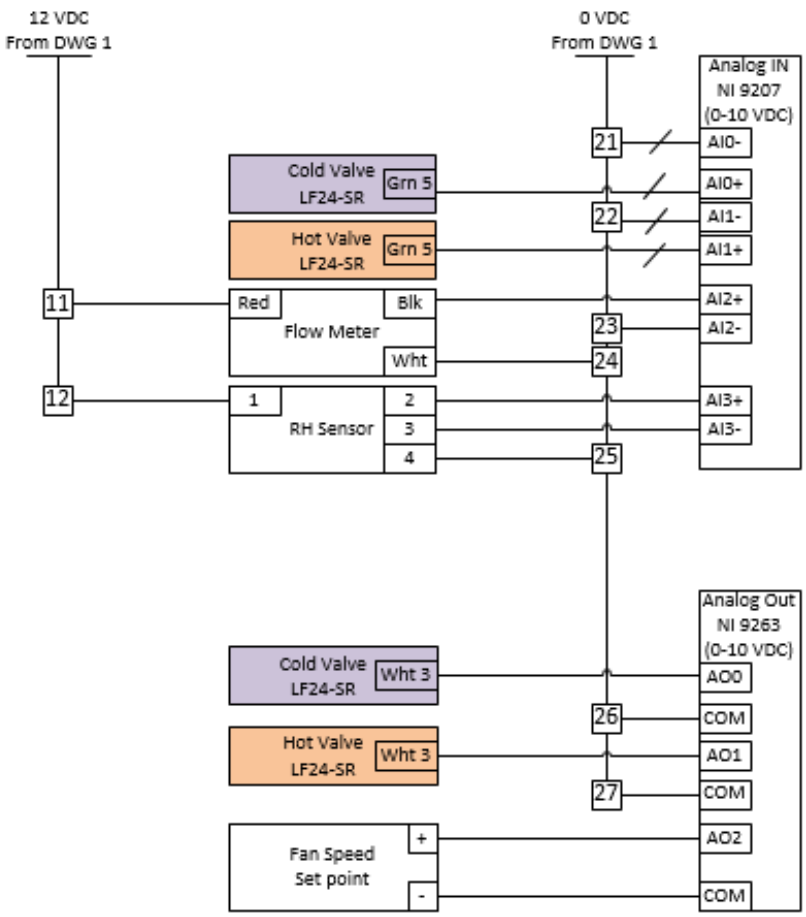

Drawing 2

Figure A.12 Wiring Diagram

Appendix D - Thermocouple Calibration

Thermocouples are composed of two dissimilar metals. The Type T thermocouple used in the experiment consists of copper and constantan. The two wires are connected at a point of measurement and a point of reference; if the two points are at different temperatures a voltage potential is generated and can be measured by a potentiometer, see Figure A.13. In the experimental set up, the thermocouples were connected to an NI9213 thermocouple card. This card electronically creates a reference temperature creating what is known as cold junction compensation (CJC). [72]

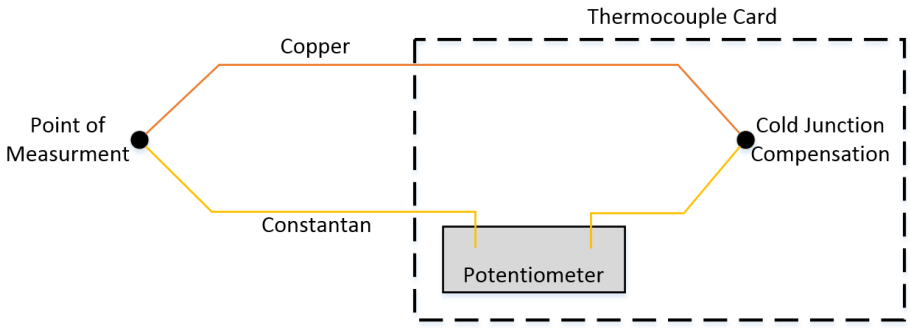

Figure A.13 Type T Thermocouple with Built-in Cold Junction Compensation

The thermocouple card sends the voltage signal and the CJC reference signal to the LabVIEW program. LabVIEW contains an internally built-in polynomial function to calculate a temperature from the acquired signals. This function does not necessarily give the best representation of the actual temperature. Thus, the thermocouples are calibrated to obtain a new polynomial to minimize error.

The calibrated polynomial function was determined by comparing the temperature from the built-in LabVIEW function to the true value. This was achieved by inserting a thermocouple into a Fluke 7102 temperature bath with a previously calibrated RTD connected to a multimeter to represent the true temperature, see Figure A.14 for set-up. A Type T thermocouple was inserted

into the temperature bath. The data recorded included the built-in CJC temperature and the thermocouple's voltage read by an NI9213 thermocouple card.

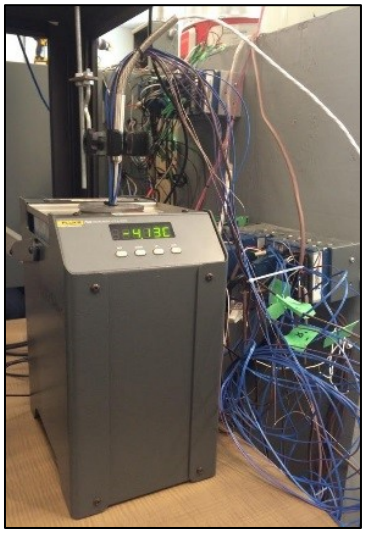

Figure A.14 Fluke 7102 Temperature Bath with Inserted RTD and Thermocouples

The temperature bath was set to an initial temperature of 5˚C and was incremented by 2˚C until a final temperature of 95˚C was reached. A time delay of 20 minutes occurred between each temperature change in order to ensure steady state was achieved. For each temperature setting 36 readings were recorded in 10 second intervals.

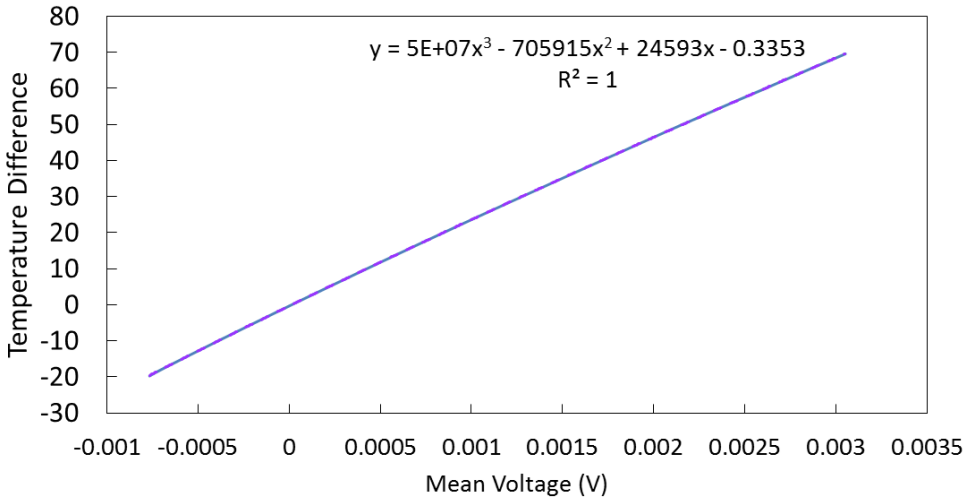

Figure A.15 Calibration Curve

The calibration polynomial was created by first taking the mean of the RTD temperature, the thermocouple voltage and the CJC temperature for each temperature interval. The mean CJC temperature is subtracted from the mean RTD temperature to obtain a temperature difference. This was done to separate the temperature (y-axis) from the voltage (x-axis) to be able to plot the polynomial function, see Figure A.15. The calibration equation was then added to the LabVIEW programming.

Appendix E - Temperature Measurement Uncertainty

The uncertainty analysis determines the potential error within a measurement. It gives the user an idea of how accurate the measurement taken was and whether it is usable for the desired application.

The uncertainty for the temperature measurement was calculated in two stages. First the error of the thermocouple from the calibration was determined and then the measurement error during general experimentation was determined. The thermocouple calibration would include the error of the instrumentation required to take the measurement which would include the voltage offset and the CJC accuracy from the thermocouple card as well as the regression error of the thermocouple. It would also include error from the instrumentation used during the calibration which would include the bath uniformity as the bath's temperature would vary slightly throughout, the error associated with the RTD which was used to measure the true temperature and the accuracy of the multimeter resistance which was used to read the resistance of the RTD. It should be noted that although the temperature measurements during experimentation were taken with the NI 9213 thermocouple card, the data for the calibration equation was obtained with the more accurate NI 9214 thermocouple card.

Most of these errors from the instrumentation specification sheets are in degrees Celsius and can be used in the RRS with the exception of the card voltage offset (6 μV for NI 9213 and 8 μV for NI 9214) and the multimeter resistance accuracy. These values needed to be converted before being included in the total calibration error. For the card voltage, this was done by taking the derivative of the calibration equation and solving using the highest voltage reading taken during calibration (0.00305 V) to find a value to relate the voltage reading to the temperature.

$$T = C_1V^3 + C_2V^2 + C_3V + C_4 \tag{A.1}$$

$$\frac{\partial T}{\partial V} = 3C_1V^3 + 2C_2V + C_3 \tag{A.2}$$

$$\frac{\partial T}{\partial V} = 3(52288560)(0.00305)^2 + 2(-706915)(0.00305) + 24593 \tag{A.3}$$

$$\frac{\partial T}{\partial V} = 21740\,\frac{℃}{\mathrm{V}} \tag{A.4}$$

The card voltage error was converted to volts and multiplied by 21740 ℃/V resulting in an error of ±0.130˚C and ±0.174˚C for cards NI 9213 and NI 9214 respectively. The multimeter resistance accuracy was converted to temperature using the same method as the card voltage. The error was determined using the highest resistance reading recorded during calibration (0.137 kΩ) for an error of ±0.00774Ω according to the manufacturer. The derivative was taken on the RTD's second order calibration equation.

$$\frac{\partial T}{\partial R} = 2C_1R + C_2 \tag{A.5}$$

$$\frac{\partial T}{\partial R} = 2(0.000997)(137\Omega) + 2.308 \tag{A.6}$$

$$\frac{\partial T}{\partial R} = 2.58\,\frac{℃}{\Omega} \tag{A.7}$$

The multimeter resistance accuracy was multiplied by the conversion factor resulting in an error of ±0.02˚C.

The errors included in the total calibration error are shown in Table A-4. The RSS was used to achieve a total calibration error of ±0.33˚C which is lower than the ±0.5˚C error specified by the manufacturer.

Table A-4 Calibration Error

Calibration Error	
Card Voltage Offset	±0.174˚C
Card CJC Accuracy	±0.25˚C
Multimeter Resistance Accuracy	±0.02˚C
Bath Uniformity	±0.02˚C
RTD Accuracy	±0.012˚C
RTD Short-term Repeatability	±0.009˚C
RTD Drift	±0.007˚C
Thermocouple Regression Error	±0.12˚C
Total Calibration Error	±0.33˚C

The temperature measurement includes the thermocouple card error and the error of the thermocouple itself. The NI 9213 card was used during experimental measurements thus the voltage offset and CJC accuracy was taken from its specification sheet. The thermocouple error is simply the total calibration error previously calculated. The total measurement error as seen in Table A-5 was calculated to be ±0.88˚C. This error is high compare to the calibration error because of the significantly higher CJC error of the NI 9213 card.

Table A-5 Temperature Measurement Error

Measurement Error	
Card Voltage Offset	±0.130˚C
Card CJC Accuracy	±0.8˚C
Thermocouple Error	±0.33˚C
Total Measurement Error	±0.88˚C

Appendix F - Temperature Reading Dynamic Response Time

The dynamic response time represents the actual time it takes for the sensor to register the true value in a changing environment. This applies to the experiment as the temperature will vary throughout.

The dynamic response time was measured by manually plunging the thermocouples into the Fluke 7102 temperature bath. The true temperature value was recorded with an RTD. One spool of Type T thermocouple wire was used throughout the entire experiment. Three thermocouple wires were used to verify any discrepancies within the spool. The initial bath temperature was set to 10˚C. The thermocouples were plunged into the bath where they rested for 5 minutes. The thermocouples were then removed, dried of the glycol and left to readjust to room temperature for an additional 5 minutes. The thermocouples where reinserted twice more for a total of three repetitions. The bath temperature was increased by intervals of 20˚C and the procedure repeated until a final temperature of 90˚C. A delay time of 20 minutes was used between temperature intervals to ensure steady state was achieved within the bath.

The data recorded from the three repetitions was averaged for each test in order to obtain more accurate results. The dynamic response time of the three thermocouples were compared to determine whether any time variance was present. Figure A.16 shows the time response of all three thermocouples with the temperature bath set at 10˚C. It was observed that all three thermocouples took slightly different paths but achieved the desired temperature reading in 2.5 seconds. Thus, it was demonstrated that there was no time variance for the thermocouple spool.

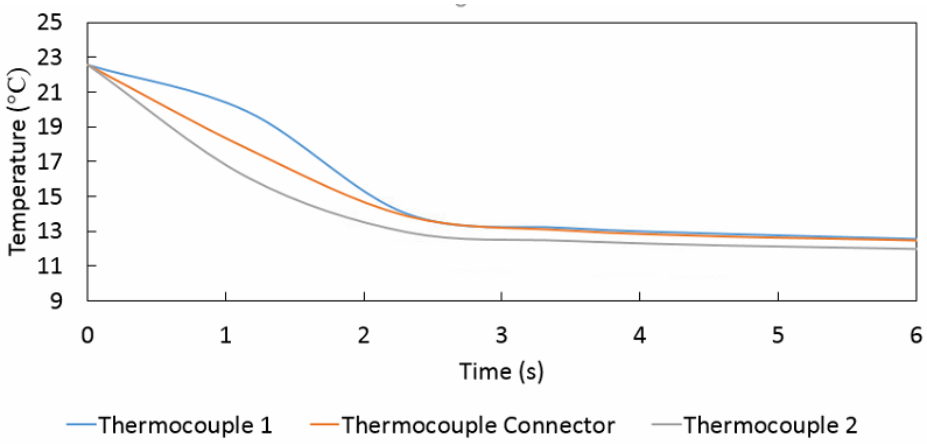

Figure A.16 Thermocouple Time Response from Room Temperature to 10˚C

The bath temperature was varied to determine whether greater temperature differences would have an effect on time response. The time response for thermocouple 1 at various temperature bath settings can be seen in Figure A.17. It was observed that for temperature differences of 10˚C and 30˚C the dynamic response time was 2.5 seconds. However, an increase in response time was observed in greater temperature differences. For instance, a response time of 8 seconds was observed for a 50˚C temperature difference and a response time of 11 s for a 90˚C temperature difference.

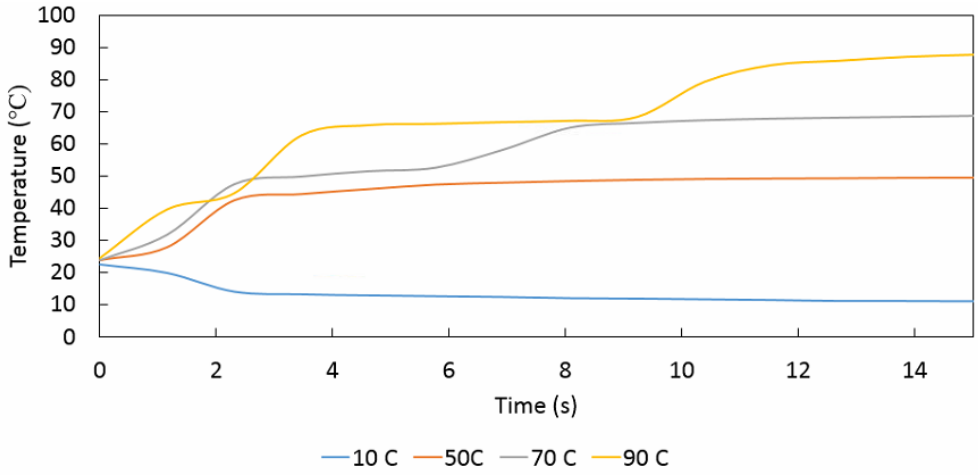

Figure A.17 Dynamic Response Time for Thermocouple 1 at Various Temperature

From these results it is concluded that dynamic response time is affected by temperature difference greater than 50˚C and will have a continuous value of 2.5 seconds otherwise. The temperature measured within the experimental equipment has an expected temperature variance of approximately 5˚C. Thus, for the application the dynamic time response was considered to be 2.5 seconds. This is useful information as it indicated that the temperature readings should be taken in time intervals of 2.5 seconds or greater.

Appendix G - Velocity Measurement Error

The errors taken into consideration for the analysis were obtained from manufacture specification sheets. The specifications for velocity measurement pertaining to error are listed in Table A-6. [73]

Table A-6 Cambridge Accusense F900 Series Air Velocity Sensor Manufacture Specifications

Cambridge Accusense F900 Series Air Velocity Sensor	
Range	0.15 m/s to 5.0 m/s
Accuracy	±5% of reading or ±0.05 m/s
Repeatability	±1% of reading

The velocity sensor's signal was read by the NI 9207 combination voltage/current input card. The card was manufacture calibrated to have an accuracy of ±0.52% of the reading. The velocity measurement error was a combination of the sensor accuracy, sensor repeatability and input card accuracy. The root-sum-squares method (RSS) was used to calculate the final uncertainty:

$$u_{\text{velocity}} = \pm\sqrt{(\text{sensor accuracy})^2 + (\text{sensor repeatability})^2 + (\text{card accuracy})^2} \quad \text{(A.8)}$$

The error for both accuracies and the repeatability are percentages of the reading meaning that the error will vary with velocity. The minimum and maximum error was determined for the range of the sensor and can be seen in Table A-7. It was noted that for the minimum velocity the accuracy error used the error of ±0.05 m/s as this value was greater than 5% of the reading.

Table A-7 Minimum and Maximum Velocity Measurement Error

Minimum and Maximum Error for Velocity Measurement		
	Minimum (0.15 m/s)	**Maximum (5 m/s)**
Accuracy	±0.05 m/s	±0.25 m/s
Repeatability	±0.0015 m/s	±0.05 m/s
Card Accuracy	±0.00078 m/s	±0.026 m/s
Total Uncertainty	±0.052 m/s	±0.33 m/s
Percent Error	35%	6.5%

There was a large difference in percent error between the minimum velocity having 35% error and the maximum velocity having 6.5% error. For a better understanding of error distribution as the velocity increases, the percent error for each value within the sensor's range was plotted and can be seen in Figure A.18. It was observed that the error remains 6.5% for values greater than 1 m/s but increase exponentially for values lower than 1 m/s until the minimum is reached. From these results, it would be advisable to only use this sensor when measuring values greater than 1 m/s.

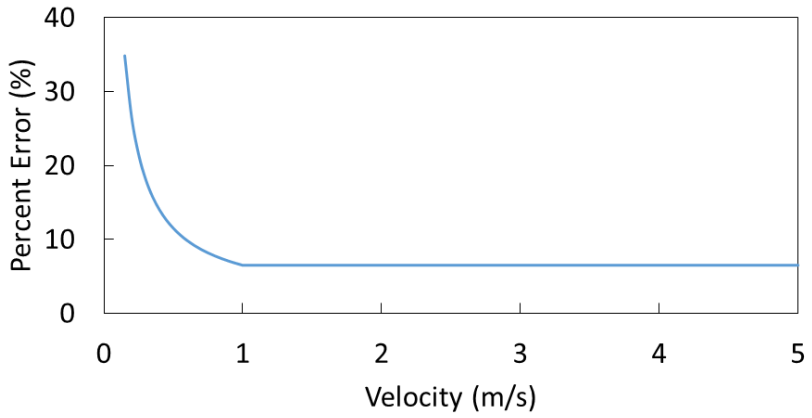

Figure A.18 Percent Error of Velocity Measurement within Sensor's Range

Appendix H Flow Rate Validation

The velocity profile test procedure described in Section 4.1 was used to determine the velocity profile at the inlet of the PCM plates. Table A-8 displays the integrated value of the equation from Figure 4.5, the average velocity and the volumetric flow rate for each of the 5 fan signals from the procedure. The maximum volumetric flow rate was determined to be 1299 CFM (2207 m³/h). The fan was rated to 890 CFM (1512 m³/h) which was lower than the maximum value of the PCM box. It was determined from the fan's manufacture specification sheet that the maximum flow was possible for a static pressure of approximately 0.3 inwg, see Figure A.19.

Table A-8 Average Velocity and Volumetric Flow Rate Values for the Five Fan Signals from the Velocity Profile Test Procedure

	Integrated Value (m²/s)	Velocity (m/s)	Flow Rate (m³/s)	Flow rate (CFM)
2V	0.269	0.441	0.164	347
4V	0.434	0.712	0.265	561
6V	0.622	1.021	0.379	804
8V	0.826	1.356	0.504	1068
10V	1.006	1.650	0.613	1299

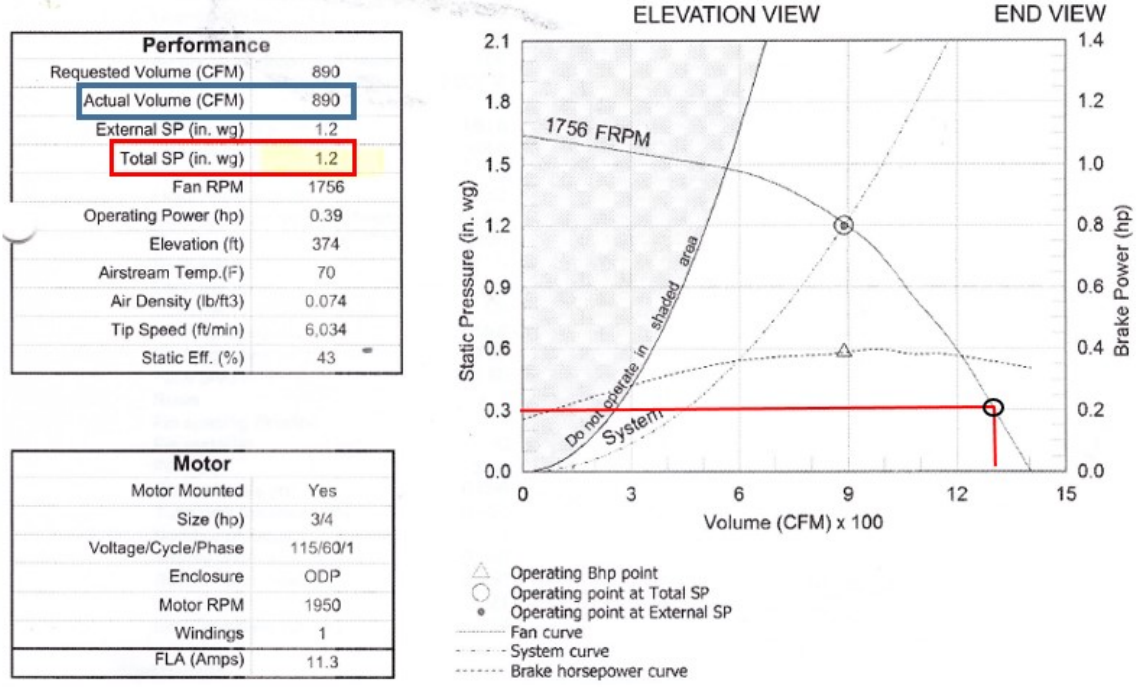

Figure A.19 Manufacture Fan Performance Sheet with the Highest Flow Rate from the Velocity Test Procedure Indicated by the Red Lines [74]

Appendix I – PCM Box Heat Loss

The PCM box would have had heat transfer to and from the surroundings. Figure A.20 shows a reference schematic indicating the wall materials and the temperature labels with Ts representing the temperature of the surroundings and Tin representing the inlet temperature in the PCM box. The thermal resistance or "R values" for 1/2" plywood and the insulation was 0.11 Km^2/W and 1.4 Km^2/W respectively. The insulation properties of the Plexiglas were considered to be negligible.

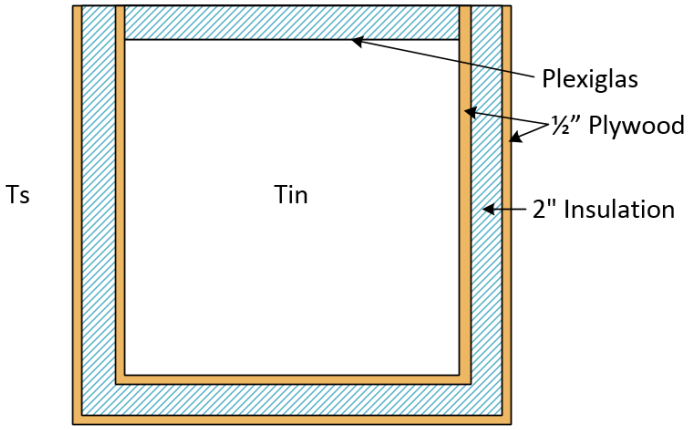

Figure A.20 Schematic of PCM Box Wall Materials

The heat transfer equation can be expressed in terms of thermal resistance [17]:

$$q = q"A = \frac{\Delta T A}{R} \tag{A.9}$$

where q represents heat transfer, q" represents heat flux, A represents area of the wall, ΔT represents the change in temperature and R represents the thermal resistance value of the material. The following is a sample calculation demonstrating how heat transfer to the surroundings was calculated using the surrounding temperature of 20˚C and the inlet temperature of 60˚C. The calculation was divided into two sections; the 3 main walls which included the base and the two sides, and the top wall.

$$q''_{(\text{3main walls})} = \frac{(60-20)}{1.4+2(0.11)} = 24.7\ \text{W/m}^2 \quad \text{(A.10)}$$

$$q_{(\text{3main walls})} = \left(24.7\frac{\text{w}}{\text{m}^2}\right)(0.45\ \text{m} * 0.61\text{m}) = 6.8\ \text{W} \quad \text{(A.11)}$$

$$q''_{(\text{top wall})} = \frac{(60-20)}{1.4} = 28.6\ \text{W/m}^2 \quad \text{(A.12)}$$

$$q_{(\text{top wall})} = \left(28.6\frac{\text{w}}{\text{m}^2}\right)(0.45\ \text{m} * 0.61\text{m}) = 7.8\ \text{W} \quad \text{(A.13)}$$

$$q = 3(6.8\ \text{w}) + 7.8\ \text{W} = 28.2\ \text{W} \quad \text{(A.14)}$$

The final heat transfer value was an instantaneous value add would change as the experiment progressed resulting in the need for it to be continuously calculated over the designated time interval until the test was done.

Appendix J PCM Plate Mass Measurements

The mass was determined for each PCM plate used in the PCM box and was recorded in Table A-9. The total mass of PCM used during experimentation was calculated by subtracting the tare mass of the aluminum case from the total mass of the plate.

Table A-9 Mass of PCM plates used during experimentation

Plate number	mass	PCM mass	Plate number	mass	PCM mass	
Top 1	856	0.506	Bottom 1	860	0.51	
Top 2	859	0.509	Bottom 2	862	0.512	
Top 3	857	0.507	Bottom 3	861	0.511	
Top 4	856	0.506	Bottom 4	861	0.511	
Top 5	855	0.505	Bottom 5	862	0.512	
Top 6	868	0.518	Bottom 6	861	0.511	
Top 7	855	0.505	Bottom 7	861	0.511	
Top 8	859	0.509	Bottom 8	857	0.507	
Top 9	860	0.51	Bottom 9	861	0.511	
Top 10	860	0.51	Bottom 10	858	0.508	
Top 11	855	0.505	Bottom 11	861	0.511	
Top 12	859	0.509	Bottom 12	861	0.511	
Top 13	859	0.509	Bottom 13	857	0.507	
Top 14	865	0.515	Bottom 14	898	0.548	
Top 15	855	0.505	Bottom 15	855	0.505	
Top 16	861	0.511	Bottom 16	860	0.51	
Top 17	858	0.508	Bottom 17	859	0.509	
Top 18	880	0.53	Bottom 18	859	0.509	
Top 19	860	0.51	Bottom 19	857	0.507	
Top 20	858	0.508	Bottom 20	854	0.504	
Top 21	859	0.509	Bottom 21	859	0.509	
Top 22	855	0.505	Bottom 22	860	0.51	
Top 23	854	0.504	Bottom 23	862	0.512	
Top 24	860	0.51	Bottom 24	860	0.51	
Top 25	862	0.512	Bottom 25	860	0.51	
Top 26	862	0.512	Bottom 26	859	0.509	
Top 27	862	0.512	Bottom 27	897	0.547	
Top 28	859	0.509	Bottom 28	856	0.506	
Top 29	855	0.505	Bottom 29	856	0.506	
Total		14.773			14.844	29.617 kg

Appendix K Additional Energy Storage

Additional energy was stored in the aluminum cases that contained the PCM and in the plywood walls that held the PCM plates. An example calculation is provide using a final temperature (inlet temperature) of 62˚C and an initial temperature of 18˚C.

K.1 Energy Stored in Aluminum Cases

Aluminum is not a PCM thus energy could only be stored sensible which can be quantified using the heat transfer rate equation, A.15. The manufactured specified mass for a single case was 0.35kg. A total of 58 plates would add to a total aluminum mass of 20.3 kg. The specific heat of aluminum was 0.91 kJ/kg K.

$$E_{\mathrm{st,al}} = mc_{\mathrm{p,al}}\Delta T \tag{A.15}$$

$$E_{\mathrm{st,al}} = (20.3\ \mathrm{kg})\left(0.91\frac{\mathrm{kJ}}{\mathrm{kgK}}\right)(62℃ - 18℃) = 813\ \mathrm{kJ} \tag{A.16}$$

The energy stored in the aluminum was an order of magnitude smaller than the energy stored in the PCM. This value made a small contribution to the over amount of energy stored.

K.2 Energy Stored in Plywood Walls

Plywood is also not a PCM and would only store energy sensible. The density of ½" plywood was approximated as 6.9 kg/m². The total mass of the plywood was determined by the density:

$$m = 3\rho A = 3 * 6.9\frac{\mathrm{kg}}{\mathrm{m^2}} * 0.2787\ \mathrm{m^2} = 5.8\ \mathrm{kg} \tag{A.17}$$

The three in the equation represent the three plywood walls as the fourth was constructed out of Plexiglas. A range of specific heat values were found for plywood ranging from 1.3 to 2.4 kJ/kgK. The average of the range was used in calculating energy storage.

$$E_{\mathrm{st,ply}} = mc_{\mathrm{p,al}}\Delta T \tag{A.18}$$

$$E_{\mathrm{st,ply}} = (5.8\ \mathrm{kg})\left(1.85\,\frac{\mathrm{kJ}}{\mathrm{kgK}}\right)(62℃ - 18℃) = 472.\,\mathrm{kJ} \tag{A.19}$$

Although the specific heat of plywood was greater than that of aluminum, plywood had about half the energy storage capacity as a result of significantly less mass of plywood present in the box. Plywood also was an order of magnitude less than PCM and contributed little to the overall energy storage capacity.

Appendix L TES PCM Type FORTRAN Code

```
57        Use TrnsysConstants
58        Use TrnsysFunctions
59
60  !------------------------------------------------------------------------
61
62  !DEC$Attributes DLLexport :: Type293
63
64  !------------------------------------------------------------------------
65  !Trnsys Declarations
66        Implicit None
67
68        Double Precision Timestep,Time
69        Integer CurrentUnit,CurrentType
70
71
72  !     PARAMETERS
73        INTEGER CUnit
74        INTEGER DUnit
75        DOUBLE PRECISION Tmelt
76        INTEGER UnitNumber
77        DOUBLE PRECISION HourChange
78        INTEGER TotalUnitNumber
79
80  !     INPUTS
81        DOUBLE PRECISION Tcharge
82        DOUBLE PRECISION Tdischarge
83        INTEGER Hour
84        INTEGER ControlSignal
85        DOUBLE PRECISION FlowCharge
86        DOUBLE PRECISION FlowDischarge
87
88  !     OUTPUTS
89        DOUBLE PRECISION EnergyStorage
90        DOUBLE PRECISION HeatTransfer
91        DOUBLE PRECISION Temperature
92        DOUBLE PRECISION Mode
93        DOUBLE PRECISION FlowOutput
94
95  !     LOCAL VARIABLE
96        INTEGER nX(4), nY(1), nIND , nXD(4), nYD(1), nINDD, j, a, k
97        DOUBLE PRECISION X(4), Y(1), XD(4), YD(1), VolumeFlow
98        DOUBLE PRECISION Energy, Tinital, Density
```

```
!------------------------------------------
!Get the Global Trnsys Simulation Variables
      Time=getSimulationTime()
      Timestep=getSimulationTimeStep()
      CurrentUnit = getCurrentUnit()
      CurrentType = getCurrentType()
!------------------------------------------

!------------------------------------------
!Set the Version Number for This Type
      If(getIsVersionSigningTime()) Then
        Call SetTypeVersion(17)
        Return
      EndIf
!------------------------------------------

!------------------------------------------
!Do Any Last Call Manipulations Here
      If(getIsLastCallofSimulation()) Then
        Return
      EndIf
!------------------------------------------

!------------------------------------------
!Perform Any "After Convergence" Manipulatior
      If(getIsEndOfTimestep()) Then
        Return
      EndIf
```

```
!Do All of the "Very First Call of the Simulation Manipulations" Here
      If(getIsFirstCallofSimulation()) Then

        !Tell the TRNSYS Engine How This Type Works
        Call SetNumberofParameters(6)           !The number of parameters
        Call SetNumberofInputs(6)                  !The number of inputs
        Call SetNumberofDerivatives(0)         !The number of derivatives
        Call SetNumberofOutputs(5)                !The number of outputs
        Call SetIterationMode(1)                            !An indicato
        Call SetNumberStoredVariables(0,12)                  !The number
        Call SetNumberofDiscreteControls(0)               !The number of

        Call SetInputUnits(1,'TE1')
        Call SetInputUnits(2,'TE1')
        Call SetInputUnits(3,'DM1')
        Call SetInputUnits(4,'DM1')
        Call SetInputUnits(5,'MF2')
        Call SetInputUnits(6,'MF2')
        Call SetOutputUnits(1,'EN1')
        Call SetOutputUnits(2,'PW3')
        Call SetOutputUnits(3,'TE1')
        Call SetOutputUnits(4,'DM1')
        Call SetOutputUnits(5,'MF2')

        Return

      EndIf
```

```
!Do All of the First Timestep Manipulations Here - There Are
      If (getIsStartTime()) Then
      CUnit = getParameterValue(1)
      DUnit = getParameterValue(2)
      Tmelt = getParameterValue(3)
      UnitNumber = getParameterValue(4)
      HourChange = getParameterValue(5)
      TotalUnitNumber = getParameterValue(6)


      Tcharge = GetInputValue(1)
      Tdischarge = GetInputValue(2)
      Hour = GetInputValue(3)
      ControlSignal = GetInputValue(4)
      FlowCharge = GetInputValue(5)
      FlowDischarge = GetInputValue(6)

      Do j=1,6
        Call SetDynamicArrayValueThisIteration(j,0.d0)
        EndDo
      k=7
      a = 0
      Mode=0
      Tinital=19+44-Tmelt
      Call SetDynamicArrayValueThisIteration(unitnumber+6,Ti


   !Check the Parameters for Problems (#,ErrorType,Text)
   !Sample Code: If( PAR1 <= 0.) Call FoundBadParameter(1,'F

   !Set the Initial Values of the Outputs (#,Value)
        Call SetOutputValue(1, 0.d0) ! EnergyStorage
        Call SetOutputValue(2, 4) ! HeatTransfer
        Call SetOutputValue(3, 0.d0) ! Temperature
        Call SetOutputValue(4, 0) ! Mode
        Call SetOutputValue(5, 0.d0) ! FlowOutput


   !If Needed, Set the Initial Values of the Static Storage
   !Sample Code: SetStaticArrayValue(1,0.d0)

   !If Needed, Set the Initial Values of the Dynamic Storage
   !Sample Code: Call SetDynamicArrayValueThisIteration(1,20

   !If Needed, Set the Initial Values of the Discrete Contro
   !Sample Code for Controller 1 Set to Off: Call SetDesired

        Return

      EndIf
```

```
!ReRead the Parameters if Another Unit of This T
      If(getIsReReadParameters()) Then
        !Read in the Values of the Parameters fr
      CUnit = getParameterValue(1)
      DUnit = getParameterValue(2)
      Tmelt = getParameterValue(3)
      UnitNumber = getParameterValue(4)
      HourChange = getParameterValue(5)
      TotalUnitNumber = getParameterValue(6)


      EndIf
!-----------------------------------------------

!Read the Inputs
      Tcharge = GetInputValue(1)+44-Tmelt
      Tdischarge = GetInputValue(2)+44-Tmelt
      Hour = GetInputValue(3)
      ControlSignal = GetInputValue(4)
      FlowCharge = GetInputValue(5)
      FlowDischarge = GetInputValue(6)


    !Check the Inputs for Problems (#,ErrorType,
    !Sample Code: If( IN1 <= 0.) Call FoundBadIn

      If(ErrorFound()) Return
```

```
    If(ControlSignal==1)Then
    k=1
    If(Mode==1) Then   !Charging
    Density=-0.0036*Tcharge+1.2832
    VolumeFlow=FlowCharge/Density*2118.88
    Energy=getdynamicarrayvaluelasttimestep(unitnumber) !Energy stored from previous timestep
    Tinital=getdynamicarrayvaluelasttimestep(unitnumber+6)
    nIND=4
    nY(1)=1
    nX(1)=30
    nX(2)=3
    nX(3)=4
    nX(4)=3
    X(1)= Energy
    X(2)= Tcharge
    X(3)= Tinital
    X(4)= VolumeFlow
    Call InterpolateData (CUnit,nIND,nX,nY,X,Y)
    HeatTransfer=Y(1)
    EnergyStorage=Energy+HeatTransfer*Timestep*3600
    Temperature=Tcharge-(HeatTransfer/(FlowCharge*1.005))-44+Tmelt
    FlowOutput=FlowCharge
    Call SetDynamicArrayValueThisIteration(unitnumber,energystorage)
    EndIf


    If(Mode==0)Then   !Discharging
    Density=-0.0036*Tdischarge+1.2832
    VolumeFlow=FlowDischarge/Density*2118.88
    Energy= getDynamicArrayValueLastTimeStep(unitnumber)*(-1)
    Tinital=getDynamicArrayValueLastTimeStep(unitnumber+6)
    nINDD=4
    nYD(1)=1
    nXD(1)=30
    nXD(2)=4
    nXD(3)=3
    nXD(4)=3
    XD(1)=Energy
    XD(2)=Tdischarge
    XD(3)=Tinital
    XD(4)=VolumeFlow
    Call InterpolateData (DUnit,nINDD,nXD,nYD,XD,YD)
    HeatTransfer=YD(1)*(-1)
    EnergyStorage=Energy*(-1)+HeatTransfer*Timestep*3600
    Temperature=(Tdischarge-(HeatTransfer/(FlowDischarge*1.005)))-44+Tmelt
    FlowOutput=FlowDischarge
    Call SetDynamicArrayValueThisIteration(unitnumber, EnergyStorage)
```

```
    If(Hour==HourChange)Then
    a=a+1
    EnergyStorage=0.d0
    Tinital=Tdischarge
    Call SetDynamicArrayValueThisIteration(unitnumber, EnergyStorage)
    Call SetDynamicArrayValueThisIteration(unitnumber+6, Tinital)
    If(a==TotalUnitNumber)Then
    Mode=1
    a=0
    EndIf
    EndIf
    EndIf

    Else
    Mode=0
    if(k<=TotalUnitNumber)Then
    k=k+1
    EnergyStorage=0.d0
    Call SetDynamicArrayValueThisIteration(unitnumber, EnergyStorage)
    Tinital=TCharge
    Call SetDynamicArrayValueThisIteration(unitnumber+6, Tinital)
    EndIf
    EndIf
```

```
!Set the Outputs from this Model (#,Value)
        Call SetOutputValue(1, EnergyStorage) ! EnergyStorage
        Call SetOutputValue(2, HeatTransfer) ! HeatTransfer
        Call SetOutputValue(3, Temperature) ! Temperature
        Call SetOutputValue(4, Mode) ! Mode
        Call SetOutputValue(5, FlowOutput) ! FlowOutput

!-----------------------------------------------------------

!-----------------------------------------------------------
!If Needed, Store the Desired Disceret Control Signal Values f
!Sample Code:  Call SetDesiredDiscreteControlState(1,1)
!-----------------------------------------------------------

!-----------------------------------------------------------
!If Needed, Store the Final value of the Dynamic Variables in
!Sample Code:  Call SetDynamicArrayValueThisIteration(1,T_FINA
!-----------------------------------------------------------

      Return
      End
!-----------------------------------------------------------
```

Appendix M TRNSYS Layouts

M.1 (L.1) Base Model

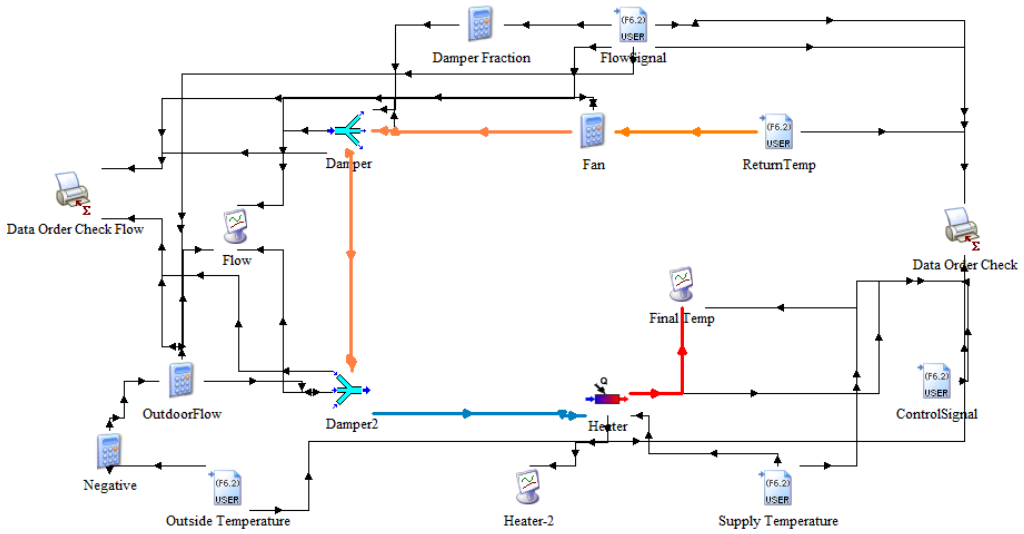

M.2 (L.2) AHU with Integrated PCM using Method 1

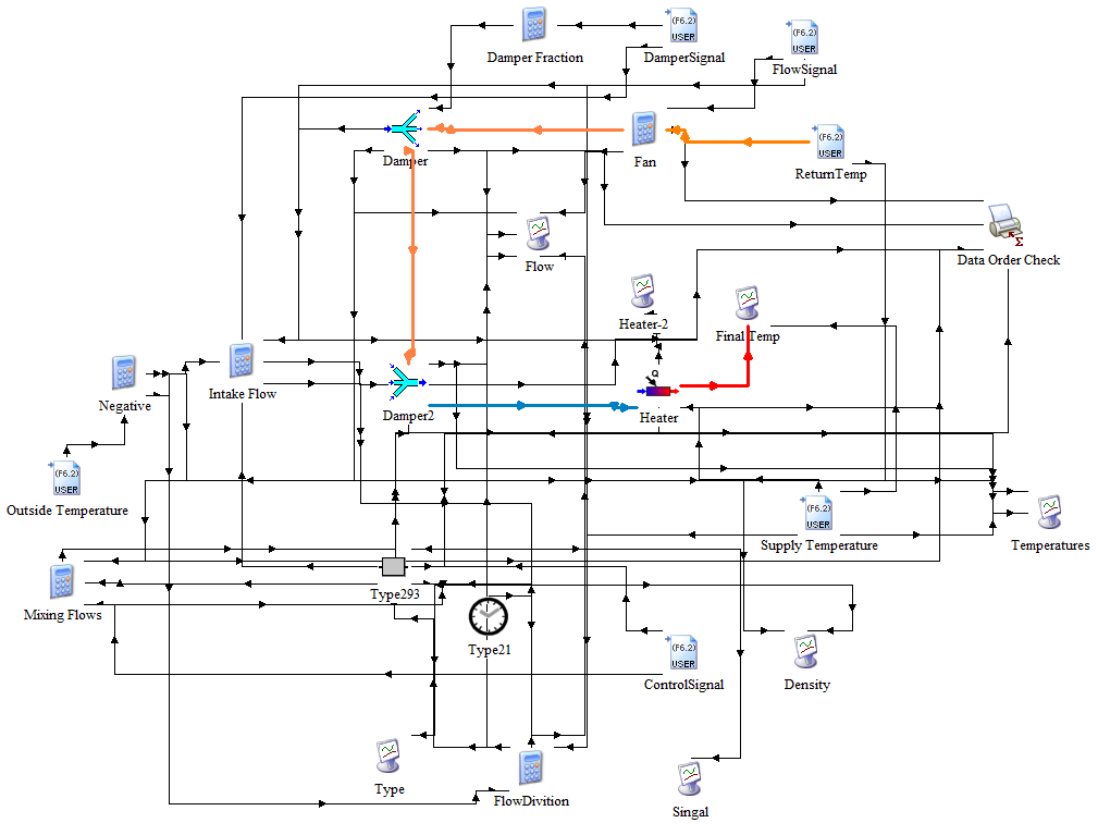

Appendix N Damper Signal Calculation

The damper signal was calculated using the known values from the AHU data set. It was used to provide a signal to the dampers indicating how much intake and exhaust flow to provide to and from the AHU. According to the controls manual of the AHU used, the intake and exhaust flow were programmed to be kept at the same value.

The analysis was done using the second damper as all temperatures at that location were known. The mix flow was a combination of some fraction of the return flow from the first damper and the intake flow with the total summing to 1;

$$\dot{m}_{\mathrm{mix}} = \dot{m}_{\mathrm{Int}} + \dot{m}_{\mathrm{Ret}} = 1 \tag{A.20}$$

were $\dot{m}_{mix}$ is the total flow, $\dot{m}_{Int}$ is the fraction of the intake flow and $\dot{m}_{Ret}$ is the fraction of the return flow from damper 1.

When mixing two fluids at different temperatures, one will gain heat and one will loss heat to the other.

$$\dot{q}_{lost} = \dot{q}_{gain} \tag{A.21}$$

$$\dot{q} = \dot{m}\Delta T c_p \tag{A.22}$$

were $\dot{q}$ is heat transfer, $\dot{m}$ is the mass flow rate, ΔT is the change in temperature and c_p is the specific heat of air. The specific heat of air is 1.005 kJ/ (kg K) for the temperature range of 40°C to -50°C in which all intake and return temperature fall. Combing Eq. (A.21) and Eq. (A.22) and rearrange;

$$c_p \dot{m}_{\mathrm{Ret}}(T_{\mathrm{Ret}} - T_{\mathrm{Mix}}) = (T_{\mathrm{Mix}} - T_{\mathrm{Int}})\dot{m}_{\mathrm{Int}} c_p \tag{A.23}$$

$$\frac{\dot{m}_{Ret}}{\dot{m}_{Int}} = \frac{(T_{Mix} - T_{Int})}{(T_{Ret} - T_{Mix})} \tag{A.24}$$

were T_{Ret} is the return temperature, T_{Mix} is the mix temperature and T_{Int} is the inlet temperature. Equation (A.21) was rearranged, inserted into Eq. (A.22) which was solved to determine the flow rate fraction of the inlet.

$$\dot{m}_{Int} = 1 - \dot{m}_{Ret} \tag{A.25}$$

$$\frac{\dot{m}_{Ret}}{1-\dot{m}_{Ret}} = \frac{(T_{Mix}-T_{Int})}{(T_{Ret}-T_{Mix})} \tag{A.26}$$

$$\dot{m}_{Ret} = \frac{\left[\frac{(T_{Mix}-T_{Int})}{(T_{Ret}-T_{Mix})}\right]}{1+\left[\frac{(T_{Mix}-T_{Int})}{(T_{Ret}-T_{Mix})}\right]} \tag{A.27}$$